

Florida Institute of Technology

Scholarship Repository @ Florida Tech

Theses and Dissertations

5-2021

Behavior of selective oxygen functional groups upon hydrothermal carbonization and pyrolysis of biomass and their roles on selective applications

Nepu Saha

Follow this and additional works at: <https://repository.fit.edu/etd>



Part of the [Chemical Engineering Commons](#)

BEHAVIOR OF SELECTIVE OXYGEN FUNCTIONAL GROUPS UPON
HYDROTHERMAL CARBONIZATION AND PYROLYSIS OF BIOMASS
AND THEIR ROLES ON SELECTIVE APPLICATIONS

by

Nepu Saha

A dissertation submitted to the Department of Biomedical and Chemical
Engineering and Sciences of
Florida Institute of Technology
in partial fulfillment of the requirements
for the degree of

Doctor of Philosophy
in
Chemical Engineering

Melbourne, Florida
May, 2021

We, the undersigned committee hereby approve the attached dissertation,
“Behavior of selective oxygen functional groups upon hydrothermal carbonization
and pyrolysis of biomass and their roles on selective applications,” by Nepu Saha.

Toufiq Reza, Ph.D.
Assistant Professor
Chemical Engineering

Pavithra Pathirathna, Ph.D.
Assistant Professor
Chemistry

James Brenner, Ph.D.
Associate Professor
Chemical Engineering

Manolis Tomadakis, Ph.D.
Professor
Chemical Engineering

Andrew Knight, Ph.D.
Professor and Department Head
Department of Biomedical and Chemical Engineering and
Sciences

Abstract

Behavior of selective oxygen functional groups upon hydrothermal carbonization and pyrolysis of biomass and their roles on selective applications

Author: Nepu Saha

Advisor: Toufiq Reza, Ph.D.

Hydrothermal carbonization (HTC) is a thermochemical process where biomass is treated in water under high temperature and corresponding vapor pressure. During HTC, biomass undergoes a series of reactions including hydrolysis, decarboxylation, dehydration, aromatization, and polymerization. As a result, a solid product is produced from biomass after HTC process, which is widely known as hydrochar. Depending on the HTC process conditions, a wide-variety of oxygen-containing groups formed on hydrochar surfaces. Many of these groups could play critical roles in applications such as adsorption, and energy and gas storage, etc. However, not all functional groups are exposed on the surface due to the low surface area and the formation of a condensate layer (secondary char) on the hydrochar surface. Pyrolysis

could be a possible pathway to expose additional functional groups by removing the volatile condensate layer. Therefore, the overall objective of this dissertation is to study HTC following by the physical activation of a model compound and real biomass (pine, paper mill sludge, winery waste, and citrus waste) to study the effects of these treatments on functional groups. HTC was primarily performed from 180-420 °C for 30 min in a batch reactor. Produced hydrochar was pyrolyzed at 400, 500, and 600 °C for 1h in a muffle furnace. Several analytical techniques such as boehm titration, Brunauer, Emmett, and Teller (BET) surface area analysis, attenuated total reflector-fourier transform infrared spectroscopy (ART-FTIR), thermogravimetric analysis (TAG), scanning electron microscope (SEM), and X-ray diffraction (XRD) were conducted to characterize the hydrochars and pyrolyzed hydrochars. Various applications of the hydrochars and pyrolyzed hydrochars, such as alternative fuel, adsorbent, and electron storage material were investigated. The results showed that the higher heating value of paper mill sludges derived hydrochars could be increased up to 1.5 times compared to the raw feedstock and that can be used as solid fuel in the existing coal-fired power plant. However, the findings suggested that the fuel properties are highly dependent on both feedstock and the HTC treatment conditions, which led me to investigate additional applications of the hydrochar. Herein, the hydrochar's potential as a solid adsorbent was investigated, where the maximum dye

adsorption capacities of citrus waste and winery waste derived hydrochars were measured 66.23 and 36.23 mg/g, respectively at 4 °C. The thermodynamic properties, such as Gibbs energy (ΔG), enthalpy (ΔH), and entropy (ΔS) were studied to understand the adsorption mechanism. The results revealed that the adsorption phenomenon of both citrus and winery derived hydrochars occurred spontaneously, as the ΔG values at all temperatures are negative. On the other hand, all positive ΔH values indicate the adsorption process was endothermic in nature and not governed by the enthalpy. It was concluded that the hydrochars produced at low HTC temperatures showed highest dye adsorption capacity and the adsorption capacity highly depended on the density of the surface functional groups. To further enhance the surface functional groups, pyrolysis of the hydrochar was conducted. Results showed that pyrolysis of hydrochar at lower temperatures exposed additional surface functionality; however, high-temperature pyrolysis removed the functional groups from the hydrochar surface. Similar to the functional groups, electron storage capacity was highest (3.25 and 2.43 mmol/g for pine and cellulose, respectively) at low pyrolysis temperature. A positive correlation between the electron storage capacity and concentration of lactonic groups on hydrochar was observed. The findings of this study are encouraging and the hydrochar could be of further use for other applications, such as gas storage materials, catalysts, etc.). As both the HTC

and pyrolysis treatments are energy intensive, the operational variables (i.e., temperature, residence time) need to be optimized, and a techno-economic analysis must be conducted prior to scale up these processes.

Table of Contents

1	Introduction	1
1.1	Background	1
1.2	Chemical structure of lignocellulosic biomass	2
1.3	Thermochemical conversion routes of biomass	5
1.3.1	Wet thermochemical conversion processes	6
1.3.2	Dry thermochemical conversion processes.....	10
1.4	Properties of char	11
1.4.1	Chemical properties of hydrochar and biochar	11
1.4.1.1	Proximate and ultimate analyses	11
1.4.1.2	Surface functional groups.....	13
1.4.2	Physical properties of hydrochar and biochar	15
1.5	Applications of hydrochar and biochar	16
1.5.1	Solid fuel.....	17
1.5.2	Soil amendment	18
1.5.3	Adsorbent.....	19
1.5.4	Precursor of catalyst.....	19
1.5.5	Electron and hydrogen storage material.....	20
1.6	Factors affecting the usefulness of char	22
1.7	Literature gaps	23

1.8	Quantification of functional groups.....	25
1.9	Project objectives.....	27
2	Materials and methods	30
2.1	Materials	30
2.2	Methods.....	33
2.2.1	Hydrothermal carbonization (HTC).....	33
2.2.2	Pyrolysis.....	34
2.2.3	Characterization	35
2.2.3.1	Moisture content, mass and energy yields.....	35
2.2.3.2	pH of hydrochar	36
2.2.3.3	pH at point of zero charge (pH _{PZC}).....	37
2.2.3.4	Elemental analysis.....	38
2.2.3.5	Inorganic analysis.....	39
2.2.3.6	Proximate analysis.....	39
2.2.3.7	Lignin analysis	40
2.2.3.8	Surface area analysis	41
2.2.3.9	Scanning electron microscope (SEM)	41
2.2.3.10	X-ray diffraction (XRD).....	42
2.2.3.11	Boehm titration.....	42
2.2.3.12	Attenuated total reflector-fourier transform infrared spectroscopy (ATR-FTIR)	46
2.2.4	Applications	47

2.2.4.1	Combustion characteristic	47
2.2.4.2	Adsorption study	48
2.2.4.3	Electron storage capacity (ESC).....	51
3	Results, discussions, and applications	53
3.1	Properties of hydrochars from a model compound.....	53
3.1.1	Mass yield, ultimate and proximate analysis	54
3.1.2	Surface morphology	57
3.1.3	Functional groups.....	62
3.1.4	pH and pH_{PZC}	69
3.2	Properties of hydrochar from waste biomasses.....	72
3.2.1	Hydrochar from wood.....	73
3.2.2	Hydrochar from citrus and winery wastes	81
3.2.3	Hydrochar from paper mill sludges	85
3.3	Properties of pyrolyzed hydrochar	97
3.3.1	Mass yield, ultimate and proximate analysis	98
3.3.2	Functional groups.....	104
3.3.3	pH and pH_{PZC}	113
3.4	Applications	116
3.4.1	An alternative energy	116
3.4.1.1	Fuel characteristics of hydrochars	117
3.4.2	Hydrochar as adsorbent material.....	124

3.4.2.1	Effect of solution's pH on adsorption	125
3.4.2.2	Adsorption isotherm.....	127
3.4.2.3	Adsorption thermodynamics	133
3.4.3	Electron storage material	135
3.4.3.1	ESC of pyrolyzed hydrochar	136
4	Conclusions	143
5	Recommendations and future research	146
6	References	148

List of Figures

Figure 1: Chemical structure of typical lignocellulosic biomass.	3
Figure 2: Major pathways of thermochemical conversion of biomass (major products corresponding to the treatment are underlined).	6
Figure 3: Thermodynamic properties of water at 30 MPa as a function of temperature.	9
Figure 4: Neutralization reactions of bases with different oxygen groups (a–f).....	26
Figure 5: pH_{PZC} determination technique using pH drift method.	38
Figure 6: A) An overview of the Boehm titration method to determine different functional groups, B) Boehm titration of a blank sample and hydrochar sample during OCAFGs measurement, C) Boehm titration of a blank sample and hydrochar sample during BFGs measurement.	44
Figure 7: Change of mass yield (MY), fixed carbon, elemental carbon, and elemental carbon yield of the hydrochar produced from cellulose at subcritical and supercritical temperatures.	54
Figure 8: The molar ratio of carbon, hydrogen, and oxygen of cellulose and its hydrochars produced at subcritical and supercritical temperatures.	56

Figure 9: SEM images and particle size distribution (PSD): (a) C-H260, (b) C-H300, (c) C-H340, (d) C-H380, and (e) C-H420.....	59
Figure 10: XRD of cellulose and its hydrochars produced at subcritical and supercritical temperatures.	61
Figure 11: Oxygen-containing functional groups of cellulose and its hydrochars produced at subcritical and supercritical temperatures	63
Figure 12: FTIR spectra of cellulose and its hydrochars produced subcritical and supercritical temperatures.	67
Figure 13: Relative transmittance area percentage of associated compounds on cellulose and its hydrochars produced at subcritical and supercritical temperatures.	69
Figure 14: FTIR spectra of wood and its hydrochars.....	80
Figure 15: Relative transmittance area percentage of associated compounds on wood-derived hydrochar surface.....	81
Figure 16: Oxygen-containing functional groups on hydrochars produced from citrus and winery wastes.	83
Figure 17: FTIR spectra of hydrochars produced from citrus and winery wastes. ...	85
Figure 18: van-Krevelen diagram for all raw PMS and their hydrochar samples including bituminous and sub-bituminous coal.	94

Figure 19: Proximate analysis of various PMS hydrothermally carbonized at 180-260 °C. The orange, gray, and blue lines represent VM, FC, and ash content, respectively.	95
Figure 20: ICP analysis of hydrochars and pyrolyzed hydrochars from cellulose and wood.	103
Figure 21: Total and individual oxygen-containing acidic functional groups on chars. A) Total, B) Carboxylic, C) Lactonic, D) Phenolic and other groups	106
Figure 22: FTIR spectra of cellulose and wood at 200 and 260 °C, and their corresponding pyrolyzed hydrochars at 400, 500, and 600 °C.	108
Figure 23: Basic functional groups on pyrolyzed hydrochars produced from cellulose and wood at different temperatures	111
Figure 24: pH and pH_{PZC} of hydrochars and pyrolyzed hydrochars from cellulose and wood; cross markup is for pH and circular markup is for pH_{PZC}	115
Figure 25: Pyrolysis thermographs (top) and DTG curves (bottom) plotted versus temperature for all 260 °C HTC treated paper mill sludges.	119
Figure 26: Combustion thermograph and DTG curves plotted versus temperature for 260 °C HTC treated PMS, coal and 50% mixtures of coal and hydrochar (TG nomenclature refers to mass loss on the left axis and DTG can be found on the right axis).	121

Figure 27: Effect of solution's pH on dye adsorption by hydrochars produced from citrus and winery wastes.	126
Figure 28: Equilibrium adsorption of dye at different temperatures on hydrochars produced from citrus wastes (top) and winery wastes (bottom).	128
Figure 29: Effect of pyrolysis temperature on the ESC of pyrolyzed hydrochars from cellulose and wood.	138
Figure 30: A correlation between ESC and lactonic functional group (top), and between ESC and carboxylic group (bottom).	140
Figure 31: Proposed electron storage mechanism by pyrolyzed hydrochars.....	141

List of Tables

Table 1: Available oxygen-containing functional groups on carbon materials	25
Table 2: A list of biomasses, their treatment conditions and purposes.....	31
Table 3: Sample nomenclature used throughout the dissertation and their respective moisture contents.	32
Table 5: Ultimate and proximate analyses of cellulose and its hydrochars produced at subcritical and supercritical temperatures.	57
Table 4: Pore size distribution, surface area, and relative crystallinity of cellulose and its hydrochars produced at subcritical and supercritical temperatures.....	60
Table 6: pH of hydrochar and process liquid at different HTC conditions.....	71
Table 7: physiochemical properties of wood and its hydrochars produced at different HTC conditions.	74
Table 8: Acidic and basic functional groups of wood and its hydrochars at different HTC conditions.	77
Table 9: Physiochemical properties of hydrochars produced from citrus and winery wastes.	82
Table 10: Mass yields and energy densification of paper mill sludges and their hydrochars (^a Not applicable).....	86

Table 11: Elemental analysis, ash, and lignin number for all raw PMS and their hydrochar samples (^a indicates it was calculated by difference; ^b below detection limit; and ^c Not applicable).	92
Table 12: Mass yield of hydrochars, pyrolyzed hydrochars and their overall from cellulose and wood.....	100
Table 13: Ultimate analysis and polarity index of hydrochars and pyrolyzed hydrochars from cellulose and wood	102
Table 14: Combustion Characteristics of determined from Combustion TGA data. (Clarion #5a coal (bituminous) was used for co-combustion).....	123
Table 15: Methylene blue adsorption by hydrochars produced from citrus and winery wastes: corresponding isotherm parameters from the Langmuir and Freundlich models.	131
Table 16: Separation factor of the Langmuir model.	132
Table 17: Thermodynamic parameters for a dye adsorption process by hydrochars produced from citrus and winery wastes.....	134

Acknowledgement

I am grateful to my thesis advisor, Dr. M. Toufiq Reza. Since my first day in graduate school, Dr. Reza believed in me like nobody else and gave me endless support. Under his supervision, I learned how to define a research problem, find a solution to it, and finally publish the results. On a personal level, Dr. Reza inspired me by his hardworking and passionate attitude. It would have been impossible for me to complete this work without his mentoring and moral supports.

I would like to express my sincere thanks to the rest of my dissertation committee members, Dr. Manolis Tomadakis, Dr. James Brenner, and Dr. Pavithra Pathirathna for their support and valuable advices.

I am thankful to Mr. Akbar Saba and Mr. Kyle McGaughy, the most helpful persons in Ohio University and Florida Institute of Technology, respectively, for their enormous supports on my research and collaborative studies. They have provided both technical suggestions and personal encouragement. I am also grateful to my research group: Pretom Saha, Jacob Steel, Ben Vancouver, Md. Tahmid Islam, Al-Ibtida Sultana, and Thomas Quaid for their assistance and creating a joyful environment in the laboratory. I would like to thank all the lab staffs of the Institute

of Sustainable Energy and the Environment (ISEE) at Ohio University and the Biofuels Lab at Florida Institute of Technology for supporting me with the laboratory supplies. It would have been impossible without their supports.

I acknowledge Florida Institute of Technology for giving me the Outstanding Student of the year (2019-2020) award. This award motivated me to focus more on the research which ultimately added value to my dissertation.

I am grateful to my collaborators Dr. Pei Chiu, and Ms. Danhui Xin at the University of Delaware, for measuring the electron storage capacity of my samples. Thanks to Dr. Kevin Holtman from Georgia Pacific, Dr Luca Fiori from University of Trento, and Drs. Maurizio Volpe and Roberto Volpe form University of Enna KORE and Queen Mary University of London, respectively for supplying some sample materials for this research work. Also, their valuable comments on my dissertation make it more organized.

I acknowledge the support from United States Department of Agriculture (USDA, grant no. 2019-67019-29288), Ohio University start-up funding support, and Florida Institute of Technology start-up funding support. Otherwise, I would not have been able to develop my scientific discoveries.

Last but not least, I would like to express my deepest gratitude to my parents. They deserve credit for all my achievements. They have supported me wholeheartedly in all my endeavors. Special thanks to Ms. Supria Saha, my wife, and Ayodhika Saha, my daughter to support me and stay beside me in all my hard times. Both have been my source of inspiration throughout my research.

Dedication

This dissertation is dedicated to my parents, who taught in me the virtues of determination and commitment and relentlessly encouraged me to strive for the excellence. My special dedication goes to my wife and daughter for the moral and spiritual support during my study.

Preface

This dissertation document is a summary of the below listed published journal articles by the author. The author has obtained permission from the publisher (e.g., Elsevier, ACS Publications, Springer Nature) for using the content in this dissertation and included those permissions in Appendix D. The author's completed dissemination list during his PhD tenure is shown in Appendix C.

Journal articles

1. **N. Saha**, A. Saba, and T. Reza, "Effect of hydrothermal carbonization temperature on pH, dissociation constants, and acidic functional groups on hydrochar from cellulose and wood," *Journal of Analytical and Applied Pyrolysis*, vol. 137, pp. 138-145, 2019. <https://doi.org/10.1016/j.jaap.2018.11.018>.
2. **N. Saha**, D. Xin, P. Chiu, and T. Reza, "Effect of pyrolysis temperature on acidic oxygen-containing functional groups and electron storage capacities of pyrolyzed hydrochars," *ACS Sustainable Chem. Eng.*, vol. 7, pp. 8387-8396, 2019. <https://doi.org/10.1021/acssuschemeng.9b00024>.
3. **N. Saha**, A. Saba, P. Saha, K. McGaughy, D. Franqui-Villanueva, W. J. Orts,

- W. M. Hart-Cooper, and T. Reza, “Hydrothermal carbonization of various paper mill sludges: an observation of solid fuel properties,” *Energies*, vol. 12, p. 858-868, 2019. <https://doi.org/10.3390/en12050858>.
4. **N. Saha** and T. Reza, “Effect of pyrolysis on basic functional groups of hydrochars,” *Biomass Conversion and Biorefinery*, vol. 1, p. 1-8, 2019. <https://doi.org/10.1007/s13399-019-00504-3>.
 5. **N. Saha**, M. Volpe, L. Fiori, R. Volpe, A. Messineo, and T. Reza, “Cationic Dye Adsorption on Hydrochars of Winery and Citrus Juice Industries Residues: Performance, Mechanism, and Thermodynamics” *Energies*, vol. 13, p. 4686, 2020. <https://doi.org/10.3390/en13184686>.
 6. **N. Saha**, K. McGaughy, and T. Reza, “Elucidating hydrochar morphology and oxygen functionality change with hydrothermal treatment temperature ranging from subcritical to supercritical conditions” *Journal of Analytical and Applied Pyrolysis*, vol. 152, p. 104965, 2020. <https://doi.org/10.1016/j.jaap.2020.104965>

1 Introduction

1.1 Background

The global biowaste production is increasing day by day. Among other biowastes, the current global production of biomass waste alone is about 140 billion tons per year [1]. Biomass wastes primarily consist of crop stalks, leaves, roots, fruit peels, and seed/nutshells that are often discarded during the crop processing. Handling this huge waste stream is always difficult due to their low bulk density, high ash, low energy content, high moisture content, and tendency to rot easily. These wastes could be potential feedstocks for various products, such as fuel, chemicals, materials, etc. However, the lack of economically viable and environmentally sustainable conversion processes hinders their utilization for value-added applications. As a result, a significant portion of biomass waste is currently being burnt on the field or being disposed at the nearby landfills. Both burning of these biomass waste or disposal on the landfills produce greenhouse gas (i.e., CO₂), which contribute to the global warming resulting climate change. Studies showed that about 18 % of total

global CO₂ emission is due to the burning of biomass residues [2, 3]. Therefore, finding sustainable applications of these wastes could convert an environmental liability to a valuable resource. Thermochemical conversions are promising technologies to convert such wet biomass into valuable products. Over the past 30 years, the primary concentration of utilization of biomass wastes was limited into the energy sector [4-8]. Due to the current volatile fuel market, it might be the time to think beyond fuel applications. However, a lack of understanding of the formation of thermochemically converted materials and their surface properties with the treatment limits the scope of these wastes as alternative uses.

1.2 Chemical structure of lignocellulosic biomass

In order to understand the conversion process like thermochemical conversion, one needs to understand the chemical structure of the biomass, as the reaction kinetics and products of thermochemical conversion would be affected by the chemical composition of specific biopolymers of biomass. Biomass waste, often known as lignocellulosic biomass, is the non-starch fibrous part of the crop plant. It mainly consists of four chemical components such as hemicellulose, cellulose, lignin, and extractives. It also contains a limited amount of inorganic materials or ash. The compositions of hemicellulose, cellulose, lignin, and extractives in typical lignocellulosic biomass are 23–32 %, 38–50 %, 15–25 %, 5–15 %, respectively,

which varies from grassy biomass to woody biomass [9]. The overall chemical structure of typical lignocellulosic biomass is shown in Figure 1. In general, cellulose can be found in a bundle, while the hemicelluloses spiral the cellulose bundles and the lignin works as a divider to separate the spiraled bundles from each other. The extractives are usually found as a thin layer over the entire cell wall configuration.

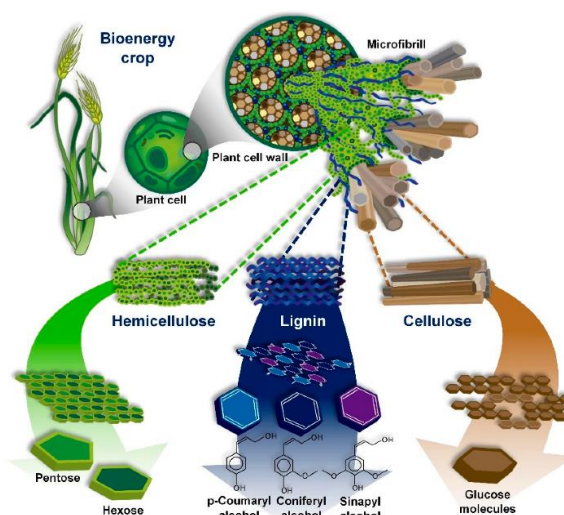


Figure 1: Chemical structure of typical lignocellulosic biomass [10].

In terms of chemical composition, hemicellulose is a polymer of different monosaccharide units of six-carbon sugars (mannose, galactose, glucose, and 4-O-methyl-D-glucuronic acid) and five-carbon sugars (xylose and arabinose) [9, 11]. The concentration of each sugar compound varies from plant types (grassy versus woody biomass) or even different parts of the same plant (stem, bark, leaves, etc.).

The backbone of hemicellulose is either a homopolymer (single sugar unit) or a heteropolymer (mixture of different sugars). These sugar molecules in hemicellulose keep short chain (typically 500–3000 units), amorphous, and side chains structure.

Unlike hemicellulose, cellulose is an unbranched long-chain (typically 7000–15000 glucose molecules) polymer of anhydro-glucose connected by β -1,4 glycosidic bonds. Due to the β -glycosidic linkages, the cellulose is a linear chain that is highly stable and resilient from the chemical attack because of highly intra- and inter molecular hydrogen bonding [12]. By forming the hydrogen bonding between the hydroxyl (-OH) groups and surrounding cellulose chains, the structure organizes in parallel and forms a crystalline structure.

Lignin is a cross-linked polymer material with high molecular weight (7400–78400 g/mol) [13]. In general, a lignin network contains different phenyl propane units such as p-coumaroyl alcohol, coniferyl alcohol, and sinapyl alcohol [14]. Lignin structure varies significantly among the biomass types. For instance, lignin in hardwood is primarily based on sinapyl alcohol and coniferyl alcohol, while in softwood is mainly based on coniferyl alcohol [15].

Extractives are the organic substances which have a low molecular weight (220–785 g/mol) [16]. It primarily contains resin, fats, waxes, fatty acids, alcohols, turpentine,

tannins, and flavonoids. Some extractives are toxic, which protects the biomass from attack by fungi and termites [17]. The ash mainly consists of inorganics, and they are mostly available on the extractives and lignin. In general, hemicellulose sticks with the cellulose and makes polysaccharide microfibrils. Lignin mainly acts as a binder and makes the structure stronger and protect the plant against microorganism or chemical attack.

1.3 Thermochemical conversion routes of biomass

Lignocellulosic biomass is available in various forms such as woody, herbaceous, animal manure, etc. Specific types of biomass have distinctive physical and chemical characteristics. In their dry form, most of these biomass can be used as a fuel without any primary treatment. However, due to low bulk density (50–200 mg/m³), low energy content (8–15 MJ/kg), and high ash content (0.5–29.5 %), thermochemical treatment is often required to enhance fuel or materials properties of the biomass. Biomass may be converted to densified fuel and/or materials by various thermochemical processes, depending on the characteristics of the raw feedstocks and the type of desired products. Figure 2 shows some of the major thermochemical conversion pathways to convert biomass to solid, liquid, and gaseous products. Regardless of the thermochemical treatment processes, a solid product is always produced as a desired product or byproduct.

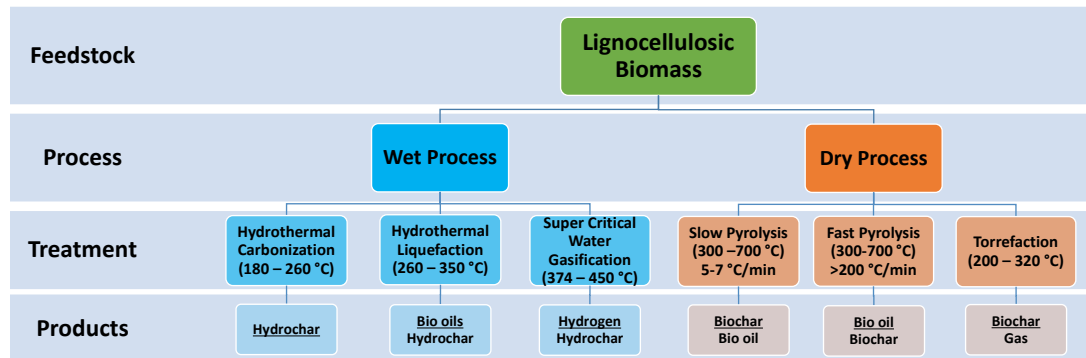


Figure 2: Major pathways of thermochemical conversion of biomass (major products corresponding to the treatment are underlined).

1.3.1 Wet thermochemical conversion processes

In the wet thermochemical processes, biomass can be used directly without any pre-drying, as water acts as the reaction medium. The critical point of water is 374 °C and 22.1 MPa. Temperature below the critical point is known as subcritical and above is known as supercritical. Thermodynamic properties of water change substantially from ambient temperature to the sub and supercritical conditions. At room temperature, water shows good solubility with the different polar compounds due to its high density and high dielectric constant. The dielectric constant is a ratio of the permittivity of a substance to the permittivity of free space, whereas permittivity is a measure of the ability of a material to resist the formation of an electric field within it. The reason for water having a high dielectric constant is its dipole moment. As a

result, water tends to polarize strongly under a given electric field, nearly canceling out the effect of the field [18]. At the same time, water conducts electricity because it contains ions (OH^- and H^+), which are highly mobile. The large dielectric constant means that substances whose molecules contain ionic bonds will tend to dissociate in water, yielding solutions containing ions. This occurs because water as a solvent opposes the electrostatic attraction between positive and negative ions that would prevent ionic substances from dissolving, and thereby water becomes a very good solvent. The dielectric constant decreases from around 80 at 25 °C to about 20 near supercritical temperature and further decreases to lower than 2 at 450 °C. This indicates that the water transforms from a polar and highly hydrogen bonded solvent at room temperature to a non-polar solvent at elevated temperature, which allows it to dissolve organic compounds. Excessive decrease of dielectric constant at supercritical condition causes a change in the dynamic viscosity and also increases the self-diffusion coefficient of water [19].

Although water is not acidic nor basic at room temperature, but it can function as both acid and base at the same time at elevated temperature. One water molecule (acting as a base) can accept a proton from a second one (acting as an acid). This can happen anywhere, even with a trace of water. The hydronium ion (H_3O^+) is a strong acid, and the hydroxide ion (OH^-) is a strong base. As fast as they are formed, they

react to produce water again. The net effect is that equilibrium is shown in equation (1).



The ionic product is the equilibrium constant for the reaction in which a reactant undergoes an acid-base reaction with itself. The equilibrium constant, K_w of water is shown in equations (2) and (3).

$$K_w = H_3O^+ [OH^-] \quad (2)$$

$$pK_w = pH + pOH \quad (3)$$

Figure 3 indicates that the ionic product of water is 10^{-14} at 25 °C, which increases with temperature and reached its highest point (1 or 2 orders of magnitude higher than at ambient temperature) at a temperature between 227 °C and 327 °C, depending upon the pressure [18, 20]. With the further increase of temperature (i.e., introduction of heat), the H-bond of water weakens, allowing the dissociation of water into H_3O^+ and OH^- ions resulting a significant decrease of ionic product (4 to 5 order of magnitude). At this condition, the network of hydrogen bonds is broken, and water then exists as separate clusters with a chain structure [18].

In addition to the dielectric constant and ionic product, the density of water changes with temperature. At room temperature, water shows the highest density, which decreases slowly with the increase of temperature up until the critical temperature

before decreasing sharply at supercritical temperature. As discussed earlier, the ionic product is lower and the dielectric constant is relatively low at supercritical temperatures, which inhibits the ionic reactions; however, the lower density favors free radical reactions that enhance the overall reaction rate.

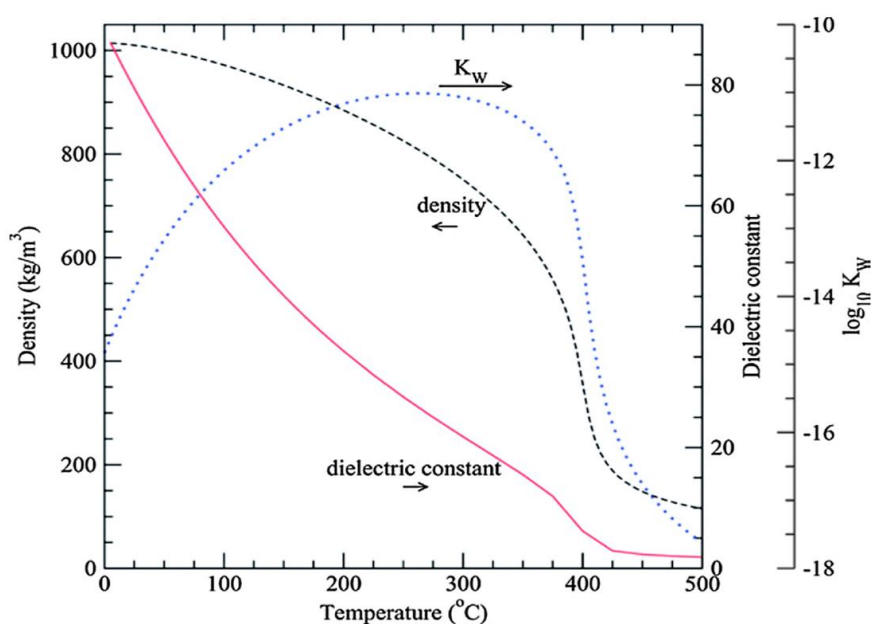


Figure 3: Thermodynamic properties of water at 30 MPa as a function of temperature [21].

Depending on the treatment temperature, the wet processes are divided into three sub-processes; i) Hydrothermal Carbonization (HTC), ii) Hydrothermal Liquefaction (HTL), and iii) Super Critical Water Gasification (SCWG). HTC is suitable at 180–260 °C, whereas HTL and SCWG are suitable at 260–350 °C and 374–450 °C,

respectively. Different hydrothermal treatments result in different main products, such as solid hydrochar is the main product of HTC, bio-oil for HTL, and syngas (or hydrogen depending on the catalyst) for SCWG. Among all the wet thermochemical processes, hydrothermal canonization is the most popular treatment for hydrochar production. As discussed earlier, the biomass mainly consists of hemicellulose, cellulose, and lignin, which are converted to hydrochar at different rates via different mechanisms. These reaction mechanisms are well-studied and shown in Appendix A.

1.3.2 Dry thermochemical conversion processes

Dry thermochemical conversion is a process where dry biomass is used as a feedstock. There are different dry treatment processes such as pyrolysis, torrefaction, gasification, etc. Torrefaction and gasification are typically conducted at 200–320 °C and >700 °C, respectively. These treatments are mainly produced solid (torrefied char) and gaseous products (synthesis gas). In contrary, during the pyrolysis process, biomass is heated typically at 300–700 °C in the absence of oxygen. Based on the heating rate, residence time, and targeted products, it can be divided into two categories, such as fast pyrolysis and slow pyrolysis. For instance, fast pyrolysis is generally used to maximize the bio-oils yield where the heating rate is generally 200 °C/min and residence time is less than 10 s [22, 23]. On the other hand, slow

pyrolysis is used to maximize the biochar yield along with a small quantity of condensed bio-oil and syngas including CO₂, CH₄, and H₂ [24, 25]. Typically, the heating rate of slow pyrolysis is 5–7 °C min, and the residence time is more than 30 min. The choice of treatment process ultimately depends on the targeted products. Similar to the HTC, different components of the biomass converted to biochar at different rates via different mechanisms under pyrolysis conditions are well studied and shown in Appendix B.

1.4 Properties of hydrochar and biochar

1.4.1 Chemical properties of hydrochar and biochar

Chemical properties of char generally indicate the ultimate and proximate analyses including the evaluation of surface functional groups. The detailed of these properties are discussed below:

1.4.1.1 Proximate and ultimate analyses

The proximate analysis is a quantitative method to determine the volatile matter (VM), fixed carbon (FC), and ash content in the char. It provides the percentage of the material that would volatilize in gaseous state (VM) and in the solid state (FC). Therefore, it is important to know for a fuel material. It is reported in the literature that the thermochemically converted material has higher FC compared to its raw

feedstock, and this number increases with the increase of treatment temperature, while the VM showed an opposite trend [4, 26, 27].

With the HTC treatment, an increased fraction of FC in the hydrochar was observed, which indicates that a significant amount of carbon was retained in the hydrochar. At the same time, the VM reduced significantly, indicating that the low volatile matters leached into the liquid phase. With these properties, hydrochar can be easily ignited at low temperatures (approximately 250 °C) and rapidly reaches a maximum weight loss when used as solid fuel [28]. Thus, it can overcome the drawbacks of raw biomass. Similar to the hydrochar, FC in biochar increased and VM decreased with the pyrolysis temperature [29].

On the other hand, the ultimate analysis consists of the elemental carbon (C), hydrogen (H), oxygen (O), nitrogen (N), and sulfur (S) content in the char. The H/C and O/C ratios in the material are important criteria for estimating the degree of de-oxygenation and the aromatic content. A higher H/C ratio indicates lower aromatic content [30]. On the other hand, a lower O/C ratio indicates the increase of calorific value. It is observed in literature that the H/C and O/C ratios decreased as the HTC and pyrolysis temperature increased for both hydrochars and biochars [29, 31-33]. As a result, it is apparent that the lignocellulose-derived hydrochar or biochar generally showed better fuel characteristics compared to raw feedstock.

1.4.1.2 Surface functional groups

Due to the complex composition of the feedstock and a wide range of treatment conditions, the hydrochar has a variety of surface functional groups. Regardless of the feedstock, the O-H stretching bonds in hydroxyl or carboxyl groups show weakening because of the dehydration that occurred during HTC [31, 34-36], which was also consistent with the reduction of H/C and O/C on the hydrochar. There are some exceptions of this behavior. For example, the hydrochar from paper mill sludges did not show any significant change in the hydroxyl groups, which could be due to the extensive thermo-mechanical or thermo-chemical pretreatment in the pulping process [37]. Ultimately, the decrease of hydroxyl groups makes the hydrochar more hydrophobic. The aliphatic and aromatic peaks are typically stronger in the hydrochar compare to the biomass because of the breakup of polymeric substances and emerge of hydro aromatic structures [35, 36].

The presence of oxygenated functional groups in hydrochars is an important characteristic. It is observed in the literature that the stretching ketone, amide, and carboxylic groups decreased in the hydrochar due to the increase of decarboxylation with the HTC temperature [36, 38]. The decrease of C=O as ketone and amide groups or carboxylic groups resulting in the conversion of the carbon compounds into CO₂ [31, 32]. Other studies reported that the C=O stretching peak was not present in

hydrochar due to the degradation of carboxyl and acetyl groups; however, a strong peak showed up at another wavenumber similar to C=O vibrations of carbonyl, quinone, ester, or carboxyl groups [34]. This could be due to the dehydration of water from the equatorial hydroxyl groups in the intermediate monomer [39]. In addition, hydrochar retains higher oxygen-containing functional groups by controlling the C-O stretching vibration in hydroxyl, ester, or ether, coupled with the vibration of O-H bending and C=O. Due to the incomplete decomposition of lignin, C-O stretching bonds can be found in higher intensity as well. Furthermore, He *et al.*, observed a drastic increase in the relative intensity of oxygen-containing functional groups due to the -C-O-R in aliphatic ethers and -C-O in alcoholic stretching [32, 40].

On the other hand, the formation of functional groups on the biochar surface occurred during the aging process of biochar. Biochar showed a decrease in stretching aliphatic, which could be due to the oxidation [41]. At the same time the stretching of C=O groups shown an increasing trend, which indicates the increase of carboxyl group in biochar [42]. During low-temperature slow pyrolysis, the biochar contains relatively high oxygen content, which allows biochar to have more functional groups [43]. With the increase of temperature, elemental oxygen stripped out from the surface, a result of reduction of oxygen-containing groups and an increase of aromatic groups on the biochar surface [44, 45].

In summary, both hydrochar and biochar surfaces consist of aromatic and aliphatic carbon with oxygen-rich functional groups. However, due to the difference in the formation mechanism, one can contain more functional groups than the other.

1.4.2 Physical properties of hydrochar and biochar

Physical properties of chars include the surface morphology parameters such as surface area, pore volume, and pore size. Generally, char shows a rough surface compare to corresponding raw feedstock due to the decomposition of raw material and/or removal of volatiles from the surface under the thermochemical conversions. For instance, at low temperature HTC, hemicellulose easily collapses and can decompose into fragments and deposit on the porous surface of the solid residue. These small fragments would further dissolve and form carbonaceous spheres on the surface. Xiao *et al.* compared scanning electron microscopy (SEM) images of different raw biomass and their hydrochars [33]. They found that the raw material showed a relatively flat and smooth surface while the hydrochar showed an irregular surface with a new microsphere. With the increase of HTC temperature, other components decompose, first hemicellulose followed by cellulose, and lignin from the main structure. However, Gai *et al.* found that a significant amount of porous structure appears on the hydrochar surface due to the decomposition of organic components during HTC [46]. At the same time, both spherical and non-spherical

shaped particles were observed on the surface by the SEM [46, 47]. Due to the decomposition of the fragments, the hydrochar typically has a lower surface area ($0.1\text{--}10\text{ m}^2/\text{g}$) [39].

On the other hand, the changes in biochar surface area are most likely due to the decomposition of organic matter from the feedstock and the formation of micropores [48]. The destruction of aliphatic and ester groups and the exposure of aromatic core under pyrolysis temperature could increase the surface area [49]. The surface area of the biochar increases with increasing of pyrolysis temperature, because at high temperature the pore blocking materials are driven off from the biomass [50]. At the same time, higher pyrolysis temperature helps to release the volatile matter and creates more pores [51]. As a result, biochar usually has a relatively higher surface area ($0.7\text{--}490\text{ m}^2/\text{g}$) [49, 52, 53].

1.5 Applications of hydrochar and biochar

Hydrochar and biochar both can be easily prepared from a variety of sources and can be used as low-cost materials in extensive applications compared to commercial materials. Combining with unique properties such as high carbon content, relatively high surface area, high pore volume, and enriched functional groups, chars can be

used in a wide range of applications such as fuel, soil amendment, adsorbent, and energy storage.

1.5.1 Solid fuel

The higher heating value (HHV) indicates the energy content of that material. In general, the HHV of polymeric composition of the biomass follows this trend: ash < extractives < hemicellulose < cellulose < lignin [54]. This trend indicates that higher carbon number has higher HHV. During the thermal treatment, removal of hemicellulose and cellulose for the biomass results in an increase of C/O ratio, which ultimately increases the HHV. During HTC process, degradation of hemicellulose forms 5-hydroxymethyl furfural (HMF), which has higher HHV (22.1 MJ/kg) compared to the hemicellulose (17.6 MJ/kg), and may increase overall HHV if HMF is deposited in the porous structure of hydrochar [55]. This may augment the HHV of hydrochar as HMF is produced at a higher reaction temperature from the degradation of hemicellulose [56]. On the other hand, pyrolysis results in the release of volatile matter and increase the fixed carbon as decarboxylation is one of the dominating reactions. Higher carbon number and lower oxygen content allow for an increased carbonization degree (C/O), resulting in a high HHV of biochar compared to feedstock [57, 58].

Although both HTC and pyrolysis treatments of biomass have increased its C/O ratio, this ratio highly depends on the feedstock. For instance, there are several waste streams, such as sewage sludges, paper mill sludges, etc., which are highly heterogeneous in nature and some of them have high inorganic content. As a result, a general treatment condition might not work for all the wastes. Thus, the initial characterizations of the feedstocks are necessary prior to treat them.

1.5.2 Soil amendment

The use of chars as a soil amendment caught attention due to its special surface structure and elemental composition. It can promote soil by improving soil structure, enhancing the cation exchange capacity, improving water retention, mitigating nutrient leaching, etc. [59]. Wang *et al.* found that the addition of 4 % of rich hulk biochar in tea gardens increase the soil quality significantly [60]. The level of soil pH including with most of the nutrient increased, while the available aluminum and lead content decreased. However, the use of char has not always a positive outcome. For example, Rillig *et al.* reported that increasing concentration of hydrochar could be harmful to plant growth [61]. Their results advised that hydrochar should be carefully tested before use as soil improvement to avoid the negative impact on the plant. This leads the researchers to find the alternative uses of hydrochar such as adsorbents, catalysts, etc.

1.5.3 Adsorbent

Biochar is thought to be a promising adsorbent of various pollutants in water, air, and soil, due to its relatively high surface area (2–490 m²/g) and pore volume (0.01–1.55 cm³/g) [52]. In contrast, hydrochars have relatively lower surface areas (0.1–10 m²/g), but they have abundant surface functionality, which make them a prominent adsorbent as well [39, 62]. The possible adsorption mechanism involves integration of several kinds of interactions such as electrostatic attraction, ion-exchange, physical adsorption, surface complexation and/or precipitation, etc. However, some heavy metals showed different adsorption mechanisms. The presence of abundant surface functional groups mainly oxygen-containing functional groups (i.e., -COOH, and -OH) enhanced the heavy metal adsorption as those functional groups have strong interactions with heavy metals, which can be evidenced by changes in functional groups of char before and after metal adsorption [63].

1.5.4 Precursor of catalyst

Biochar is considered as a promising supporting material or catalyst because of its relatively larger surface area (2–490 m²/g) [52]. In addition, the presence of surface functional groups enhances its activity such as the O-H and C=O groups for the ammonium adsorption [64], and O-H group for Norfloxacin adsorption [65].

Although hydrochar has a relatively low surface area, it has high surface functionality. So, the thermal activation of hydrochar could give us a material with high in both surface area and surface functionality, which could be an ideal catalyst support.

1.5.5 Electron and hydrogen storage material

In addition to the above-discussed applications, char has been used for other purposes such as electron and energy storage materials. Hydrogen has attracted significant attention as a replacement for fossil fuels because of its high energy efficiency and zero greenhouse gas emission. However, the critical problem of hydrogen use as an alternative energy source is the difficulty in storage. It has been reported that along with the adsorption parameters (e.g., high microporous surface area $> 2000 \text{ m}^2/\text{g}$, small pore size $< 20 \text{ \AA}$, and large pore volume $> 1 \text{ g/L}$), the adsorption sites (oxygen functional groups with atomic O/C ratio ≈ 0.2) and the interaction between adsorption sites with H_2 are vital for storing a large volume of H_2 [66]. According to literature, the hydrochar spheres are produced in the range of $0.6 - 6.0 \text{ \mu m}$. Increasing reaction temperature, precursor concentration, or reaction time results in larger spheres [67, 68]. In addition, carbon content increases from ~ 42 to 65% , where the O/C atomic ratio decreases from 1.0 (precursor) to ~ 0.35 with the increase of reaction temperature. It is also observed that the ether and hydroxyl bonds are reduced into ester, carbonyl, and alkene bonds with increase in HTC temperature. Although the

total number of oxygen functional groups increases significantly in the hydrochar compared to raw feedstock, the other parameters, such as pore size, micropore volume, and specific surface area are not up to the mark where the H₂ storage capacity is maximum. As a result, further activation (thermal or chemical) will be required to enhance H₂ storage.

Electrical energy storage systems are becoming widely used in consumer electronics and electric vehicles, as well as in the storage of renewable energy sources. Electrochemical energy storage devices, such as supercapacitors and Li-ion batteries, have shown great potential and attract broad interests. An electrochemical energy storage material should have a high surface area and tunable pore size, high electric conductivity, and easy accessibility [69]. Both chars (hydrochar and biochar) can donate, accept, or transfer electrons in their surrounding environments, either abiotically or via biological pathways [44, 70]. These abilities of chars to reduce (or oxidize) their environment strongly vary with the nature of the feedstock and the treatment conditions. Oxygen-containing functional groups are probably forming most of this “redox pool”. A certain fraction of these compounds can be reversibly oxidized and reduced, giving the chars, the property of a redox buffer [44]. The electron-donating moieties (i.e., reducers) from the chars are likely phenolic species, while the compounds accepting electrons (i.e., oxidants) are believed to be quinones

and polycondensed aromatic structures [44]. So, the functional groups such as carboxylic and phenolic groups in char determine its surface charge and redox properties and play an important role in the retention of cations and anions in soil and aqueous environments

1.6 Factors affecting the usefulness of char

The application of char is highly dependent on the specific properties of the char, which are governed by both the feedstock and the treatment conditions. For example, carbon and oxygen contents are most important to use the material as fuel. High carbon and low oxygen in the char have showed better fuel properties. On the other hand, for the adsorption application, surface area and pore size are very important. However, researchers have been recently claiming that surface functionality is also important [71, 72]. For example, Lu *et al.* proposed that free carboxylic groups played a significant role in heavy metal adsorption [71]. Samsuri *et al.* studied heavy metal adsorption by using oil palm and rice husk biochars [72]. Their results showed that oil palm biochar with the relatively low surface area has higher adsorption than rich husk biochar, which suggests the surface area is less important than functionality. Qiu *et al.* found that the overall dye adsorption depends on the π - π interaction between the dye molecule and char surface, the direct dye-char electrostatic attraction and repulsion, as well as the intermolecular hydrogen bonding [73]. They

also observed that the rich phenolic hydroxyl groups on char surface were expected to enhance π - π interaction which will ultimately increase the adsorption.

The surface functionality of char plays an important role in its redox properties (e.g., electron exchange or storage capacity) [70, 74-76]. Electron storage capacity is the amount of electrons that can be stored within a unit mass of char through chemical redox reactions with a reductant or an electron transfer mediator [70, 76-78]. Saquing *et al.* found that electron storage capacity could be a source of reversible electron donor and acceptor [70]. On the other hand, Klüpfel *et al.* and Emmerich *et al.* proposed that quinone functional groups are primarily responsible for the electron storage capacity [76, 79]. Since the carboxylic, lactonic groups are available on the hydrochar and biochar vary with the treatment conditions, the electron storage capacity of the char could also be varied under different conditions [80].

1.7 Literature gaps

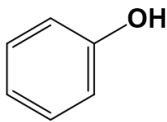
In the past years, literature reported biomass upgrading via both pyrolysis and HTC individually. The solid products from those treatments (i.e., biochar and hydrochar) have also been used in various applications, which were discussed in the earlier sections. Although, use of hydrochars as an alternative fuel is well established, how the wastes from similar industries behave differently under HTC conditions are not

studied yet, which is one of the bottlenecks in current literature. Among all of the above-discussed applications, energy and electron storage material and precursor of catalysts are newly added to the list. These new applications are highly controlled by the surface functionality along with the surface morphology [63, 66, 71]. Not only these applications, one of the well-established applications (i.e., adsorption) also highly dependent on the surface functionality. Due to the complex composition of the char, until now, Fourier Transform Infrared Spectroscopy (FTIR) technique is employed in most studies to analyze the surface functional groups and gives a qualitative indication. However, the quantitative determination of functional groups is very important in regard to their applications. Additionally, it is also crucial to know how those functional groups behave with different thermochemical conversions. Although researchers have been developing methods to utilize hydrochar and biochar for various purposes, the applications in other fields are limited because of a lack of understanding of their surface functionality. To use these chars in an efficient way, it is essential to know the optimum treatment conditions where these functional groups are maximized. Additionally, knowing how each and every functional group varies with the treatment conditions is also important to use them in any particular application.

1.8 Quantification of functional groups

Based on the previous discussion, it is important to quantify the oxygen functional groups on the hydrochar surface. This will allow to make a correlation between the application of that material and their functional groups. There are two types of such functional groups, namely: i) oxygen-containing acidic functional groups (OCAFG), and ii) basic functional groups (BFG). Table 1 showed some common OCAFG and BFG available on the char.

Table 1: Available oxygen-containing functional groups on carbon materials.

Name	Functional Group
Alcohols	$R-OH$
Phenols	
Ethers	$R-O-R'$
Aldehydes	$R-\overset{\text{O}}{\parallel}-H$
Ketones	$R-\overset{\text{O}}{\parallel}-R'$
Carboxylic Acid	$R-\overset{\text{O}}{\parallel}-OH$
Esters	$R-\overset{\text{O}}{\parallel}-O-R'$

There is no direct method to quantify the OCAFG and BFG. However, after a detailed search in literature, a well known acid-base titration method known as Boehm titration (BT) was discovered which could be used to determine both OCAFG and BFG on the char.

Figure 4 shows how the surface functional groups have been measured by using the BT method. Using different strength bases will give different types of surface groups.

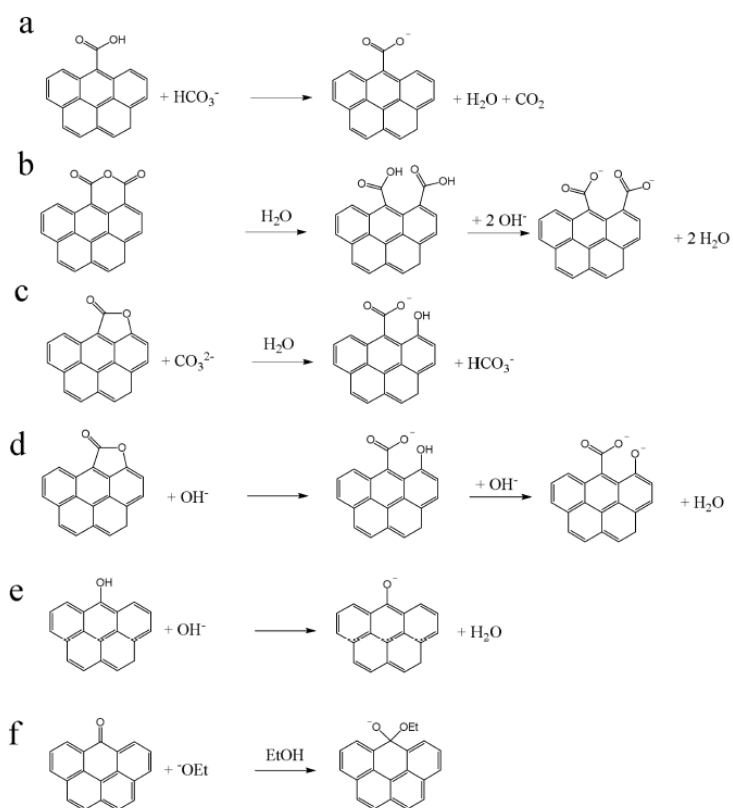


Figure 4: Neutralization reactions of bases with different oxygen groups (a–f) [81]

The acidic groups are often donated as Brønsted acids (H^+ donors) [82, 83]. The donation of proton applies to carboxylic and phenolic groups shown in Figure 4(a, e). As the lactonic group has no proton that can be eliminated, the determination of this group is a little different. According to literature, the conversion of oxygen groups is based on induced hydrolysis [84]. So, a hydroxide ion (OH^-) from the water molecule comes to the lactone group and cleaved the bond and released a proton that ultimately neutralizes the base shown in Figure 4c.

1.9 Project objectives

The overall objective of this research was to study the alternative uses of waste biomasses, such as fuel, adsorbent, and electron storage material. This study extensively focused on the surface properties of hydrochar and the pyrolyzed hydrochar following by their importance on various applications, such as an alternative fuel, adsorbent, and electron storage material. The specific objectives of this research are outlined below:

Objective 1: Investigate the physiochemical properties (e.g., pH, elemental and proximate analyses, surface area, etc.) of thermochemically converted chars.

Rationale: Physiochemical properties of a material are the basic information one needs to know prior to moving forward with them. This will allow one to see how the different feedstocks changed differently under thermochemical conversion.

Objective 2: Investigate the effect of HTC temperature on OCAFGs and BFGs on the hydrochar surface.

Rationale: Surface functionality is the key among all other properties of hydrochar material upon their applications. It is observed in the literature that HTC is better thermochemical treatment compared to the pyrolysis when functionalization is the ultimate goal [85]. As a result, the HTC of a model compound and a lignocellulosic biomass were conducted at a different temperature between 180–420 °C. The results will allow us to recognize the effect of HTC temperature on functional groups.

Objective 3: Examine the effect of pyrolysis temperature on OCAFGs and BFGs on pyrolyzed hydrochars.

Rationale: Although HTC functionalizes the biomass, the surface area remains relatively low, which hinders its application. As pyrolysis treatment is used to increase the surface area, this treatment has been implemented on the hydrochar produced in objective 2. The results will demonstrate whether we can increase the surface area by keeping the functionality or whether this also changes with the pyrolysis temperature.

Objective 4: Various applications of hydrochars and pyrolyzed hydrochars in regard to finding alternative uses of waste biomasses.

Rationale: The first three objectives are to synthesize the material while this objective is on the application side. This will give an indication of whether all the hydrochars can be used as fuel or not. Also, it will establish a pathway to use the hydrochar as adsorbent and their favorable condition. In addition, the electron storage capacity of pyrolyzed hydrochar has been examined that will express how important the surface functional groups of material for the electron storage application.

2 Materials and methods

2.1 Materials

In this dissertation, a model compound (cellulose), woody biomass (hardwood), various paper mill sludges (PMS), citrus waste (orange peel), and winery industry waste (grape skin) were investigated. In order to understand the change of the surface properties under various treatments, a model compound cellulose was chosen, as cellulose is a common biopolymer in all waste biomasses. Furthermore, waste wood is the most abandoned biomass in the world, which was the reason for chosen woody biomass in this study. Wet waste biomasses, such as paper mill sludges, grape skin, and orange peel are mostly discarded to landfill. Due to the strict landfill policy, none of these wastes is recommended as a land filler (soil improver) because paper mill sludges contain ink, chemicals, etc. whereas the orange peel is acidic in nature and grape skin is a rich source of phenolic compounds and high sugar content. As all of these wastes are wet in nature, it is also not economically favorable to use them as fuel directly. This study investigated the alternative uses of these biomasses shown in Table 2.

Table 2: A list of biomasses, their treatment conditions and purposes.

Biomass	HTC condition		Pyrolysis condition		Purposes
	Temp (°C)	Time (min)	Temp (°C)	Time (min)	
Cellulose	180–420	30	400–600	60	Investigated the effect of HTC and pyrolysis treatment on oxygen functional groups and the application of pyrolyzed char as an electron storage material.
Wood	180–260	30	400–600	60	Investigated the effect of HTC and pyrolysis treatment on oxygen functional groups and the application of pyrolyzed char as an electron storage material.
PMS	180–260	30	NA	NA	Investigated the fuel properties of hydrochar.
Winery waste	180–250	60	NA	NA	Investigated the usefulness of hydrochar as an adsorbent.
Citrus waste	180–250	60	NA	NA	Investigated the usefulness of hydrochar as an adsorbent.

* NA = Not applicable

Microcrystalline cellulose (extra pure, avg. particle size 90 μm) was purchased from Acros Organic (Fair Lawn, NJ). Meanwhile, debarked hardwood (*Prunus avium*) was harvested from Ohio University Ridges Land Lab (Athens, OH). Wood was chopped with a power saw to make the particle size less than 5 mm. The initial moisture contents of cellulose and wood were measured as $3.9 \pm 0.1 \%$ and $4.9 \pm 1.4 \%$, respectively.

Six different PMS were obtained from an industrial partner's different pulp and paper mill plants found throughout the USA specifically for this study. Table 3 displays the sample names and how they are referenced throughout the manuscript. Samples PS, DPS, PSS₁, PSS₂, and PFR are all from different plants; PTS was obtained from the

same plant as PFR samples. Meanwhile, Clarion #5a (bituminous coal) was used for co-combustion studies. All samples were dried in an oven at 105 °C for 24 h and sealed in Ziploc bags until further use. The nomenclature of the samples and their moisture contents (MC) are shown below in Table 3.

Table 3: Sample nomenclature used throughout the dissertation and their respective moisture contents.

Sludge Sample	ID	MC (%)
Primary Sludge	PS	60.1 ± 1.5
De-inked Paper Sludge	DPS	63.5 ± 0.5
Primary and Secondary Sludge 1	PSS ₁	64.1 ± 1.0
Primary and Secondary Sludge 2	PSS ₂	76.5 ± 1.0
Primary Sludge and Fiber Rejects	PFR	57.1 ± 1.2
Pre-thickened Sludge	PTS	98.7 ± 0.1

The wet citrus waste (orange peel) was provided by the Misitano and Stracuzzi citrus juices and essential oils factory located in Messina province, Sicily, Italy, while the winery waste (grape skin) was collected from a wine-production plant at Trentino, Italy. The freshly collected citrus waste (CW) and winery waste (WW) wastes were wet and content 78 and 70 wt. % moisture, respectively. These wet feedstocks were dried overnight in an oven at 105 °C, milled, sieved to particle size lower than 800 µm, stored in plastic bags, and put into a desiccator until use.

In order to perform various analyses, different types of salts, acids, and bases were purchased from various suppliers. For instance, 0.01 N hydrochloric acid (HCl) and

0.01 N sodium hydroxide (NaOH) solutions were purchased from Fisher Scientific, while 0.1 M sodium bicarbonate (NaHCO₃) and 0.1 M sodium carbonate (Na₂CO₃) solutions were purchased from Sigma Aldrich. In addition, 99 wt.% potassium nitrate (KNO₃) salt was purchased from Alfa Aesar.

A cationic dye, 1 % (w/v) methylene blue (MB) was purchased from Fisher Scientific to be used in this adsorption study. The dye was diluted as per requirement by using deionized (DI) water. For electron storage capacity (ESC) measurements, titanium (III) chloride (20 % w/v, in 2 N HCl) and sodium citrate (99 %) were acquired from Acros Organics (Morris Plains, NJ) and used as received. Each pyrolyzed hydrochar sample was individually ground and sieved, and the < 100 μm fraction was collected and dried at 65 °C for 24 h. Dried samples were weighed immediately before use, and all reported ESC values are based on the dry weight.

2.2 Methods

2.2.1 Hydrothermal carbonization (HTC)

All HTC experiments were performed in 100, 600, and 2000 mL Parr reactors (Moline, IL). The reaction temperature was controlled with a Parr proportional-integral-derivative (PID) controller (Model 4843) with an accuracy of ± 3 °C. The auto-generated pressure (mainly the vapor pressure of water) of the reactor was

monitored during the experiment. All experiments consisted of 1:9 feedstock to deionized water (DI). The reactor content was stirred at 175 ± 2 rpm from the initial heating up of the reactor until it cooled down to ensure product homogeneity. HTC experiments were performed at various temperatures between 180-420 °C. The reactor was heated at an average heating rate of 10 °C/min to the desired temperature and held isothermally for 30 min at that temperature. At the end of the HTC reaction time, the heater was turned off, and the reactor was cooled down rapidly to room temperature (~30 °C) by placing it in an ice-water bath. The gaseous products produced during the reaction were vented in a fume hood. The slurry was filtered by using a vacuum filtration unit with a Whatman filter paper, Grade 41 (20 µm), to separate the hydrochar from the HTC process liquid. Around 50 mL of process liquid was refrigerated in a Fisherbrand centrifuge tube for the forthcoming examination. The wet hydrochar was dried at 105 °C in an oven for 24-48 hr. Dried hydrochar was kept in a centrifuge tube (Fisherbrand®) and stored in a desiccator for further analyses. Each HTC experiment was replicated twice to ensure its reproducibility.

2.2.2 Pyrolysis

Hydrochars produced from cellulose and wood were pyrolyzed in a GCF Series Controlled Atmosphere Muffle Furnace (Livingston, NJ). The hydrochars were pyrolyzed at three different temperatures: 400, 500, and 600 °C. The pyrolysis was

conducted in two stages. In the first stage, the furnace was heated from ambient temperature to 100 °C at 10 °C min⁻¹ and kept it constant for 1 minute to stabilize the temperature and to remove moisture from the hydrochar. In the final stage, the furnace was heated from 100 °C to the set pyrolysis temperature at a rate of 20 °C/min, which was followed by an isothermal period of 60 min at the same temperature. Afterward, the furnace was cooled to 200 °C at a rate of 20 °C/min by a built-in forced draft fan and then cooled to room temperature by natural cooling. An inert gas (N₂) was passed through the furnace at 1.0 ml/min during the entire experiment to avoid any unwanted combustion or gasification. Pyrolyzed hydrochars were kept in a centrifuge tube (Fisherbrand[®]) and stored in a desiccator for further analyses. Each pyrolysis experiment was replicated twice to ensure its reproducibility.

2.2.3 Characterization

2.2.3.1 Moisture content, mass, and energy yields

Moisture content (MC) of a feedstock was measured by drying the feedstock in an oven (Quincy Lab, Inc., Chicago, IL) for 24 hours at 105 °C. MC was calculated via equation (4). The mass yield (MY) was calculated using equation (5), and it shows how much of the initial feedstock was converted into hydrochar. Higher heating

value (HHV) was also determined for hydrochars using a Parr 6200 adiabatic oxygen-bomb calorimeter (Moline, IL) calibrated with benzoic acid. Dry ash-free HHV (HHV_{daf}) was calculated via equation (6). Energy densification (ED) was calculated via equation (7) to evaluate how HHV changes from the untreated feedstock to hydrochar.

$$MC (\%) = \frac{\text{Mass of wet feedstock} - \text{Mass of dry feedstock}}{\text{Mass of wet feedstock}} \times 100\% \quad (4)$$

$$MY (\%) = \frac{\text{Mass of dry hydrochar}}{\text{Mass of untreated dry feedstock}} \times 100\% \quad (5)$$

$$HHV_{daf} = \frac{\text{HHV of the sample}}{1 - \text{Fraction of dry ash into the sample}} \quad (6)$$

$$ED = \frac{\text{HHV of dry hydrochar}}{\text{HHV of untreated dry feedstock}} \quad (7)$$

2.2.3.2 pH of hydrochar

The acidity and basicity of the hydrochar surface were measured using a pH probe (Fisher Scientific, AE 150). The hydrochar was washed with DI water until the pH of the washed water became constant. This step was required to remove most foreign materials (process liquid in this study) adhered on the hydrochar surface. The washed hydrochar was dried and stored in a desiccator until the pH measurement. To measure pH, a known amount of washed and dried hydrochar (~ 1.5 g) was added into a 30

mL of DI water. The solution was shaken for 24 h at 200 rpm and was filtered using Whatman filter paper, Grade 41 (20 μm). Then, pH of the liquid was measured using the above-mentioned pH probe, which is expressed as hydrochar's pH throughout this study. It should be noted that the pH is an equilibrium parameter, which in this study depends on the DI water added to the hydrochar.

2.2.3.3 pH at point of zero charge (pH_{PZC})

There are several techniques to measure the pH at the point of zero charge (pH_{PZC}) on solid surface e.g., mass titration, potentiometric titration, immersion technique, and pH drift method [86]. In this study, two measurement techniques (immersion technique and pH drift method) were used for selective samples to examine the differences in results. However, no significant differences were found in the measurement. As a result, only the pH drift methodology was followed for the rest of the sample measurements. This method was chosen because of the simplicity between the two methods. In this method, 30 mL of 0.03 M KNO_3 solution was poured into six different volumetric flasks, and pH of those solutions were adjusted to pH 2, 4, 6, 8, 10, and 12 by adding HCl and NaOH, where necessary. Around 1.5 g of washed hydrochar sample was added to each of the volumetric flasks, and all the flasks were agitated for 24 h at 250 rpm on an automatic shaker. Afterward, the liquids were filtered and the final pH's of the solution were measured. A plot was

drawn by using the initial pH placed in the x-axis and final pH placed on the y-axis. A tie line was drawn in the same axis, where the final pH was considered equal to the initial pH. The intersecting point between those two lines, shown in Figure 5 was recognized as pH_{PZC} .

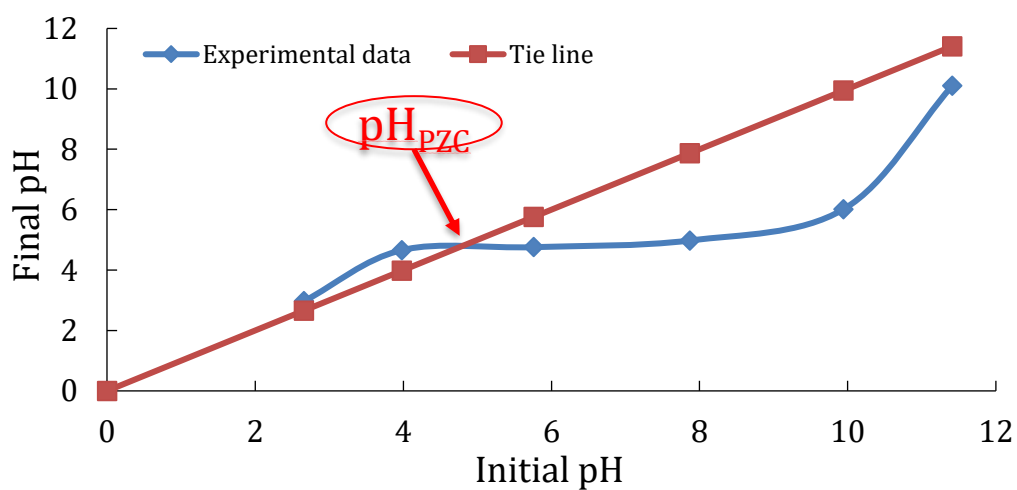


Figure 5: pH_{PZC} determination technique using pH drift method.

2.2.3.4 Elemental analysis

Elemental analysis of the hydrochars, as well as the raw cellulose, were carried out in a Flash 2000 Organic Elemental Analyzer (Waltham, MA) to determine elemental carbon, hydrogen, nitrogen, and sulfur content. For the analysis, BBOT (Cystine sulphanilamide methionine) was used as a calibration standard and V_2O_5 (vanadium

oxide) as a conditioner for the samples, which were combusted around 950 °C in ultra-high purity oxygen with a helium carrier gas and passed over copper oxide pellets and then electrolytic copper. The gases were then analyzed by a thermal conductivity detector (TCD), with the peak areas of detection being compared to that of BBOT standards. The calibration was such that blank samples had an area of nitrogen less than 1 % of actual samples, this area was caused by impurities in the oxygen feed and small amounts of gas entering with the sample. All samples were dried before combustion, so all hydrogen is likely from the sample itself and not from any residual water. Oxygen content was calculated separately by the difference method.

2.2.3.5 Inorganic analysis

A Thermo iCAP 6000 inductively coupled plasma (ICP) (Waltham, MA) was used to identify the presence of inorganic ions (Al, Cr, Cu, Cr, Mn, Ni, Zn) in the hydrochars. The lower detection limits for ICP-OES were 0.005 ppm for Ca, Fe, Mg, and S, up to 0.05 ppm for Na; up to 0.02 ppm for Al and Si, and 0.1 ppm for K.

2.2.3.6 Proximate analysis

A thermogravimetric analyzer (TGA) Q500 (TA instruments, DE) was used for proximate analysis of the raw feedstock and resulting hydrochars to determine the

percentage of volatile matters (VM), fixed carbon (FC), and ash content. All the samples were heated upto 900 °C at a heating rate of 20 °C/min. An inert atmosphere was maintained to avoid an unexpected burning of the material by following nitrogen (N₂) at 50 mL/min. The temperature was held at 900 °C for 5 minutes, and then the air was introduced to combust the remaining sample. The mass loss under N₂ atmosphere at 900 °C was considered as VM. Mass remaining at the end of the combustion process was considered as ash. FC was determined by subtracting the VM and ash from 100%.

2.2.3.7 Lignin analysis

Lignin analysis was performed by the standard TAPPI method [87]. A modified method of Sequeira and Law [88] was used to quantify the sugar content. In this method, DI-water at 50 °C was used for making and blending a 5% solid slurry for one minute; three extractions were performed. Solid was filtered in a pressurized air filter (OFI Testing Equipment, model 140-31) by using Whatman no. 4 filter paper. The filtration process was operated just above atmospheric pressure to ensure liquor was extracted from the sludges or hydrochars. Final extraction was conducted in an autoclave (L30 cycle) to make sure no free sugar remained in the solid. HPLC (Agilent 1200 series) was used to analyze the sugar and sugar alcohols. HPLC was equipped with a binary pump, an HPX-87P (Bio-Rad) column, and an refractive

index (RI) detector. Water was used as a mobile phase with a flow rate of 0.5 mL/min. The column was heated to 85 °C for enhancing the separation and the RI detector was used at 55 °C. An external calibration was used to quantify the contents (lactose, glucose, xylose, galactose, arabinose, mannose, and fructose).

2.2.3.8 Surface area analysis

The Brunauer, Emmett, and Teller (BET) surface area of the hydrochars was measured using a surface area analyzer (Micromeritics ASAP 2020, Norcross, GA). A five points measurement technique was used, where the BET surface area was calculated from a linear isotherm plot up to the relative pressure (P/P_0) of 0.3. Liquid nitrogen was used to maintain a constant temperature throughout the experiment. Ultrapure N₂ gas was used as an adsorption medium in this analysis

2.2.3.9 Scanning electron microscope (SEM)

The surface morphology of all samples was examined with a scanning electron microscope (SEM) (JSM-6390, JEOL, Peabody, MA). The samples were sputtered with palladium (Pd) of 50-150 nm coating thickness to increase conductivity. To avoid charging effects, relatively even surfaces were chosen for investigation. The applied voltage for the SEM was 15 kV, the working distance was 15 mm, and the spot size was 40-50 mm. The highest magnification reached up to 5,000 times and

the smallest focal length was 5 μm . The SEM images were then processed with Image J software to determine the particle size distribution of each sample.

2.2.3.10 X-ray diffraction (XRD)

The crystal structure was explored with the help of the Rigaku X-ray diffraction (XRD) analyzer (Woodlands, TX). The operating voltage and electric current of the X-ray emitter were 40 kV and 40 mA, respectively. Additionally, the scan conditions were adjusted from 5° to 85° in 2θ range with a step interval of 0.0167° and counter-time of 2 s/step. The percentage of crystallinity was calculated from the XRD spectra where the area under the crystalline peaks of specific spectra was divided by the total area under that spectra.

2.2.3.11 Boehm titration

A standard titration procedure known as Boehm's method was carried out to quantify the oxygen containing functional groups on the surface of hydrochars [89]. According to the method, a back titration was conducted to quantify the oxygen-containing acidic functional groups (OCAFG), where a forward titration was conducted for basic functional groups (BFG) measurement. A detailed methodology is shown in Figure 6A.

As per the back-titration method, a known amount of washed hydrochar (~ 0.25 g) was added into a 30 mL of each of the three bases i.e., NaOH, NaHCO₃, and Na₂CO₃. The samples were agitated on a shaker for 24 h at 250 rpm. The solution was then filtered using a Whatman filter paper, TE 37 (1.0 μm) to remove the hydrochar from the solution. Exactly 10 mL of filtered sample was taken by pipette and this sample was acidified by the addition of 30 mL of HCl solution to ensure complete neutralization of the base. The acidified solution was then titrated with the titrator base (0.01 N NaOH). All the titrations were performed using an automatic titrator (Mettler Toledo, T50). A blank titration (without hydrochar sample) was performed every time prior to the titration with a sample. The volume of the titrator base required at endpoint was noted from the titration graph (pH vs base volume). The targeted end-point pH was 7.0 in this study. The extra volume of titrator base required to obtain the endpoint for the titration with the sample (see Figure 6B) was considered to be responsible for the functional groups. This volume was taken into account to calculate the functional groups. It was assumed that NaOH reacted with all acidic functional groups (carboxylic (C), lactonic (L), and phenolic and other acidic groups (PO)) on the surface, Na₂CO₃ reacted with C and L groups, and NaHCO₃ reacted only with the C group. Hence, the total and individual groups can be calculated by using equations (8)-(12).

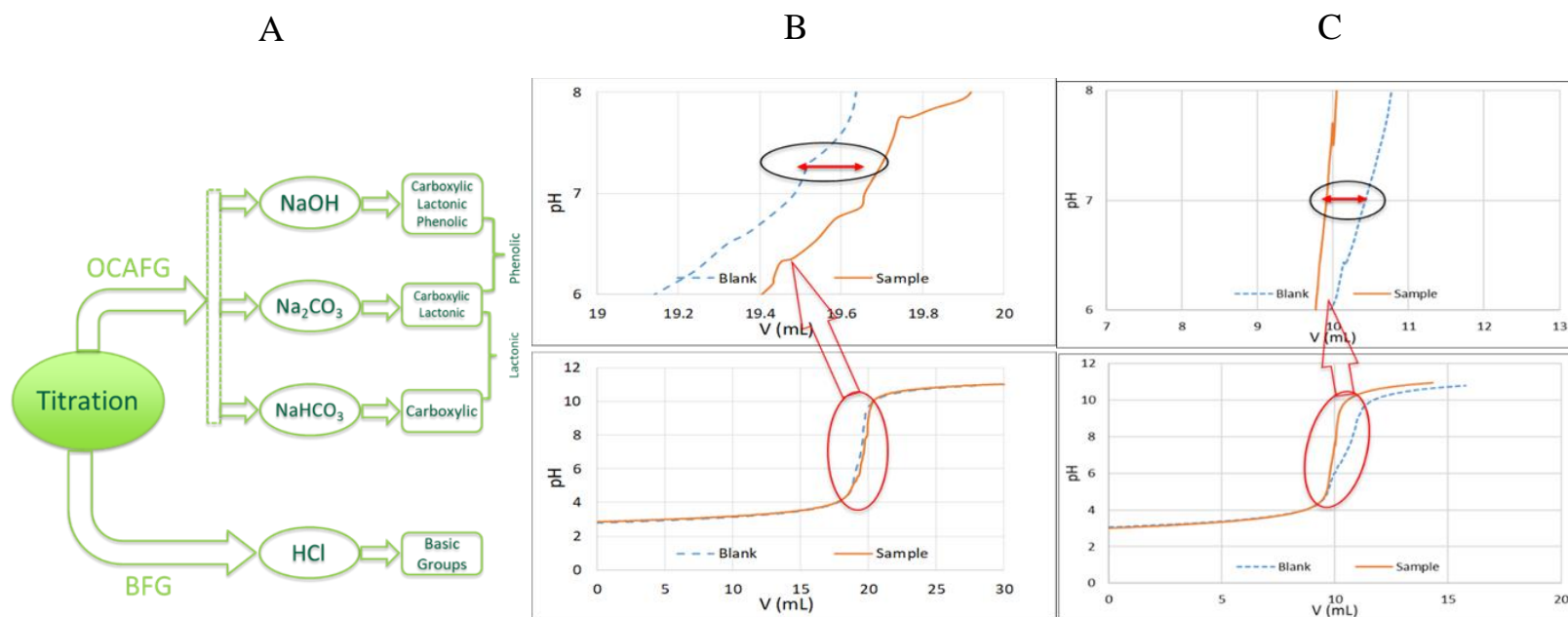


Figure 6: A) An overview of the Boehm titration method to determine different functional groups, B) Boehm titration of a blank sample and hydrochar sample during OCAFGs measurement, C) Boehm titration of a blank sample and hydrochar sample during BFGs measurement.

$$C+L+PO = \frac{V_{B(NaOH),S} - V_{B(NaOH),E}}{M_S} \times C_{B(NaOH)} \times 10^3 \quad (8)$$

$$C+L = \frac{V_{B(Na_2CO_3),S} - V_{B(Na_2CO_3),E}}{M_S} \times C_{B(Na_2CO_3)} \times 10^3 \quad (9)$$

$$C = \frac{V_{B(NaHCO_3),S} - V_{B(NaHCO_3),E}}{M_S} \times C_{B(NaHCO_3)} \times 10^3 \quad (10)$$

$$L = (C+L) - C \quad (11)$$

$$PO = (C+L+PO) - (C+L) \quad (12)$$

where C, L, and PO stand for carboxylic, lactonic, and phenolic and other acidic groups in $\mu\text{mol/g}$, respectively. Meanwhile, $V_{B,S}$ and $V_{B,E}$ stand for volumes of base (in mL) required to reach at the endpoint of the titration with and without a sample, respectively. C_B and M_s are the molar concentration of base and the mass of char samples, respectively.

For the BFGs measurement, a known amount of sample (~ 0.25 g) was added into 40 mL of HCl in a 125 mL Erlenmeyer flask. The flask was kept on an orbital shaker for 24 h at 250 rpm for continuous agitation. The solution was then filtrated using a 5- μm PTFE membrane filter paper to remove the solid sample from the solution. Exactly 10 mL of filtrated solution was taken by pipette and diluted with an additional 30 mL of DI water. The diluted solution was then titrated with the titrator base (0.01 N NaOH). All the titrations were performed using the same titrator mentioned above. A blank titration (without sample) was also performed every time prior to the titration with the sample. The volume of the titrator base required to reach

the endpoint (pH 7.0) was noted from the titration graph (see Figure 6C). The less amount of titrator base required for the sample is considered to be responsible for the BFGs. The total and individual groups can be calculated by using equation (13).

$$BFG = \frac{V_{TB,E} - V_{TB,S}}{M_S} \times C_{TB} \times 10^3 \quad (13)$$

where BFG stands for basic functional group in $\mu\text{mol/g}$. Meanwhile, $V_{TB,S}$ and $V_{TB,E}$ stand for volumes of titrator base (both in mL) required to reach at the endpoint of the titration with and without the sample, respectively. C_{TB} and M_S are the normal concentration of titrator base (N) and the mass of char sample (g), respectively.

2.2.3.12 Attenuated total reflector-fourier transform infrared spectroscopy (ATR-FTIR)

The primary organic compounds on the surface of the hydrochar samples were identified using Perkin Elmer attenuated total reflector-fourier transform infrared spectroscopy (ATR-FTIR Model: 65 FTIR Spectrometer, Waltham, MA). ATR operating conditions were set at a scan rate of 256 s^{-1} , data wavenumber range of $500\text{-}4000 \text{ cm}^{-1}$, and accumulations of 64. Transmittance was plotted on the y-axis with wavenumber on the x-axis to evaluate the stretching and/or bending of the chemical bonds' on the hydrochar surface. To understand the dominant of each bond in each sample, individual areas above the spectra were calculated. The individual areas were divided by the total area above that spectra to determine the relative

transmittance area percentage (RTAP). A bond's RTAP should not be interpreted as the bond's abundance in a sample; rather it should be used to compare the same bond in another sample, with respect to feedstock.

All the above mentioned characterizations were replicated at least twice to ensure their reproducibility. In addition, the equal variance analysis was conducted to determine the P-value and found that all data are statistically significant within the 95 % confidence level.

2.2.4 Applications

2.2.4.1 Combustion characteristic

To determine the fuel properties of hydrochar, an oxidative reactivity was performed which was similar to the proximate analysis method described earlier using the same equipment. Similar heating rates, gas flows, and temperature increments were used, but the air was the only gas used during the entire run. Combustion thermograms and derivative of the mass relative to temperature (DTG) curves were plotted as shown in the literature [90]; calculation of ignition (equation (14)) and burnout (equation (15)) indices are presented below [91]:

$$D_i = \frac{|DTG_{max}|}{t_p t_i} \quad (14)$$

$$D_B = \frac{|DTG_{max}|}{\Delta t_{1/2} t_p t_B} \quad (15)$$

where, DTG_{max} is the maximum rate of combustion, in magnitude, found in the combustion DTG curves; t_p is the time where DTG_{max} occurs; t_i and t_B are the time at which the ignition temperatures and burnout temperatures are obtained, respectively; and $\Delta t_{1/2}$ is the time when the combustion DTG value is one-half of the DTG_{max} . Lower values of D_i and D_B indicate an ideal ignition and burnout (i.e. overall combustion) behavior.

2.2.4.2 Adsorption study

Adsorption tests were performed in a set of 15 ml vials, where approximately 25 mg of dry hydrochar samples were placed. An equal volume of 10 ml of MB dye solutions with initial concentrations of 10–500 mg/L were added into the vials. All the vials were placed in a tube revolver and shaken at 40 rpm and 20 °C for 24 h to reach equilibrium. Similar procedures were followed for the other two sets of vials containing the same initial dye concentrations and the same amount of hydrochars but kept at different temperatures: 4 and 36 °C. All samples were filtered prior to analysis, in order to minimize interference of the fine particles with the analysis. The concentrations of MB in the supernatant solutions were determined using a Hach-6000 UV-vis spectrometer (Loveland, CO) at 665 nm. The amount of adsorption at equilibrium, q_e (mg/g), was calculated by:

$$q_e = \frac{(C_0 - C_e)V}{W} \quad (16)$$

where C_0 and C_e (mg/L) are the liquid-phase concentrations of dye at initial and equilibrium conditions, respectively. V is the volume of the dye solution and W is the mass of dry adsorbent used (g).

The adsorption isotherm of this study was fitted on Langmuir and Freundlich isotherm models. The applicability of the isotherm models to the adsorption experimental data was evaluated considering their correlation R^2 values. The linear forms of the Langmuir's and Freundlich's isotherm models are as follows:

$$\frac{C_e}{q_e} = \frac{1}{Q_{max}K_L} + \frac{C_e}{Q_{max}} \quad (17)$$

$$\ln q_e = \ln K_F + \frac{1}{n_F} \ln C_e \quad (18)$$

where C_e (mg/L) and q_e (mg/g) indicate the equilibrium concentrations of MB and the amount of MB adsorbed, respectively. Q_{max} (mg/g) is the maximum adsorption capacity and K_L is the Langmuir isotherm coefficient. K_F and n_F are the Freundlich adsorption constants. The separation factor (R_L) of the Langmuir model, which is a dimensionless parameter, can be calculated as follows:

$$R_L = \frac{1}{1 + C_0 K_L} \quad (19)$$

where C_0 (mg/L) is the initial concentration of the MB solution. The factor indicates the following characterizations by changing the R_L value:

$$R_L = \begin{cases} \text{reversible} & \text{if } R_L = 0 \\ \text{favorable} & \text{if } 0 < R_L < 1 \\ \text{linear} & \text{if } R_L = 1 \\ \text{unfavorable} & \text{if } R_L > 1 \end{cases} \quad (20)$$

The thermodynamic properties, such as Gibbs energy (ΔG), enthalpy (ΔH), and entropy (ΔS) for the adsorption process were obtained from the experiments carried out at different temperatures using the following equations:

$$\ln K_c = \frac{\Delta S}{R} - \frac{\Delta H}{RT} \quad (21)$$

$$\Delta G = \Delta H - T\Delta S \quad (22)$$

where, R (8.314 J/mol K) is the universal gas constant, T (K) is the absolute temperature, K_c is equilibrium constant which must be dimensionless. The K_c can be easily derived by multiplying the Langmuir constant (K_L) by the molecular weight of MB (319.85 g/mol), 1000, and the number of moles of pure water (55.5) per liter [92, 93]. Equation (21) is known as van't Hoff equation, where the values of ΔH and ΔS were determined from the slope and the intercept of the linear plot of $\log(K_c)$ vs. $1/T$. These values were used to calculate ΔG .

The effect of solution pH on dye adsorption capacity was measured by mixing 10 ml of 300 mg/l with approximately 25 mg of hydrochar sample at various pH of 2–12. The pH of the solutions was maintain using 0.01 N HCl and 0.01 N NaOH solutions. The equilibrium adsorption capacity, q_e (mg/g), was calculated by using equation (16).

2.2.4.3 Electron storage capacity (ESC)

The reversible ESCs of pyrolyzed hydrochars were determined using a chemical method recently developed based on Soil Reef Biochar (SRB) [77, 78]. In this study, dissolved O₂ (DO, +0.80 V vs. standard hydrogen electrode (SHE) at pH 7, P_{O₂} = 0.21 atm) and Ti(III) citrate (-0.36 ± 0.01 V vs. SHE at pH 6.4) were used as the oxidant and reductant, respectively, to obtain the ESC of pyrolyzed hydrochars for three consecutive redox cycles. All ESC measurements were conducted in duplicates in an anaerobic glove box ($2.0 \pm 0.5\%$ H₂ in N₂, P_{O₂} < 25 ppm, Coy, MI), except when samples were being oxidized by DO. Samples of SRB from the same batch used for method development, as well as blank without char, were included in all measurements for quality control [77, 78]. The ESCs of SRB measured between +0.80 V and -0.36 V were 3.69 ± 0.03 mmol/g for the first cycle and 3.35 ± 0.05 mmol/g for the subsequent cycle, consistent with the results of the previous work and confirming the reproducibility of the method [77].

Prior to reduction with Ti(III) citrate, any stored electron in each sample was first drained completely through DO oxidation for 72 h. The DO-oxidized samples were then transferred to an anaerobic glove box, deoxygenated, and reduced by 30 mM Ti(III) citrate solution (pH 6.4 ± 0.2). After reduction for 72 h, a 2-mL aliquot was collected, 3-fold diluted, and passed through a 0.22- μ m PVDF syringe filter for

Ti(III) analysis. Using the Beer-Lambert law shown in equation (23), Ti(III) citrate was quantified by absorbance using a Vernier LabQuest 2 UV-vis spectrophotometer (Vernier, OR). The ESC of pyrolyzed hydrochar was calculated based on electron balance using equation (24).

$$A_i = \varepsilon b C_i \quad (23)$$

$$e^- \text{ transferred (mmol/g)} = (C_i - C_n) \times V_i / M \quad (24)$$

where A_i and C_i are the absorbances at 400 nm and the concentration of Ti(III) citrate solution, respectively, ε is the extinction coefficient of Ti(III) citrate ($91.5 \pm 3.3 \text{ M}^{-1} \text{cm}^{-1}$ at 400 nm), b is the path length (1 cm), C_i and V_i are the initial concentration and volume of Ti(III), respectively, C_n is the final Ti(III) concentration at redox equilibrium, and M is the sample mass (dry weight).

To evaluate the ESC reversibility of each sample, DO oxidation and Ti(III) reduction were repeated for two additional cycles, using the same procedures as described above. After each redox cycle, the char sample was collected on a glass microfiber filter, rinsed thoroughly with deionized water, and dried fully for the next cycle. Further information about the ESC analysis method for black carbons is detailed in Xin *et al.* [77, 78].

3 Results, discussions, and applications

3.1 Properties of hydrochars from a model compound

Hydrothermal treatment (HTT) of biomass is one such method that has been used to produce fuel, fertilizers, platform chemicals, adsorbents, and countless other products. This treatment is usually conducted between 180–420 °C depending on the product requirement. HTC is a mild HTT treatment where biomasses are treated at 180–260 °C. increasing HTT temperature to near critical conditions (260–374 °C), is commonly referred as HTL, while HTT above critical point of water (374 °C, commonly up to 420 °C) is known as SCWG. Regardless of the treatment temperature, hydrochar is either a desired or an undesired product from the hydrothermal treatment process. To understand the hydrochar formation and their properties, such as surface functionality, morphology, and elemental composition, an extensive study was conducted where a model compound (microcrystalline cellulose) was hydrothermally treated at 180–420 °C. The properties of hydrochars were examined by using Boehm titration, FTIR, XRD, and SEM analyses. The findings are discussed in the following sections.

3.1.1 Mass yield, ultimate and proximate analyses

The fraction of initial solid mass remaining after the hydrothermal treatment is referred to as the mass yield (MY). The obtained results of MY shown in Figure 7 were like the results reported in the literature [80, 94].

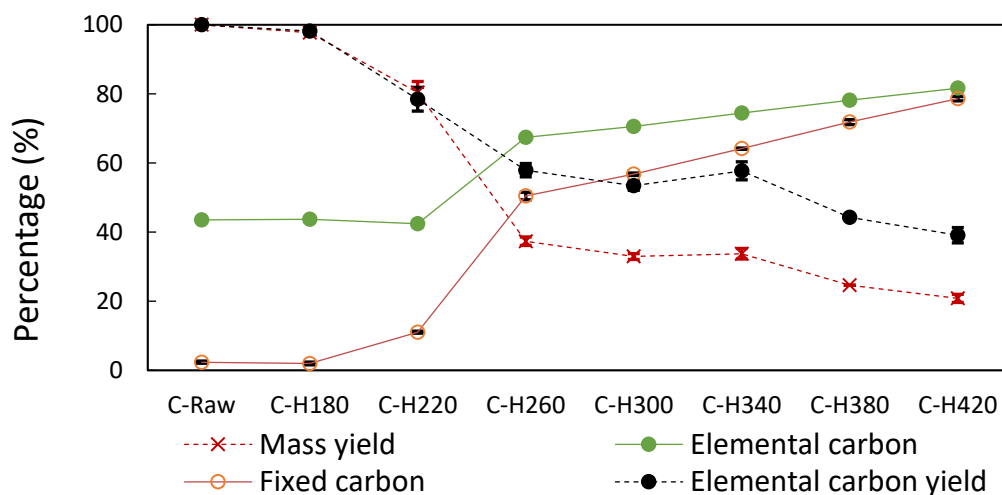


Figure 7: Change of mass yield (MY), fixed carbon, elemental carbon, and elemental carbon yield of the hydrochar produced from cellulose at subcritical and supercritical temperatures [95].

The MY of the hydrochars decreases with the increase of HTT temperatures. However, the decrease of MY in subcritical and supercritical regions occurred due to different reasons. At the subcritical region (180–374 °C), liquid water has high concentrations of ionic products, which means the local concentrations of hydronium and hydroxide ions are far higher than at room temperature [96], leading to acid/base

catalyzed reactions that can be broadly defined as decarboxylation, hydrolysis/ dehydration, and polymerization/condensation of carbon fragments [96-98]. As decarboxylation and hydrolysis/ dehydration of the biomass occurs, fragments are broken off into the liquid phase. Part of the fragments condenses and repolymerize to add additional layers to the hydrochar product [99, 100]. However, the rate of hydrolysis might be larger than the rate of polymerization; as a result, the continuous decrease of the MY of the hydrochars resulted in the HTT temperatures. As the HTT temperature was increased from the subcritical to the supercritical region, the effect of dehydration occurred again, as shown in Figure 8. These net effects of dehydration, decarboxylation, and then further dehydration occur in addition to the overall mass loss. The movement of the elemental composition, along with the overall MY shown in Figure 7, shows the dominant reactions that occur throughout the process. The reaction routes in the diagram were drawn by using the stoichiometric ratio of carbon, oxygen, and hydrogen. Though there is little change in the MY between 260 and 340 °C, the elemental composition changes significantly as oxygen is stripped away from the hydrochar through decarboxylation. Minimal change in the MY paired with significant change in elemental composition suggests that the condensation reactions must be occurring. These condensation reactions helped to return the species (which were removed during the heating process) from the liquid phase to the surface of the hydrochar. As the elemental carbon and oxygen change differently compare to MY

with respect to HTT temperature, it is necessary to see how the surface oxygen functionality and morphology have changed. Figure 7 shows that fixed carbon increases with the temperature, which leads to an overall carbonizing effect.

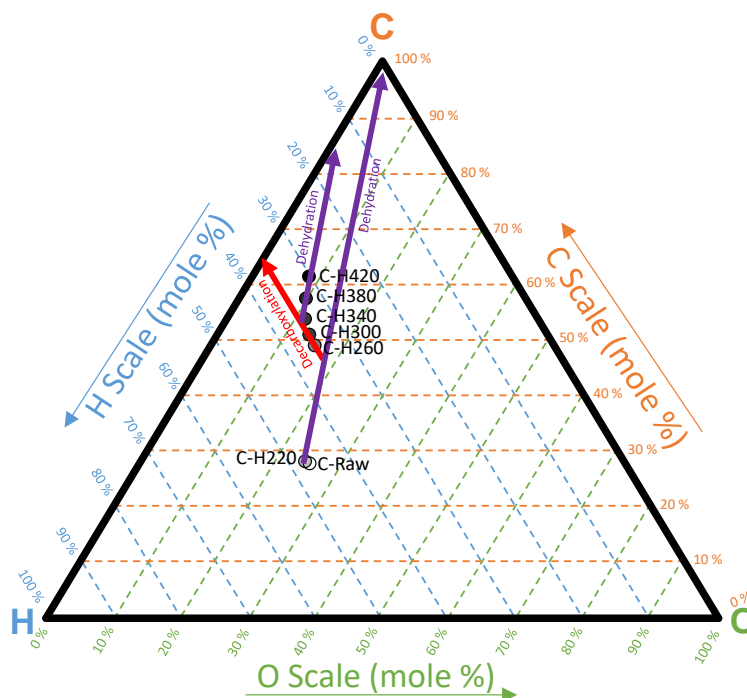


Figure 8: The molar ratio of carbon, hydrogen, and oxygen of cellulose and its hydrochars produced at subcritical and supercritical temperatures [95].

At higher HTT temperatures, more volatile carbons are stripped from the hydrochar surface into the liquid phase. At 420 °C, nearly 80 % of the carbon is in a fixed form (see Table 4), but the overall carbon yield is only 40 %, meaning that 60 % of the initial carbon moved to the liquid phase as non-condensable species. There was no

direct correlation between the fixed carbon and crystallinity observed in this study as fixed carbon increased with the treatment temperature; on the other hand, hydrochar moved from crystalline to amorphous and back to the crystalline structure, telling us that the orientation of the fixed carbon is more important than the percent present in the hydrochar.

Table 4: Ultimate and proximate analyses of cellulose and its hydrochars produced at subcritical and supercritical temperatures.

Sample ID	C (%)	H (%)	N (%)	S (%)	O (%)	VM (%)	FC (%)	Polarity index
C-Raw	43.5 ± 0.1	6.1 ± 0.1	BD	BD	50.4 ± 0.2	97.6 ± 0.7	2.4 ± 0.3	1.2 ± 0.0
C-H180	43.7 ± 0.4	6.1 ± 0.2	BD	BD	50.3 ± 0.6	98.0 ± 0.8	2.0 ± 0.4	1.2 ± 0.0
C-H220	42.4 ± 0.8	6.0 ± 0.1	BD	BD	51.6 ± 1.0	88.9 ± 0.4	11.1 ± 0.3	1.2 ± 0.1
C-H260	67.4 ± 0.3	4.1 ± 0.0	BD	BD	28.5 ± 0.4	49.6 ± 0.8	50.4 ± 1.1	0.4 ± 0.0
C-H300	70.6 ± 0.1	4.1 ± 0.0	BD	BD	25.3 ± 0.1	43.2 ± 0.5	56.8 ± 0.4	0.4 ± 0.0
C-H340	74.4 ± 0.2	4.0 ± 0.0	BD	BD	21.6 ± 0.2	35.9 ± 0.9	64.1 ± 0.2	0.3 ± 0.0
C-H380	78.2 ± 0.5	3.7 ± 0.0	BD	BD	18.1 ± 0.5	28.2 ± 0.3	71.8 ± 0.7	0.2 ± 0.0
C-H420	81.7 ± 0.1	3.4 ± 0.1	BD	BD	15.0 ± 0.0	21.4 ± 0.4	78.6 ± 0.6	0.2 ± 0.0

3.1.2 Surface morphology

The SEM images are shown in Figure 9 (a-e) demonstrate that hydrochars synthesized at different HTT reaction temperatures have variations in their morphology and particle size distribution (PSD). As the morphology of the raw cellulose (rod-shaped particle, size of 70–350 μm) has been well-studied [101, 102] and it remains primarily unchanged up to 220 °C [80, 103], the SEM images of C-Raw and C-H220 are not been shown in Figure 9. A drastic change was observed at

reaction temperature 260 °C, where, a spherical shape with a particle size lower than 1.0 μm appears. Under this condition, the size of the particles was sufficiently uniform as 75 percentile of the particles fell between 0.4-0.6 μm. With the increase of the HTT reaction temperature (260–340 °C), aggregation and cross-linking of the spheres began to occur. As a result, the particle size of the derived hydrochars increased up to 7.0 μm. As Figure 9 shows, the distribution shifted towards the right side of the x-axis, which means the frequency of the larger spheres increased with increasing of the HTT temperature. This is probably because, during the generation of hydrochar, nucleation took place, and once nuclei formed, the nuclei grew outwards and formed larger particles [39, 100]. This outcome suggests that the increase of HTT temperature contributed to the hydrolysis of cellulose and played a decisive role in the formation of the particle size. However, when the HTT temperature was increased to 380 °C, the spheres lost their uniformity. This was the time where the spheres were large enough to burst (bigger particles broke down to smaller particles) as observed at 420 °C. From earlier sections, it is evident that dehydration reaction dominates at the supercritical conditions. This water molecule can form inside the hydrochars and accumulate energy to come out from the hydrochars.

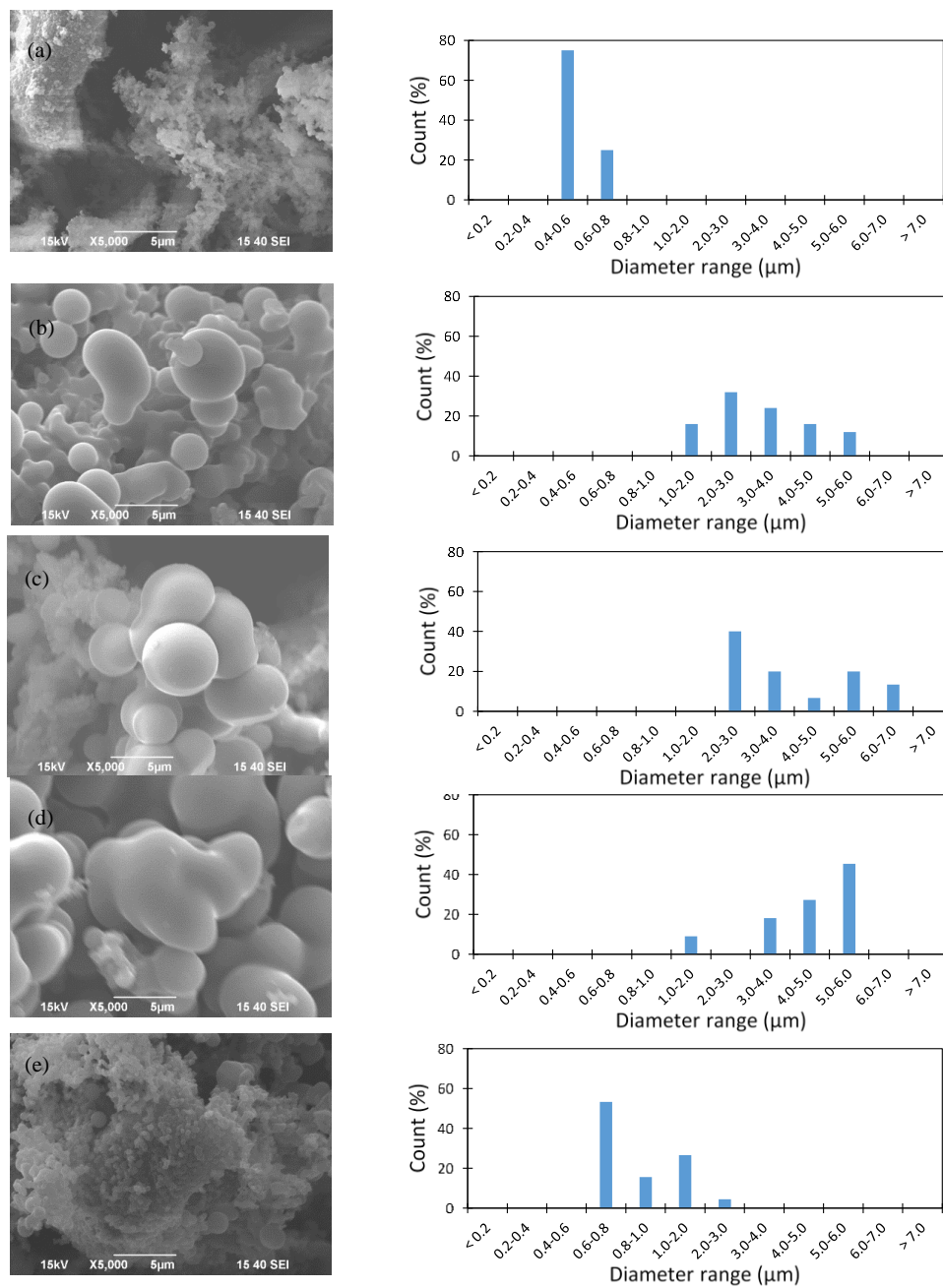


Figure 9: SEM images and particle size distribution (PSD): (a) C-H260, (b) C-H300, (c) C-H340, (d) C-H380, and (e) C-H420.

When the energy exceeded the bursting energy of the hydrochar, it came out from the hydrochar by breaking hydrochar's structure. This could be the reason of the bursting. Due to the bursting, the larger spheres broke down and formed small spheres, which had a similar particle size distribution (PSD, about 70 percentile particles have less than 1.0 μm diameter) as observed in C-H260.

A similar observation was found in the BET analysis shown in Table 5, where the low surface area ($< 1.5 \text{ m}^2/\text{g}$) was measured for the C-Raw and C-H220. However, the surface area increased by approximately eight times at C-H260 due to the formation of the microspheres. As seen in the SEM analysis, the size of the sphere increased during the HTT temperature between 300–380 $^{\circ}\text{C}$; as a result, the BET surface area decreased. As the larger spheres broke down at 420 $^{\circ}\text{C}$ and formed smaller spheres, the surface area also increased to $15.41 \text{ m}^2/\text{g}$, similar to the surface area of C-H260, which had comparable particle size.

Table 5: Pore size distribution, surface area, and relative crystallinity of cellulose and its hydrochars produced at subcritical and supercritical temperatures

Sample ID	Particle size distribution (μm)	Surface area (m^2/g)	Relative crystallinity (%)
C-Raw	> 10.00	1.30 ± 0.05	89.90
C-H220	> 10.00	1.27 ± 0.07	77.68
C-H260	0.40–0.80	10.82 ± 0.18	-
C-H300	1.00–6.00	2.62 ± 0.04	-
C-H340	2.00–7.00	3.69 ± 0.23	-
C-H380	1.00–6.00	4.63 ± 0.57	58.75
C-H420	0.60–3.00	15.41 ± 0.18	49.93

The XRD patterns for cellulose and corresponding hydrochar products obtained at different temperatures are shown in Figure 10. The diffractogram of cellulose exhibited three characteristic peaks of cellulose around $2\theta = 16^\circ$, 22.6° , and 35° , which are considered to represent typical cellulose form. The crystallinity of each sample was also calculated by taking the percentage of the area of the crystalline peak over the total area as shown in Table 5.

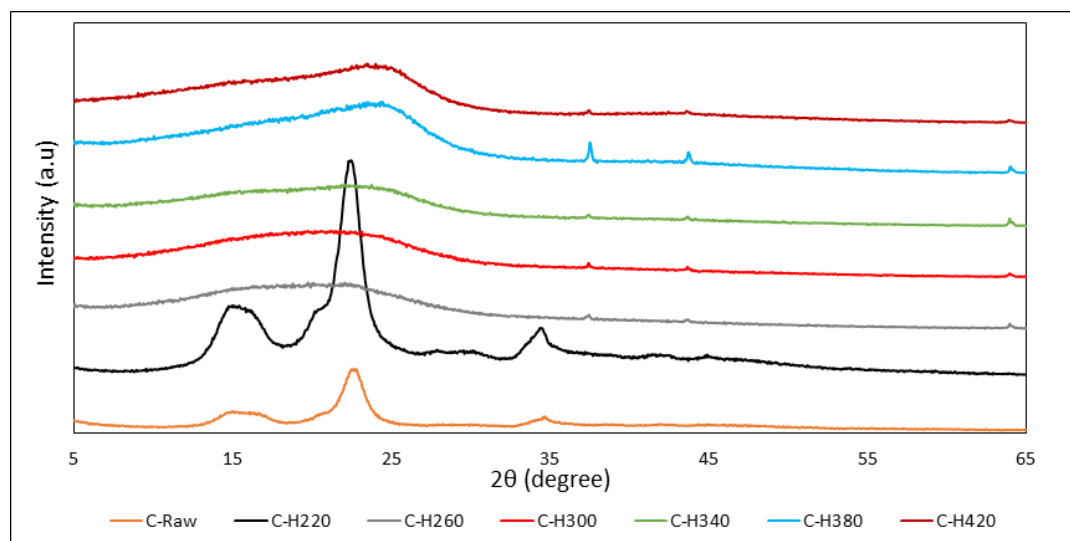


Figure 10: XRD of cellulose and its hydrochars produced at subcritical and supercritical temperatures.

Hydrochar produced from cellulose at a low temperature (220°C) revealed a similar XRD pattern as raw cellulose, indicating the crystalline structure of cellulose in C-

H220 had been preserved. However, a slightly low crystallinity was observed in C-H220 (78 %) compared to C-Raw (90 %), which attributed to the hydrolysis of a portion of cellulose in the amorphous region during HTT [104, 105].

3.1.3 Functional groups

The OCAFGs are categorized into the carboxylic groups, lactonic groups, and phenolic groups, whereas the BFGs consist of alcohol and amine groups. As there was no nitrogen present in any of the samples, it was assumed that no amine groups were present on the cellulose and its hydrochars. Therefore, all BFGs determined in this study were considered as alcoholic groups. The OCAFGs on the produced hydrochar at different temperatures are shown in Figure 11. Although cellulose is a long-chain polymer of glucose monomers, the OCAFG was observed in the C-Raw ($20.5 \pm 0.3 \mu\text{mol/g}$) because of carboxylic groups ($-\text{COOH}$) that are attached to the end of its polymeric chain. OCAFG increases with the increase of the HTT temperature until it reaches a maximum ($1495 \pm 25 \mu\text{mol/g}$) at C-H260. Interestingly, the ultimate analysis showed the elemental oxygen decreased with the increase of the HTT temperature.

It is also shown in Figure 8 that the molar ratio of carbon and oxygen did not change between C-Raw and C-H220. However, it changed significantly between C-H220 and C-H260, where both dehydration and decarboxylation reactions dominated.

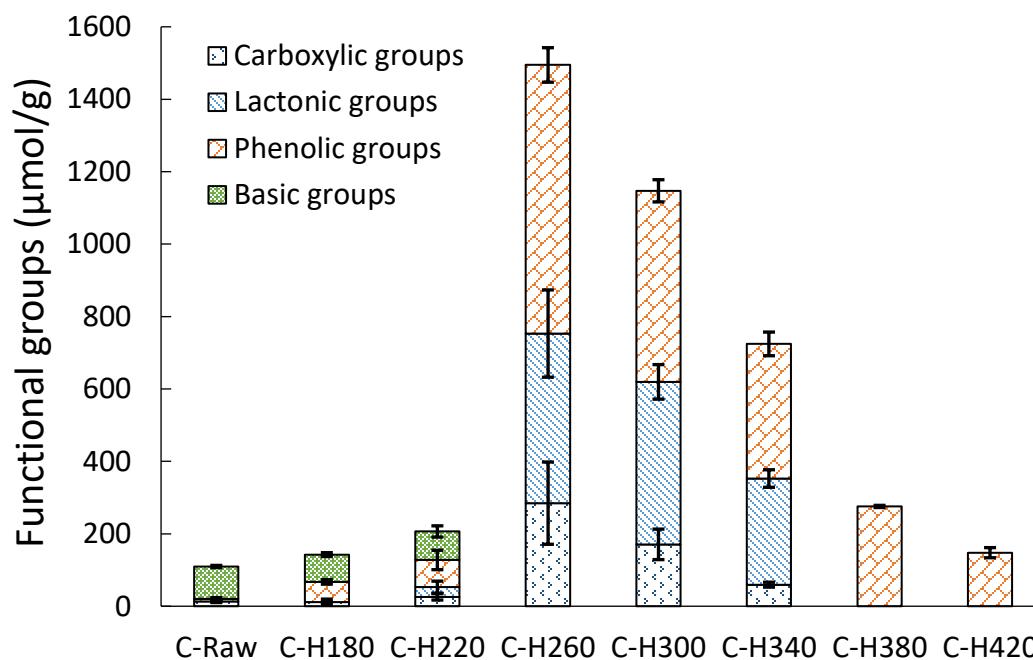


Figure 11: Oxygen-containing functional groups of cellulose and its hydrochars produced at subcritical and supercritical temperatures [95].

Due to the dehydration reaction, one mole of oxygen was removed from the hydrochar with two moles of hydrogen while one mole of carbon and two moles of oxygen were removed during the decarboxylation reaction. These effects are shown with purple and red lines, respectively, in Figure 8. Due to these two major reactions along with other side reactions (e.g., demethylation), the net effect was in between the dehydration and decarboxylation lines. The dominant reaction shifts to the decarboxylation in the rest of the subcritical conditions where the cellulose's

structure continues to breakdown and release CO₂ gas. This was previously reported as the main gaseous product in the HTT of biomass, which is the result of breaking down the carboxylic acids and carboxyl functional groups those are formed from the previous reactions [106-108]. The loss of elemental oxygen as H₂O and CO₂ could be resulted in from the surface rather than oxygen associated with the functional groups. With the further increase of the HTT temperature, the OCAFG is decreased and ended at $148 \pm 14 \mu\text{mol/g}$ at C-H420. Wang *et al.* and Saha *et al.* have discussed previously that HTT can only increase surface functionality to a certain maximum, after which the reaction severity begins to remove surface groups [43, 100]. The loss of oxygen functionality could be due to the increased reactivity of the groups with the medium, as hydroxide and hydronium concentrations increase with temperature up to supercritical conditions. In the case of cellulose, the maximum OCAFG appeared at 260 °C, where cellulose undergoes hydrolysis, dehydration, and decarboxylation reactions and is fully reacted [109]. Like the literature, a decreasing trend of total OCAFGs was observed at temperatures above 260 °C [43, 80, 100]. However, different OCAFGs decrease at different rates, with carboxylic groups degrading first, followed by the lactonic groups and then phenolic groups (see Figure 11), so, it can be concluded that the carboxylic groups are the most unstable groups under higher temperatures (300–420 °C) and the phenolic groups are the most stable groups compared to the carboxylic and lactonic groups regardless of the HTT

temperature. This difference in stability of different OCAFG acidic groups could be caused by several different reaction phenomena. Firstly, with the increase of HTT temperature, the carboxylic group ($-\text{COOH}$) breaks down and forms $\text{C}=\text{O}$ and $-\text{OH}$ groups [110]. At the same time, the primary alcoholic group ($\text{C}-\text{O}$) forms due to the breakdown of the lactonic group ($\text{C}=\text{O}$) [111]. Although the creation and destruction of different functional groups were observed at higher HTT temperature temperatures (300-420 °C), the carboxylic groups were only degraded; on the other hand, the lactonic and phenolic groups were created at the same time some of them were destroyed. As a result, the carboxylic groups were extinct first, followed by the lactonic and phenolic groups. Secondly, due to the domination of polymerization and condensation reactions at the higher temperatures, a secondary hydrochar formed that covered some of the functional groups, especially the carboxylic groups, which would result in low functional groups at higher temperatures [112, 113]. In addition, this secondary hydrochar has a higher atomic C/O ratio, which indicated the increase of energy properties instead of oxygen functional groups of the hydrochar [113].

The amount of BFG in the raw cellulose was measured at $89.3 \pm 3.0 \mu\text{mol/g}$, which is mainly attributed to the $-\text{CH}_2\text{OH}$. This number reduced slightly at H220 as the hydration reaction started to occur, possibly demolishing some $-\text{OH}$ groups. With the increase of the HTT temperature, in the case of 260 °C, the reaction approached the end stage, which means all the dehydration and decarboxylation reactions on the

hydrolyzed products have occurred. This could be the reason to dismiss all the BFG from the surface of the hydrochar produced at a temperature higher than 220 °C. A similar finding was observed in the FTIR spectra shown in Figure 12, where a broader peak appeared at 3200-3500 cm^{-1} for C-Raw and C-H220, which indicated the presence of alcoholic (-OH) groups. Besides OCAFG and BFG, other functional groups (e.g., alkene, aliphatic, etc.) could be present on hydrochars. Unfortunately, Boehm titration only allowed us to determine BFG (titration) and OCAFG (back titration). In order to find other functionality, the RTAP of each FTIR spectrum was calculated (see Figure 13). RTAP is expected to give a better understanding of the change of peak intensities with the treatment for respective hydrochar samples. The calculation procedure of the RTAP was adopted from Saha *et al.* [80].

A bond's RTAP should not be interpreted as the bond's abundance in a sample; rather, it should be used to compare the same bond in another sample, with respect to raw feedstock. C-Raw and C-H220 shared similar peaks with mostly alcohol/phenol and primary alcohols. However, a significant change was observed in C-H260, where the primary alcohol converted into mostly ester (C-O) and some aromatic (C-H) bonds. Further increases of the HTT temperature increased the aromaticity of the hydrochar as shown in Figure 13. At the same time, hydrophobicity of the hydrochar increased, which can be explained in context with the polarity index, which is a ratio of

elemental oxygen and elemental carbon. The polarity indices of the hydrochars decrease from 1.16 to 0.18 as shown in Table 4.

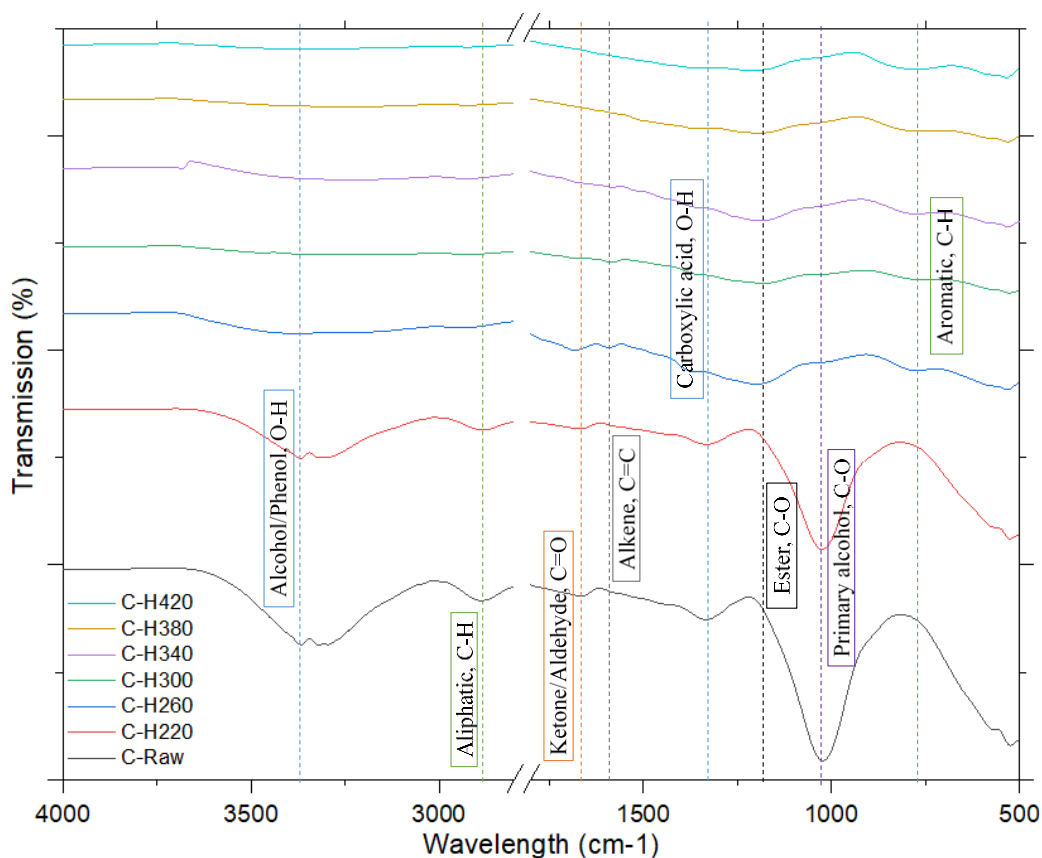


Figure 12: FTIR spectra of cellulose and its hydrochars produced subcritical and supercritical temperatures.

The increased hydrophobicity is primarily due to the removal of the hydrophilic hydroxyl groups (3400 cm^{-1}), evidenced by the elimination of the water band in cellulose (1660 cm^{-1}), which is lowered in the hydrochars. Cellulose hydrolysis in

C-H260 contributed to the peak intensity decreasing for aliphatic C–H and aliphatic esters C–O (1190 cm^{-1}).

An increase in C–O intensity can be attributed to glucose monomers produced from cellulose; dehydration and decarboxylation following hydrolysis fragmentation also contributed to the larger presence of the C–O band [97]. New peaks were also present for alkene C=C (1590 cm^{-1}) and aromatic C–H (780 cm^{-1}) bonds as a result of aromatization and polymerization that contributed to the formation of hydrochars [27]. These peaks slowly disappeared with the increase of the HTT temperature (shown in Figure 12), as the produced hydrochar took part in the dehydration reaction as discussed earlier.

Regardless of the HTT temperature, hydrochar was produced, although solid mass yield decreases with the increase of HTT temperature. In addition, the change in surface morphology and functionality with HTT temperature were observed. The key finding from here was that the surface functionality increased up to a point, after which excessive dehydration actually removed them. The formation, presence, and degradation of these functional groups are reflected in the overall surface composition of the hydrochar. It was found that the surface functionality was highest at $260\text{ }^{\circ}\text{C}$, where nearly equal amounts of lactonic, carboxylic, and phenolic groups. As HTT temperature rises to $340\text{ }^{\circ}\text{C}$, the carboxylic groups are almost fully

diminished, and the lactonic and phenolic groups are reduced by a third and a half, respectively, compared to C-H260. After supercritical conditions, there are only phenolic groups present at the hydrochar surface. As a result, from now on, 260 °C is the maximum hydrothermal treatment temperature discussed in this dissertation.

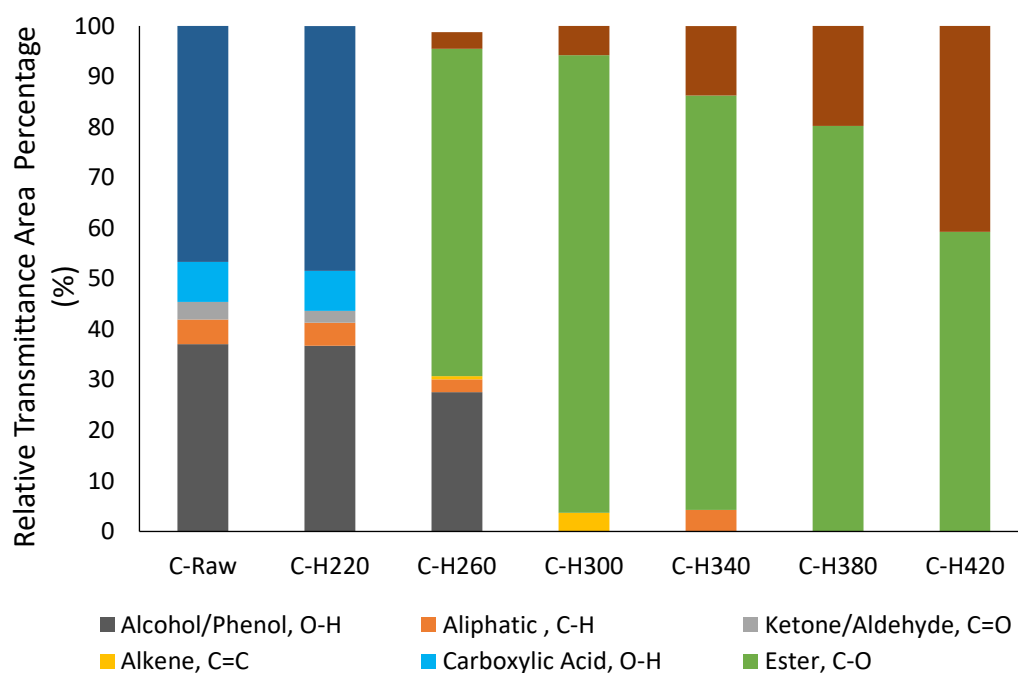


Figure 13: Relative transmittance area percentage of associated compounds on cellulose and its hydrochars produced at subcritical and supercritical temperatures.

3.1.4 pH and pH_{PZC}

The acidity or basicity of a char can be determined by measuring its pH. Table 6 shows pH of hydrochars produced from cellulose. The pH of the raw cellulose

sample was measured 6.1 ± 0.0 which is in the range of the pH reported in the literature (5.0–7.5) [114]. The pH values decreased around 4.3, 19.6, and 38.2 % with respect to raw cellulose at C-H180, C-H220, and C-H260, respectively. The reduction of pH indicates the formation of acidic functional groups on the hydrochar surface. The reduction of pH indicates that the solid-solid reaction still continued at higher HTC temperature and hydrochar becomes more acidic. These acids also catalyze the hydrolysis of unreacted biomass [115]. Thus, pH started to drop down and continued to decrease with HTC temperature.

A decrease of pH means either an increase of H^+ ion or reduction of OH^- . Since hydrolysis occurred during HTC, a reduction of OH^- ions happened on the hydrochar surface and went into the liquid phase. As a result, the liquid phase pH is supposed to be higher than the solid phase. However, it was observed in this research that the pH in the liquid phase is always lower than the solid phase shown in Table 6. The pH of C-PL180 was 4.7 ± 0.0 which was further reduced to 2.8 ± 0.1 at 220 °C and 2.5 ± 0.0 at 260 °C. It is speculated that the difference in pH between process liquid and hydrochar happened mainly because of the formation of acetic, formic, lactic acids in the liquid phase due to condensation reactions [115]. Another reason behind this phenomenon might be that the formation of organic products are much faster than the increase of OH^- ions into the liquid phase.

Table 6: pH of hydrochar and process liquid at different HTC conditions.

Sample ID	pH	pH _{PZC}
C-Raw	6.1 ± 0.0	3.7 ± 0.2
C-H180	5.8 ± 0.1	3.7 ± 0.1
C-PL180	4.7 ± 0.0	NA*
C-H220	4.9 ± 0.0	3.4 ± 0.1
C-PL220	2.8 ± 0.1	NA*
C-H260	3.8 ± 0.1	3.3 ± 0.2
C-PL260	2.5 ± 0.0	NA*

* NA = Not applicable

Table 6 also shows the measured values of pH_{PZC} for both feedstocks at different HTC temperatures. The pH_{PZC} of raw cellulose was found to be 3.7 ± 0.2 which was lower than the pH of raw cellulose. This means that the hydrochar surface is negatively charged. Mosur *et al.* reported that the microcrystalline cellulose is negatively charged with a pH_{PZC} of 3.2 [116]. The discrepancy between this study and Mosur *et al.* might result from the different feedstocks for cellulose or due to the presence of impurities in cellulose. With the increase of HTC temperature, the pH_{PZC} was decreased to 0.3, 8.7, and 10.6 % for C-H180, C-H220, and C-H260, respectively compared to raw cellulose. This can be explained by the same concept as discussed in pH changes. Due to the hydrolysis, a significant amount of positive charge (H⁺ ions) increases on the surface which will reduce the net negative charges on it [117]. Hence, hydrochars are getting closer to the neutral charge (equal amount of positive and negative charge) with the rise of HTC temperature. The surface of hydrochar is

negatively charged while the pH of hydrochar is higher than the pH_{PZC} . This type of hydrochar could interact with positively charged matters. On the other hand, hydrochar is positively charged while its pH is lower than pH_{PZC} and this could interact with negatively charged matters [86]. It is clear from Table 6, low HTC temperature produced more negatively charged hydrochar, which mainly attracts positive charges. On the other hand, higher temperatures produced almost neutral charged hydrochar, which can interact with both charges. Depending on the application, whether it requires to adsorb only positive or negative charge or both positive and negative charges from the system of interest (i.e., bio-waste, soil, etc.), HTC temperature might vary.

3.2 Properties of hydrochar from waste biomasses

It is always recommended that before digging into a complex material, investigating a model material, and understanding its formation, degradation, and product properties under various treatment conditions. In the previous section, a detailed examination of cellulose hydrochar was conducted. As of now, we know the behavior of a model compound's properties. However, the availability of the model compound in nature is limited. As a result, it is necessary to study the waste stream and understand their behavior with treatment conditions for their better uses. Thus, various properties of hydrochar produced from four different wastes, such as wood,

paper mill wastes, citrus, and winery wastes were investigated. The findings are discussed in the following sections.

3.2.1 Hydrochar from wood

The elemental and proximate analyses of wood and their corresponding hydrochars are shown in Table 7. Both analyses indicate that wood starts to degrade slowly at 180 °C as wood is a combination of lignin, hemicelluloses, and cellulose. At 260 °C, the carbon and oxygen content reach similar contents to that of cellulose hydrochar (see Table 4). The VM gradually decreases with the HTC temperature, while the FC increases. pHs of wood-derived hydrochars are shown in Table 7. The pH of raw wood was found to be 6.2 ± 0.1 and reduced by 21.9, 27.9, and 36.1 % for wood hydrochar at 180, 220, and 260 °C, respectively, compared to raw wood. The change in pH from raw to W-H180 was higher than W-H180 to W-H220 and W-H220 to W-H260. A possible reason behind that is that wood contains lignin, cellulose, and hemicelluloses where hemicelluloses start hydrolyzing from 180 °C [21].

Table 7: Physiochemical properties of wood and its hydrochars produced at different HTC conditions.

Sample ID	Mass yield [‡] (%)	Elemental analysis					Proximate analysis			pH	pH _{pzc}
		C (%)	H (%)	N (%)	S (%)	O (%)	VM (%)	FC (%)	Ash (%)		
W-Raw	NA*	48.1 ± 0.6	5.6 ± 0.3	BD*	BD*	46.3 ± 0.8	97.4 ± 0.1	2.6 ± 0.9	BD*	6.2 ± 0.1	4.8 ± 0.1
W-H180	68.3 ± 0.9	50.6 ± 0.7	5.7 ± 0.0	BD*	BD*	43.7 ± 0.6	85.9 ± 1.1	14.1 ± 2.0	BD*	4.8 ± 0.1	4.4 ± 0.1
W-H220	60.3 ± 0.2	52.4 ± 1.1	5.8 ± 0.2	BD*	BD*	48.8 ± 1.3	80.1 ± 0.1	19.9 ± 0.3	BD*	4.5 ± 0.1	3.9 ± 0.0
W-H260	43.2 ± 1.3	67.4 ± 0.3	5.0 ± 0.2	BD*	BD*	27.6 ± 0.3	58.7 ± 0.8	41.3 ± 0.9	BD*	4.0 ± 0.1	3.7 ± 0.1

* NA = Not applicable ‡ Mass yield = $\frac{\text{Final mass of feedstock (dry basis)}}{\text{Initial mass of feedstock (dry basis)}} \times 100 \%$

Conversely, cellulose starts to break down slowly at 220 °C and lignin at 255 °C [118, 119]. This can be confirmed from the mass yield data shown in Table 7 and Figure 7, where, the mass yield of C-H180 was 97.7 ± 0.4 % and W-H180 was 68.3 ± 0.9 %, indicating that significant reactions did not occur to cellulose at 180 °C. The mass yields of HTC at 220 °C were found to be 80.8 ± 3.1 % and 60.3 ± 0.2 % for cellulose and wood, respectively. Showing that cellulose starts to degrade at 220 °C. On the other hand, at 260 °C, the mass yield of cellulose and wood were similar 41.5 ± 1.5 % and 43.2 ± 1.3 %, respectively, as more of the macromolecules have broken down at this temperature. As a result, HTC of wood at 180 °C produced a noteworthy amount of organic acid that changes the pH of the hydrochar significantly. At high temperature, lignin first decomposes by hydrolysis and de-alkylation, which yields phenolic products, and then these intermediates undergo a cross-linking reaction and re-polymerize into phenolic char [120]. Although additional acids are produced at 220 and 260 °C, the change of pH was not significant compared to W-H180. It might be due to the lower content of cellulose in wood than pure cellulose and/or the formation of alkaline groups, which are competing with acidic groups.

Table 7 also shows the measured values of pH_{PZC} at different HTC temperatures. The pH_{PZC} of raw wood was found as 4.8 ± 0.1 , which was lower than its pH. The pH_{PZC} declined around 7.7, 19.5, and 22.5 % for W-H180, W-H220, and W-H260, respectively compared to the raw wood. The changes of pH_{PZC} for wood is

significantly higher compared to cellulose (see Table 6). It is speculated that the change is higher at 180 and 220 °C because of the hemicellulosic nature of wood, as hemicellulose starts to breakdown at 180 °C and cellulose at 220 °C [21]. Similarly, the changes are higher at 260 °C because of its lignocellulosic nature, as lignin breaks down at 255 °C [119].

Table 8 shows the functional groups on the wood and its hydrochar. The carboxylic group was reduced around half from its initial amount 140.3 to 71.7 $\mu\text{mol/g}$ at HTC temperature of 180 °C. This number started to increase from 220 °C and ended with a number which was about two times (261.1 $\mu\text{mol/g}$) compared to raw wood while HTC was conducted at 260 °C. The existence of lactonic groups appeared on all wood hydrochars (W-H180, W-H220, and W-H260) even though it was missing in the raw wood just like it was missing for raw cellulose. This group was found in an increasing trend (about three times) between 180 °C and 220 °C, while it further increased around two times from 220 °C to 260 °C. Adversely, phenolic groups had a decreasing trend and it was decreased by four folds on the W-H260 surface compare to the raw surface. Although individual functional groups did not follow the increasing trend like the model compound (cellulose), the total number of functional group increases with the increase of HTC temperature. As wood is a combination of cellulose, hemicellulose, and lignin, hydrolysis of different compounds occurs at

different HTC temperatures. At high temperatures, some of the functional groups decompose simultaneously [115]. As a result, individual functional groups did not follow any specific increasing or decreasing trend.

Table 8: Acidic and basic functional groups of wood and its hydrochars at different HTC conditions.

Sample ID	OCAFG ($\mu\text{mol/g}$)				BFG ($\mu\text{mol/g}$)
	Carboxylic	Lactonic	Phenolic	Total	
W-Raw	140.3 ± 2.0	BD*	436.3 ± 8.2	576.6 ± 7.8	160.0 ± 10.0
W-H180	71.7 ± 16.2	52.6 ± 11.6	483.2 ± 3.5	607.5 ± 5.5	120.8 ± 8.6
W-H220	82.3 ± 23.7	168.6 ± 15.2	397.3 ± 18.4	648.2 ± 21.4	59.6 ± 10.8
W-H260	261.1 ± 76.4	310.4 ± 21.4	109.3 ± 60.1	680.8 ± 18.8	64.7 ± 6.5

* BD = Below detection limit

As the ultimate analysis of the studied materials showed both nitrogen (N) and sulfur (S) contents were below the detection limit, it was assumed that no $-\text{NH}_2$ groups were present on wood-derived hydrochars. Therefore, all the BFGs determined in this study were the alcoholic groups shown in Table 8. The raw wood contains $160 \pm 10 \mu\text{mol/g}$ of BFGs and this was reduced to around $60 \mu\text{mol/g}$ on its hydrochar products. This supports the FTIR spectra, which showed weaker peaks on the wood hydrochars compared to raw wood. Wood has a mixture of a polymer matrix containing hemicellulose, cellulose, and lignin, although the composition might be different depending on the origin of it [121]. As hemicellulose starts to react hydrothermally at $180 \text{ }^\circ\text{C}$, cellulose by $230 \text{ }^\circ\text{C}$, and lignin remain unreacted until

260 °C, it can be assumed that hemicellulose reacted completely at 220 °C with hydration following by the dehydration and decarboxylation reactions [21]. As a result, there is a decrease in BFGs, to $57 \pm 11 \mu\text{mol/g}$, observed for W-H220. With the increase of HTC temperature, no further change in BFGs was observed on W-H260, as the remaining lignin is a thermally stable biopolymer compared to hemicellulose and cellulose. Therefore, the BFGs stayed similar to $65 \pm 7 \mu\text{mol/g}$ for-H260.

Figure 14 shows the IR spectra of untreated/treated wood; peak identification has been determined through various literature [122-124]. Figure 15 shows the relative transmittance area percentage (RTAP) of each IR spectrum in order to compare how peak intensities change with treatment, for respective samples. A bond's RTAP should not be interpreted as the bond's abundance in a sample; rather, it should be used to compare the same bond in another sample, with respect to feedstock.

Due to the lignocellulosic nature of wood, Figure 14 has similar peaks to cellulose (see Figure 12), in addition to peaks for bonds found in hemicellulose and lignin. The same cellulosic peaks for O-H stretching ($3430\text{-}3350 \text{ cm}^{-1}$), aliphatic C-H bonds (2900 cm^{-1}), and ether C-O stretching (1040 cm^{-1}) are observed; however, the same bands are indicative to O-H in phenolics, aromatic aliphatics, and aliphatic ether C-O-C bonding in pyranose rings, respectively, found in lignin [98]. Carbonyl C=O

peak (1690 cm^{-1}) from hemicelluloses and cellulose and lignin aliphatic ether C-O (1350 and 1230 cm^{-1}) were also found in wood. Small peak changes and RTAP occur for W-H180 and W-H220 (Figure 14b, Figure 14c, and Figure 15) as a result of hemicellulose being hydrolyzed at 180°C [21]. Specifically, the C=O hemicellulose band intensity is minimal and an O-H carboxylic acid band appears (1440 cm^{-1}), most likely due to dehydration and decarboxylation of hemicellulose hydrolysis products [125]. The intensity of the aliphatic ether group is also reduced. As a result, a reduction is observed in the carboxylic and phenolic groups shown in Table 8.

W-H260 (Figure 14d) shows more intensity for aliphatic C-H and aromatic C-H due to lignin remaining in the sample after the hydrolysis of hemicellulose and cellulose and is indicated so by the higher RTAP. Likewise, the carboxylic group determined by Boehm titration is higher at W-H260. The re-emergence of a C=O (1690 cm^{-1}) is due to more dehydration and decarboxylation products forming and remaining in the hydrochar, which indicates the presence of a more lactonic group (shown in Table 8). Similarly, the O-H carboxylic acid group is also more defined, this peak can also be attributed to O-CH₃ ether bonds in remaining lignin [98]. As a result, more phenolic groups were found on the W-H260 compared to the W-H220. Lignin remaining without hemicellulose in hydrochar product results in C-O ether RTAP

decreasing and their peaks become smaller and more defined. An alkene C=C band (810 cm^{-1}) is produced from hydrochar aromatization or polymerization.

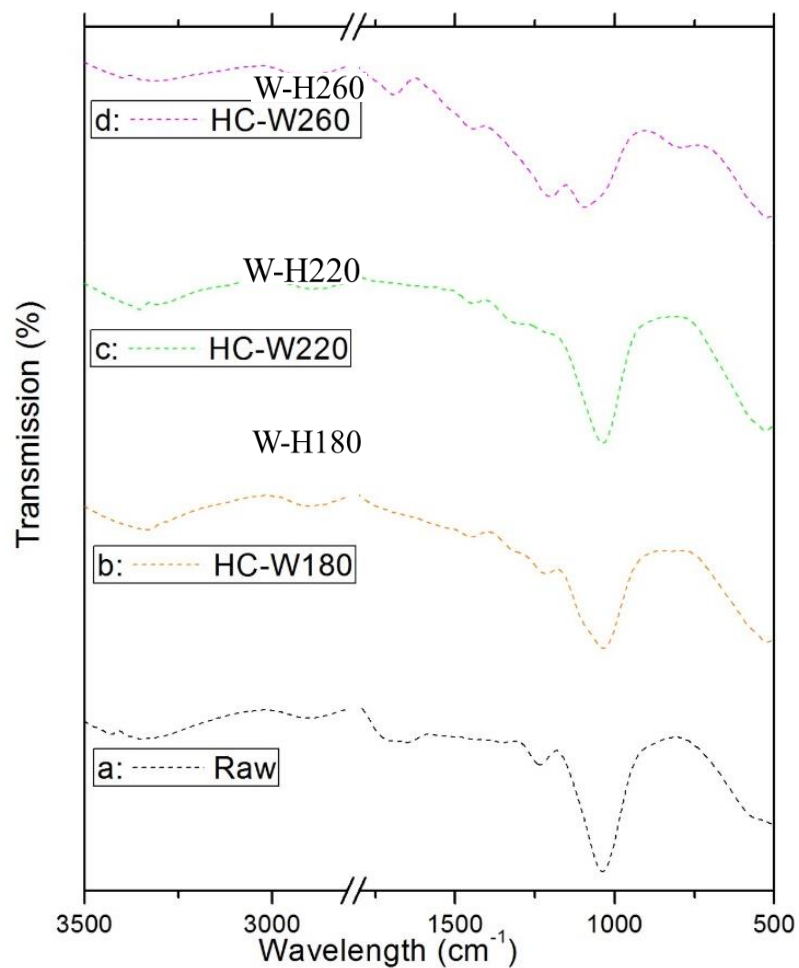


Figure 14: FTIR spectra of wood and its hydrochars.

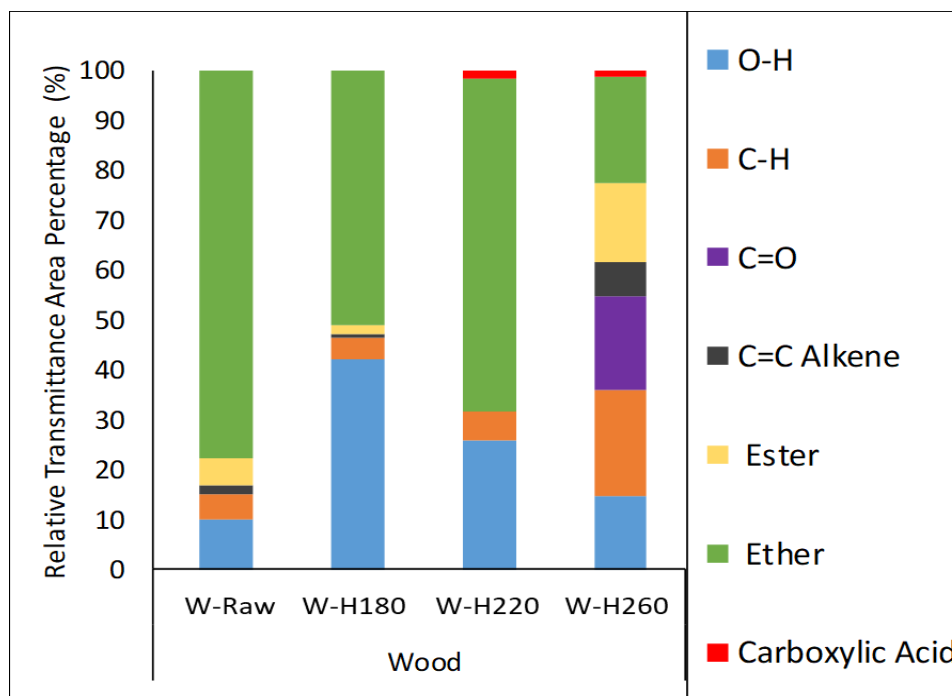


Figure 15: Relative transmittance area percentage of associated compounds on wood-derived hydrochar surface.

3.2.2 Hydrochar from citrus and winery wastes

The chemical state of the hydrochar was characterized by the pH, while the electrical state was characterized by the pH_{PZC} . The pH and pH_{PZC} values of the hydrochar samples are shown in Table 9. The results showed that both pH and pH_{PZC} increased with the increase of treatment temperature for both CW and WW. However, CW hydrochar showed a minimum difference in pH and pH_{PZC} , while WW showed higher pH compared to its pH_{PZC} at all conditions. According to the literature, the

surface of the hydrochar is typically negatively charged when the pH is higher than its pH_{PZC} and it is positively charged if the pH is lower than its pH_{PZC} [43], which indicates that the WW hydrochars are negatively charged while CW hydrochars are mostly neutral.

Table 9: Physiochemical properties of hydrochars produced from citrus and winery wastes.

Sample ID	pH	pH_{PZC}	BET surface area (m^2/g)	Density of surface functional groups ($\mu mol/m^2$)
CW-H180	4.74 ± 0.06	4.72 ± 0.15	46.16 ± 0.11	23.24 ± 0.22
CW-H220	5.24 ± 0.05	5.29 ± 0.08	47.60 ± 0.90	23.36 ± 0.51
CW-H250	5.68 ± 0.02	5.61 ± 0.04	63.82 ± 2.08	16.61 ± 0.59
WW-H180	4.72 ± 0.06	4.22 ± 0.06	34.08 ± 1.23	32.69 ± 1.39
WW-H220	6.52 ± 0.08	5.41 ± 0.04	41.96 ± 0.88	24.33 ± 0.54
WW-H250	6.91 ± 0.11	5.67 ± 0.06	48.04 ± 1.61	21.45 ± 0.81

Furthermore, Figure 16 provides quantitative information on the acidic and basic groups on the hydrochars' surfaces. It is observed that the total oxygen functional groups (acidic and basic) on hydrochar surfaces did not vary significantly. Surprisingly, with a deeper look at the specific functional groups, it was noticed that acidic oxygen functional groups decreased with HTC temperature and basic oxygen functional groups increased with HTC temperature. As a result, the overall sum of oxygen functional groups remains similar to the increase of HTC temperature. For instance, the carboxylic groups decreased from $499 \mu mol/g$ on CW-H180 to $353 \mu mol/g$ on CW-H250, while on WW they decreased from $433 \mu mol/g$ to $221 \mu mol/g$.

The basic functional groups increased with the HTC temperature for both samples. On CW, they increased from 67 to 148 $\mu\text{mol/g}$ and, correspondingly, from 64 to 227 $\mu\text{mol/g}$ for WW. Although no lactonic groups were found in CW samples, the WW samples showed an increasing trend with the HTC temperature.

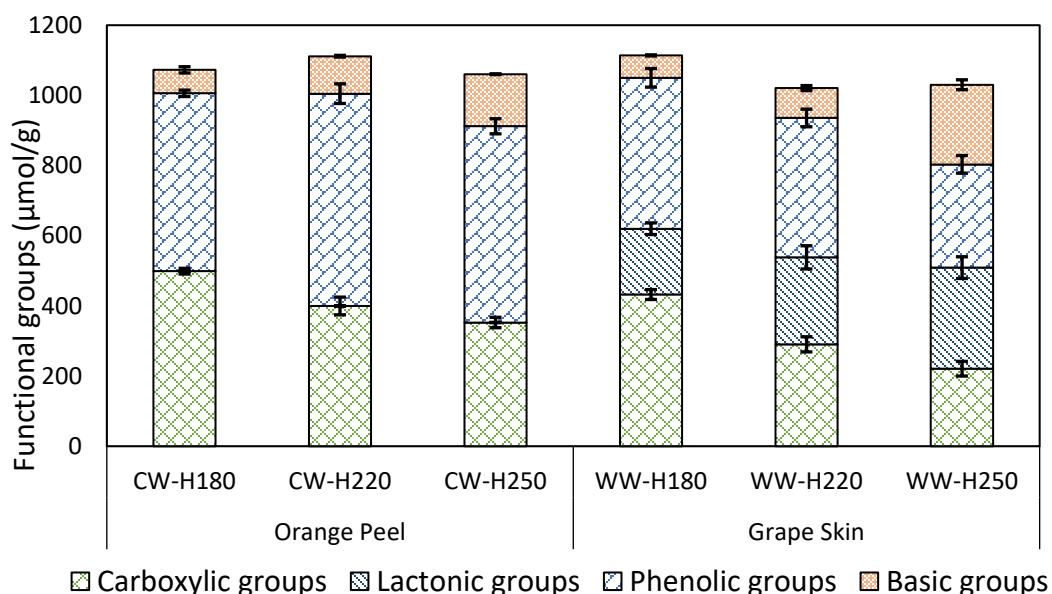


Figure 16: Oxygen-containing functional groups on hydrochars produced from citrus and winery wastes.

This is confirmed by the FTIR spectra (see Figure 17) where no peak for aliphatic ketone at $1705\text{--}1725\text{ cm}^{-1}$ appeared on CW hydrochars, but it appeared on WW-H180 and stayed more visible at higher temperatures (220 and 250 $^{\circ}\text{C}$). By contrast, the phenolic groups showed an opposite trend whereby they increased for the CW

samples from 507 to 560 $\mu\text{mol/g}$, but decreased for WW samples from 430 to 294 $\mu\text{mol/g}$ at 180 and 250 $^{\circ}\text{C}$, respectively. In general, any carbon material contains both acidic and basic properties. However, the dominant property is highly dependent on the pH_{PZC} of that material. While the pH_{PZC} of carbon material is less than 7.0, the material should be dominated by the acidic groups, otherwise, the basic groups should be dominant [126]. The measured pH_{PZC} values are following the domination of total acidic and basic groups in this study.

The BET surface areas of the hydrochars are shown in Table 9. Both CW and WW hydrochars showed an increased surface area with increasing HTC temperature. This could be related to the removal of volatiles from hydrochars at high-temperature HTC. As the surface area increased and the total functional groups remained almost unchanged, the density of functional groups decreased significantly. The density of functional groups of material represents the number of active sites present per unit surface area. The density of functional groups was 23.24 $\mu\text{mol/m}^2$ on CW-H180 which reduced to 16.61 $\mu\text{mol/m}^2$ on CW-H250. While this number reduced from 32.69 to 21.45 $\mu\text{mol/m}^2$ for WW hydrochar at 180 and 250 $^{\circ}\text{C}$, respectively. The density of functional groups could play an important role if the mechanism of adsorption is of the monolayer type.

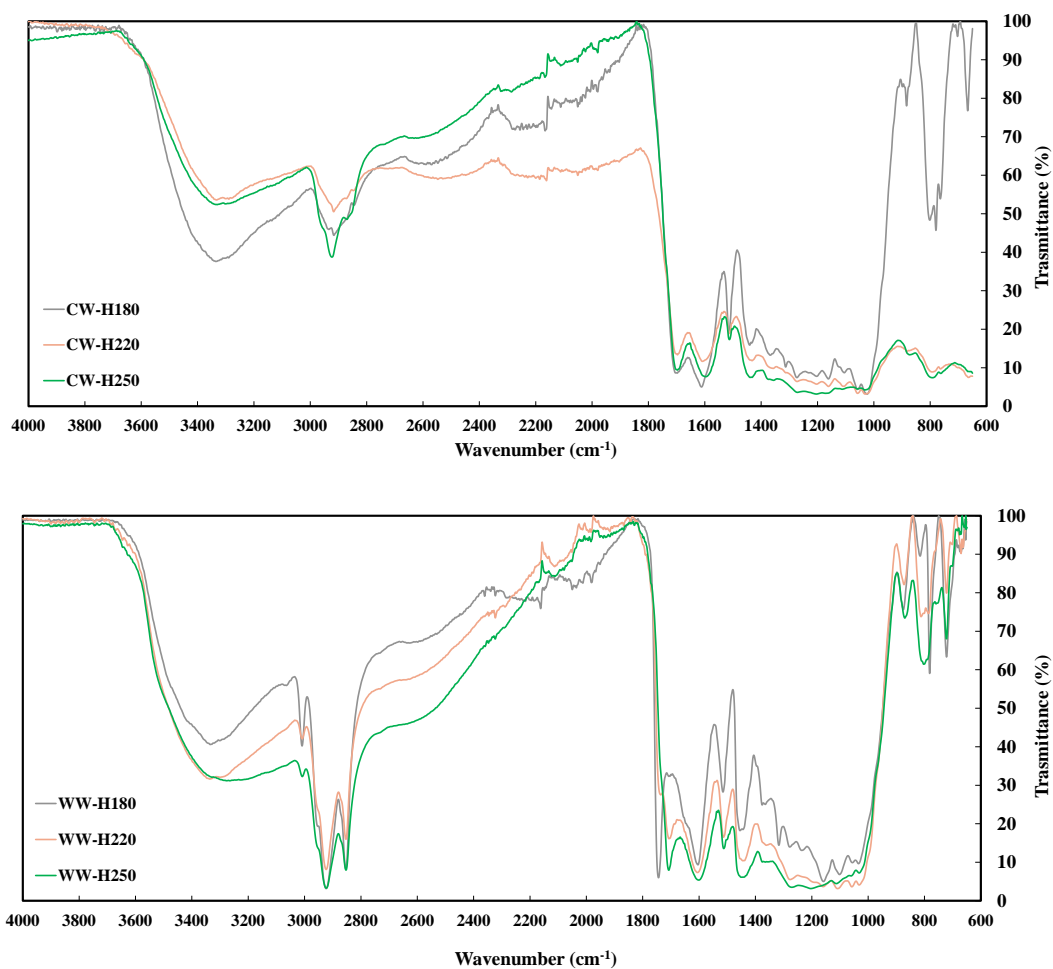


Figure 17: FTIR spectra of hydrochars produced from citrus and winery wastes.

3.2.3 Hydrochar from paper mill sludges

The mass yields of hydrochars with respect to different HTC temperatures are shown in Table 10. With the increase of HTC temperature, mass yield decreases in the

output. Since the reactivity of biomass increases with the HTC temperature, lower mass yields were expected with the increase of HTC temperatures.

Table 10: Mass yields and energy densification of paper mill sludges and their hydrochars (aNot applicable).

Sample	HTC Temperature (°C)	Mass yield (%)	HHV _{daf} (MJ/kg)	ED
PS	Raw	NA ^a	15.5 ± 0.0	NA ^a
	180	96.2 ± 2.0	15.1 ± 0.4	1.0 ± 0.0
	220	85.4 ± 2.0	15.3 ± 0.4	1.0 ± 0.0
	260	30.3 ± 1.1	22.8 ± 0.1	1.5 ± 0.0
DPS	Raw	NA ^a	13.0 ± 0.0	NA ^a
	180	91.7 ± 0.9	13.0 ± 0.2	1.0 ± 0.0
	220	84.4 ± 0.9	12.9 ± 0.1	1.0 ± 0.0
	260	58.4 ± 2.0	11.4 ± 0.7	0.9 ± 0.1
PSS ₁	Raw	NA ^a	21.4 ± 0.1	NA ^a
	180	81.2 ± 0.3	21.7 ± 0.1	1.0 ± 0.0
	220	74.1 ± 0.0	21.7 ± 0.1	1.0 ± 0.0
	260	54.1 ± 2.0	27.4 ± 0.1	1.3 ± 0.0
PSS ₂	Raw	NA ^a	19.6 ± 0.2	NA ^a
	180	90.9 ± 0.5	19.6 ± 0.1	1.0 ± 0.0
	220	78.9 ± 1.2	20.2 ± 0.1	1.0 ± 0.0
	260	41.1 ± 1.7	28.9 ± 0.1	1.5 ± 0.0
PFR	Raw	NA ^a	19.7 ± 0.2	NA ^a
	180	93.2 ± 2.1	18.5 ± 0.0	0.9 ± 0.0
	220	81.9 ± 1.2	19.3 ± 0.2	1.0 ± 0.0
	260	45.4 ± 1.2	25.2 ± 0.3	1.3 ± 0.0
PTS	Raw	NA ^a	17.1 ± 0.7	NA ^a
	180	87.5 ± 2.9	18.6 ± 0.5	1.1 ± 0.0
	220	69.8 ± 2.8	21.6 ± 0.1	1.3 ± 0.0
	260	43.8 ± 1.1	31.5 ± 3.7	1.8 ± 0.3
Clarion # 5a coal	Raw	NA ^a	30.5 ± 0.3	NA ^a

The variation of HTC product distribution resulting from different PMS feedstocks can be found in Table 10. Mass yields of HTC treated PSS₁ and PSS₂ considerably decreased as reaction temperature increased, reaching yields as low as 54.1 % and

41.1 %, respectively at 260 °C. Even though both are mixtures of primary and secondary sludges, their mass yields were significantly different. The reason could simply be the variation of ratios of primary to secondary sludges in the samples. This result shows that sludge feedstocks can vary in a manner that impacts HTC performance, even amongst the same category of sludges. The yields at 180 and 220 °C were quite high for both feedstocks, which may indicate that both sludges were rich in cellulose and lignin. As the cellulose and lignin react with water during HTC at approximately 220-230 °C and 255–265 °C, respectively, PMS remains mostly unreacted at 180 and 220 °C [119, 127-129]. These findings are consistent with the literature values, where the mass yield is in a range between 29 to 65 % depending on the mixing ratio of primary to secondary sludges when the HTC was conducted at 260 °C [130, 131].

Mass yield of HTC treated PS significantly decreases at the high reaction temperature, reaching a yield as low as 30.3 % at 260 °C. However, minimal changes were observed at 180 and 220 °C, which indicates that the PS is rich in cellulosic material that did not completely react until 260 °C. The mass yield of PFR was similar to PS at low temperatures (180 and 220 °C), while the mass yield of PFR was higher than the mass yield of PS at 260 °C. The reason for this higher mass yield for PFR could be the presence of higher lignocellulosic material in PFR compared to PS, as PFR

contains tree branches and barks. These lignin-rich compounds break down slowly and likely remain unreacted at these treatment conditions.

Since PTS is basically the PS prior to the dewatering step [132], the mass yields for PTS are expected to be similar to PS. However, a significant difference was observed between their mass yields, especially at 260 °C. The mass yield was 43.8 % for PTS while it was 30.3 % for PS. Although the yields were different, they fall within the literature values of PS (29 to 65%). This difference indicates that the PTS might have an even distribution of lignin and cellulosic compounds, as it seems a similar degradation from 180 to 220 to 260 °C. With PS, a significant difference occurs between 220 and 260 °C than 180 and 220 °C. This is indicative that the PS is composed of more hardy lignin compounds that break down at higher temperatures. These differences in mass yield with respect to temperature are consistent with previous literature, which has traditionally explained this observation as being the result of differences in feedstocks. A mild change in mass yield at 260 °C was observed for DPS, which was 58.4 %. This higher mass yield, compared to the other sludges, may be due to either the sludge contains more inorganic components which remain unreacted during HTC, or the sludge contains more lignocellulosic fiber wastes which do not degrade as readily under these conditions.

It was observed from the mass yields that minimal carbonization happened to the PMS at 180 and 220 °C, even though cellulose degradation is expected to occur at 220 °C. Meanwhile, significant changes happened to all PMS only at 260 °C. This indicates that the cellulosic mass may be stabilized by the other lignin components in the PMS, requiring a higher temperature to initiate the HTC process. Mass yields alone, however, do not give a full account of the benefits of the HTC process; it is necessary to check additional fuel characteristics (i.e., HHV or ED) of all hydrochars to evaluate the more impactful hydrochars for further analysis.

The HHV of a fuel is defined as the amount of heat released by a specified quantity once it is combusted. Meanwhile, how the energy is concentrated into the hydrochar with respect to its raw sample is known as energy density (ED). The dry ash-free HHV (HHV_{daf}) and ED, relative to the raw samples, are shown in Table 10. The HHV_{daf} of raw sludges varies from 13.0 to 21.4 MJ/kg, where DPS has the minimum, PSS_1 has the maximum, and the others fall in between. The HHV_{daf} of all sludges are lower than the HHV of bituminous coal (25.4-27.4 MJ/kg) [133, 134]. The HHV_{daf} of hydrochars produced at 180 and 220 °C were similar to their individual raw samples. However, the HHV_{daf} of hydrochars produced at 260 °C were significantly higher than the corresponding raw samples, with the exception of DPS. Some of them are even higher than the HHV_{daf} of coal (e.g., hydrochar of PSS_1 , PSS_2 , and PTS

produced at 260 °C). Most of the PMS sludges are the combination of hemicellulose, cellulose, lignin, and other inorganics. The HHVs of hemicellulose and cellulose have a range between 16.8–18.6 MJ/kg and break down around 180 and 220–230 °C [127, 128, 135]. On the other hand, lignin not only has a higher HHV (23.3–25.6 MJ/kg) but also has HTC initiation around 255–265 °C [119, 129]. As a result, the component that has higher HHV stays in the hydrochar product at higher HTC temperature. The only exception was observed in DPS, where the HHV decreases with the increase of HTC temperature. This decrease in HHV, which is unique to the DPS char, is due to the loss of carbon and a relative increase in oxygen (both must be compared to the total mass loss of the sludge). The lack of carbonization could be due to the higher amount of inorganics present in the DPS, which is shown in its high ash content.

Table 10 shows that ED remains 1.0 for all hydrochars produced at 180 and 220 °C, which indicates that almost nothing favorable happened for PMS in terms of energy content at those HTC conditions. However, the energy contents by the hydrochars produced at 260 °C were 1.3 to 1.8 times higher than their raw samples except for DPS, which had ED lower than 1.0 at 260 °C. So, the types of feedstocks are more significant than HTC reaction temperature for densifying the energy in PMS. As the

highest ED was observed at HTC 260 °C, from now on, the characteristics of hydrochars produced from PMS at 260 °C will only be discussed.

It was observed that the solid mass yield decreases and ED generally increases with the HTC temperature. Therefore, it is important to evaluate how the organics and lignin in the hydrochars produced at 260 °C vary from their raw sludges, including their significant impact on ED. Table 11 presents the elemental analysis including ash, lignin, and sugar (C₅ and C₆) content of all PMS and their corresponding hydrochars produced at 260 °C. Hydrochar of each sample has higher carbon content compared to its raw sample, except DPS. The carbon content increases from 34.6 to 44.3 %, 38.4 to 40.5 %, 42.8 to 62.2 %, 39.8 to 57.6 %, and 23.9 to 40.2 % for PS, PSS₁, PSS₂, PFR, and PTS, respectively. However, this content decreases for DPS from 27.1 to 22.2 %.

Table 11: Elemental analysis, ash, and lignin number for all raw PMS and their hydrochar samples (^aindicates it was calculated by difference; ^bbelow detection limit; and ^cNot applicable).

Sample	HTC temperature (°C)	C (%)	H (%)	N (%)	S (%)	O ^a (%)	Ash (%)	Lignin (%)	C ₅ and C ₆ sugar (mg/g)
PS	Raw	34.6 ± 0.4	4.7 ± 0.1	0.3 ± 0.0	BD ^b	44.4 ± 0.8	16.0 ± 0.0	5.2 ± 0.4	2.7 ± 0.3
	260	44.3 ± 3.3	3.8 ± 0.3	0.2 ± 0.0	2.0 ± 0.0	18.5 ± 7.5	33.1 ± 1.7	36.9 ± 1.3	3.0 ± 0.3
DPS	Raw	27.1 ± 0.2	3.4 ± 0.1	0.7 ± 0.0	BD ^b	37.0 ± 0.9	31.9 ± 0.4	10.0 ± 1.2	2.0 ± 0.2
	260	22.2 ± 1.7	1.8 ± 0.2	0.4 ± 0.1	0.1 ± 0.0	29.6 ± 3.4	46.0 ± 0.3	19.7 ± 0.8	1.9 ± 0.3
PSS ₁	Raw	38.4 ± 0.8	5.3 ± 0.1	2.3 ± 0.2	0.9 ± 0.1	30.3 ± 2.2	22.8 ± 0.4	20.2 ± 0.1	4.0 ± 1.1
	260	40.5 ± 1.5	4.2 ± 0.3	2.1 ± 0.0	1.3 ± 0.0	16.0 ± 4.4	36.0 ± 1.3	46.8 ± 0.8	1.4 ± 0.0
PSS ₂	Raw	42.8 ± 0.0	6.1 ± 0.2	0.7 ± 0.1	0.2 ± 0.0	45.8 ± 0.7	4.5 ± 0.1	17.6 ± 0.5	3.5 ± 1.2
	260	62.2 ± 0.7	5.7 ± 0.1	1.6 ± 0.1	0.3 ± 0.0	25.0 ± 1.5	5.2 ± 0.1	87.8 ± 5.9	3.5 ± 2.5
PFR	Raw	39.8 ± 0.1	5.3 ± 0.0	0.6 ± 0.1	0.3 ± 0.0	34.6 ± 0.5	19.5 ± 0.1	22.6 ± 0.3	3.8 ± 2.2
	260	57.6 ± 2.6	5.5 ± 1.2	0.6 ± 0.1	0.4 ± 0.1	9.2 ± 6.1	26.8 ± 0.3	57.9 ± 1.2	2.8 ± 0.3
PTS	Raw	23.9 ± 2.7	3.9 ± 0.4	0.6 ± 0.0	6.2 ± 0.6	48.4 ± 5.2	17.1 ± 0.1	20.4 ± 0.5	3.2 ± 2.2
	260	40.2 ± 1.4	4.3 ± 0.1	0.4 ± 0.1	1.3 ± 0.2	3.3 ± 1.5	50.5 ± 1.5	44.2 ± 0.6	2.4 ± 1.2
Clarion # 5a coal	Raw	63.8 ± 1.2	4.1 ± 0.1	1.5 ± 0.0	4.6 ± 0.8	14.9 ± 1.8	11.1 ± 0.6	NA ^c	NA ^c
Bituminous coal [136]	Raw	75.1 ± 2.8	5.3 ± 0.4	1.5 ± 0.1	1.1 ± 0.8	6.9 ± 2.6	10.0 ± 1.4	NA ^c	NA ^c
Sub-bituminous coal [137]	Raw	55.8 ± 3.5	6.2 ± 0.2	0.7 ± 0.1	0.3 ± 0.1	32.7 ± 2.8	4.3 ± 0.9	NA ^c	NA ^c

The oxygen content, on the other hand, has a decreasing trend for all sludges from raw to its hydrochar. The oxygen content decreases from 44.4 to 18.5 %, 37.0 to 29.6 %, 30.3 to 16.0 %, 45.8 to 25.0 %, 34.6 to 9.2 %, and 48.4 to 3.3 % for PS, DPS, PSS₁, PSS₂, PFR, and PTS, respectively. The loss of hydroxyl groups due to the dehydration reaction during HTC results in lower oxygen content [133]. The increase in carbon and a decrease in oxygen content complement the HHV increases after HTC treatment. Although the oxygen content decreases for DPS, the carbon content also decreases with HTC resulting in a decrease of HHV. Hydrogen and nitrogen content change minimally and remain approximately the same. Fuel qualities of the PMS hydrochars were further analyzed with the van-Krevelen diagram (Figure 18). In the van-Krevelen diagram, a sample closer to the origin indicates a higher quality fuel (i.e., anthracite) and a sample far from the origin specifies a poor quality fuel (i.e., lignite or biomass). Fuel quality of all PMS except DPS being vastly upgraded with HTC at 260 °C and falls between bituminous and sub-bituminous region shown in Figure 18.

The proximate analysis of various raw and PMS hydrochars at 180, 220, and 260 °C are presented in Figure 19. The figure indicates that the raw PMS samples were high in volatile matters and low in fixed carbon. Among the raw PMS samples, PSS₂ contained the highest volatile matters and the lowest ash while PSS₁ had the highest fixed carbon. Figure 19 also shows the change of ash, fixed carbon, and volatile

matters present in various sludges with respect to HTC temperatures compared to raw samples.

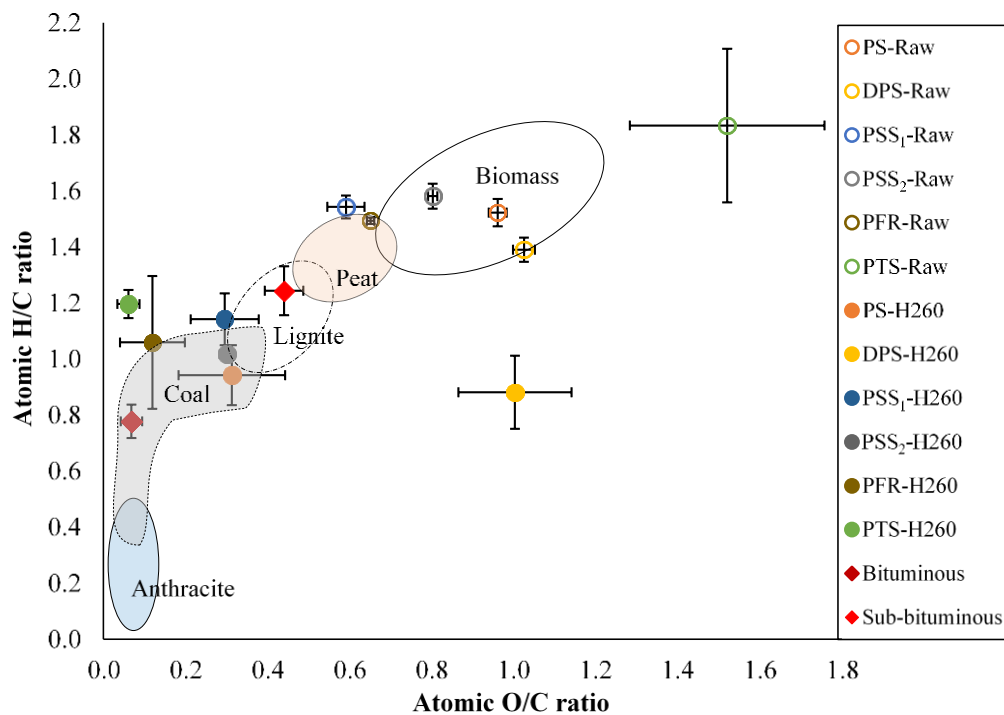


Figure 18: van-Krevelen diagram for all raw PMS and their hydrochar samples including bituminous and sub-bituminous coal.

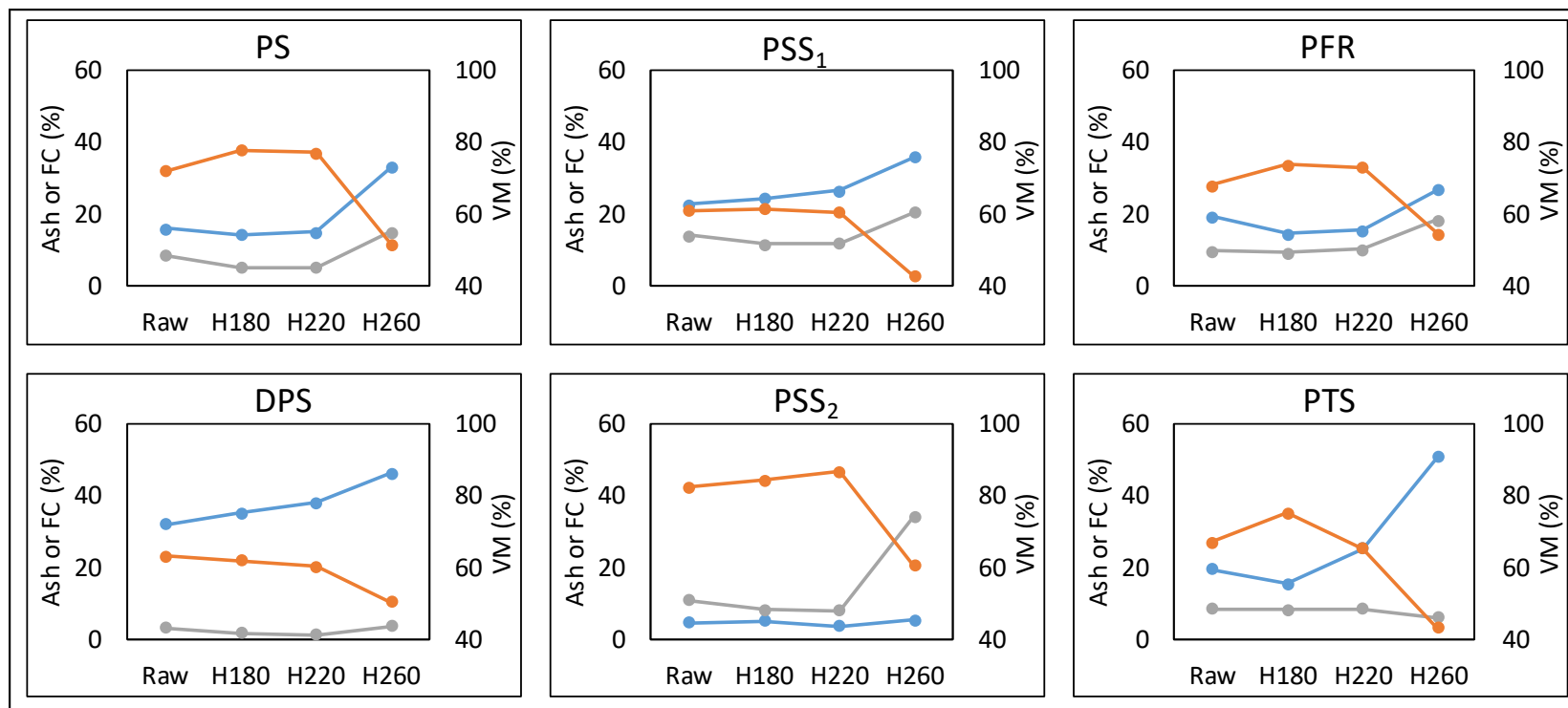


Figure 19: Proximate analysis of various PMS hydrothermally carbonized at 180-260 °C. The orange, gray, and blue lines represent VM, FC, and ash content, respectively.

The figure also illustrates that HTC of PMS at 180 and 220 °C did not significantly affect the volatile materials, fixed carbon, and ash content compared to raw PMS samples. However, the ash and fixed carbon were increased and volatile matters of PMS decreased remarkably when HTC temperature increased from 220 to 260 °C. The presence of high inorganic materials, which were trapped in the solid phase of the product instead of leached into the liquid phase, could be a possible reason for the increase in ash. The decrease in volatile materials could be attributed to the decomposition of cellulose and hemicellulose producing gaseous species like CO, CO₂, and short-chained hydrocarbons [138, 139]. The decomposition of volatile materials also increased the fixed carbon in 260 °C hydrochars [32]. Among the PMS hydrochars, PSS₂ contained the maximum volatile materials and fixed carbon as well as the lowest ash percentage.

Ash content in each hydrochar was higher from its raw sample also shown in Table 11. Ash is predominantly inert in the HTC process, so it is expected to become concentrated as the HTC process progresses. Higher ash content in treated samples is a result of HTC breaking down organic biomass constituents (release into liquid phase) and keep concentrating the inorganic content in the solid phase [140, 141]. Similar to the ash content, lignin content was also higher in hydrochar compared to its raw sludge. This number increases from 5.2 to 36.9 %, 10.0 to 19.7 %, 20.2 to

46.8 %, 17.6 to 87.8 %, 22.6 to 57.9 %, and 20.4 to 44.2 % for PS, DPS, PSS₁, PSS₂, PFR, and PTS, respectively. As lignin breaks down between 255–265 °C [119, 129], unreacted lignin is concentrated in the solid phase. Higher lignin content in hydrochar can be supported by the increase in HHV for most sludges following treatment as a result of reactive, less energy-dense cellulose being removed from the char more at higher temperatures.

Total sugar content in raw samples and their hydrochar was almost the same, as shown in Table 11. The short-chain sugar molecules (C₅ and C₆) are likely the product of hydrolyzed cellulose and hemicellulose [100]. However, these sugar molecules are highly reactive at HTC conditions, and they tend to dehydrate into furan derivatives (e.g., furfural, hydroxymethylfurfural, etc.) or decarboxylated to short-chain acids, CO₂ and water [100]. However, in PMS, the number did not increase, which could indicate that dehydration and decarboxylation of sugars are more dominant than hydrolysis of PMS.

3.3 Properties of pyrolyzed hydrochar

In the previous sections, it is observed that HTC could increase the surface functionality up to a certain limit and then drop down. As pyrolysis is a process that is generally used for volatiles removal from lignocellulose structure and increases

surface area. Pyrolysis of hydrochar may allow a further increase in the functional group on the surface. Thus, the effect of pyrolysis temperature on surface functionality including with physical properties of the hydrochar were investigated. For this investigation, the hydrochars from a model compound (cellulose) and waste biomass (wood) were used. The properties of the pyrolyzed hydrochars are discussed in the following sections.

3.3.1 Mass yield, ultimate and proximate analyses

The fraction of the initial mass remaining after HTC or pyrolysis can be referred to as mass yield. As the reactivity of biomass increases with temperature, lower mass yields were expected with the increase of both HTC and pyrolysis temperatures. Meanwhile, overall mass yield can be referred to as the product of individual mass yields of HTC and pyrolysis. Table 12 shows the mass yields of HTC, pyrolysis, and overall for both feedstocks. The HTC mass yields of cellulose are around 80.4 % and 41.5 % for C-H220 and C-H260, respectively. In contrast, the HTC mass yields of wood are around 60.3 % and 43.2 % for W-H220 and W-H260, respectively. These yields are consistent with the literature for similar HTC conditions [80]. Table 12 also shows that the pyrolysis mass yield of C-H220 was 28.2 % at P400, and it was further decreased with an increase of pyrolysis temperature to 20.2 % at P600. It can also be noticed that pyrolysis mass yields of C-H260 decreased with pyrolysis

temperature, the pyrolysis yields were higher compared to C-H220. This phenomenon indicates that C-H220 might be different from C-H260. Similarly, the pyrolysis yields of W-H260 were higher than W-H220, and they were different from cellulose hydrochars. The higher mass yield of C/W-H260 stipulates that hydrochars produced at 260 °C were more thermally stable than hydrochars produced at 220 °C. As the pyrolysis mass yields were significantly higher for C/W-H260 compared to C/W-H220, higher overall mass yields were observed for C/W-H260 as shown in Table 12. However, the overall mass yields for all H220 are lower than the mass yields of H260. This might be due to the opposite trend of mass yield for HTC and pyrolysis. However, the decrease of mass yields was different for HTC and pyrolysis, which can be explained from the ultimate analysis.

During HTC and pyrolysis, both carbon and oxygen content change differently, which may affect the overall mass yield. The change of carbon and oxygen content would be different in pyrolyzed hydrochars for the hydrochars produced at different temperatures. The ultimate analysis of hydrochars and their pyrolyzed chars are shown in Table 13.

Table 12: Mass yield of hydrochars, pyrolyzed hydrochars and their overall from cellulose and wood

Feedstock	HTC		Pyrolysis		Overall mass yield (%)**
	Temperature (°C)	Mass yield (%)*	Temperature (°C)	Mass yield (%)*	
Cellulose	220	80.4 ± 3.1	400	28.2 ± 1.0	22.8 ± 2.4
			500	22.9 ± 1.2	18.6 ± 2.4
			600	20.2 ± 0.1	16.3 ± 1.0
	260	41.5 ± 1.5	400	76.0 ± 1.1	31.6 ± 2.2
			500	66.2 ± 1.0	27.5 ± 2.0
			600	59.7 ± 0.3	24.8 ± 1.4
Wood	220	60.3 ± 0.2	400	43.0 ± 0.9	25.9 ± 0.9
			500	35.5 ± 0.2	21.4 ± 0.3
			600	31.9 ± 0.6	19.2 ± 0.6
	260	43.2 ± 1.3	400	69.2 ± 1.1	29.9 ± 1.9
			500	56.7 ± 0.1	24.5 ± 1.0
			600	50.8 ± 1.1	22.0 ± 1.5

$$* \text{ Mass yield} = \frac{\text{Final mass of feedstock (dry basis)}}{\text{Initial mass of feedstock (dry basis)}} \times 100 \%$$

$$** \text{ Overall mass yield} = \frac{\text{HTC mass yield (\%)} \times \text{Pyrolysis mass yield (\%)}}{100 \times 100} \times 100 \%$$

The carbon content was increased from 43.9 to 69.8 % and from 52.4 to 67.4 % for cellulose and wood from H220 to H260, respectively, which is consistent with the literature [80]. Correspondingly, the oxygen content was decreased from 49.9 to 26.1 % and from 41.8 to 27.6 % for cellulose and wood from H220 and H260, respectively. Now, carbon content has been significantly increased while pyrolysis was performed to the C-H220 sample at 400 °C. At the same time, the oxygen content was significantly decreased. With the increase of pyrolysis temperature, the carbon content continued to increase, and the oxygen content continued to decrease. Similar trends were observed for the pyrolysis of W-H220. The volatile matters (VM) are around 91.3 and 77.5 % for C-H220 and W-H220, respectively [80]. As a result, the noteworthy conversion happened during pyrolysis at 400 °C. On the other hand, both cellulose and wood were mostly converted into small fragments during HTC 260 °C. Moreover, less VM was observed in C-H260 and W-H260 [80]. Thus, pyrolysis could remove less volatiles from the chars resulting in higher mass yield. Nitrogen, sulfur, and ash content were below detection limits for all samples. The detection limits of the instrument were 1.6, 1.8, and 0.2 wt % for nitrogen, sulfur, and ash, respectively.

Table 13: Ultimate analysis and polarity index of hydrochars and pyrolyzed hydrochars from cellulose and wood

Sample	C (%)	H (%)	N (%)	S (%)	O (%)	Ash (%)	Polarity index	Surface area (m²/g)
C-H220	43.9 ± 0.1	6.2 ± 0.0	BD*	BD*	49.9 ± 0.1	BD*	1.14	1.8 ± 0.0
C-H220-P400	70.9 ± 2.7	3.3 ± 0.2	BD*	BD*	25.9 ± 2.9	BD*	0.37	2.7 ± 0.0
C-H220-P500	78.1 ± 4.3	2.8 ± 0.1	BD*	BD*	19.2 ± 4.3	BD*	0.25	95.9 ± 0.5
C-H220-P600	84.2 ± 2.3	2.3 ± 0.0	BD*	BD*	13.6 ± 2.3	BD*	0.16	357.9 ± 2.7
C-H260	69.8 ± 0.2	4.1 ± 0.1	BD*	BD*	26.1 ± 0.1	BD*	0.37	2.2 ± 0.0
C-H260-P400	69.0 ± 3.6	3.0 ± 0.4	BD*	BD*	28.1 ± 3.9	BD*	0.41	5.5 ± 0.0
C-H260-P500	79.8 ± 6.4	2.8 ± 0.3	BD*	BD*	17.5 ± 6.6	BD*	0.22	81.4 ± 1.3
C-H260-P600	83.4 ± 2.8	2.3 ± 0.0	BD*	BD*	14.3 ± 2.8	BD*	0.17	307.9 ± 1.9
W-H220	52.4 ± 1.1	5.8 ± 0.2	BD*	BD*	41.8 ± 1.3	BD*	0.80	0.4 ± 0.0
W-H220-P400	68.4 ± 3.2	2.9 ± 0.3	BD*	BD*	28.7 ± 3.5	BD*	0.42	1.6 ± 0.0
W-H220-P500	75.9 ± 2.9	2.5 ± 0.1	BD*	BD*	21.5 ± 3.0	BD*	0.28	102.7 ± 1.7
W-H220-P600	80.1 ± 5.7	2.3 ± 0.1	BD*	BD*	17.6 ± 5.6	BD*	0.22	340.3 ± 2.7
W-H260	67.4 ± 0.3	5.0 ± 0.2	BD*	BD*	27.6 ± 0.3	BD*	0.41	1.9 ± 0.0
W-H260-P400	68.7 ± 2.7	3.2 ± 0.0	BD*	BD*	28.1 ± 2.7	BD*	0.41	2.4 ± 0.2
W-H260-P500	77.1 ± 2.1	2.6 ± 0.1	BD*	BD*	20.3 ± 2.2	BD*	0.26	23.7 ± 0.8
W-H260-P600	83.7 ± 3.7	2.3 ± 0.1	BD*	BD*	14.0 ± 3.8	BD*	0.17	298.1 ± 2.7

* Below detection limit

On the other hand, the maximum inorganic was observed around 0.14 % for pyrolyzed hydrochar of wood. According to Zhang *et al.*, the inorganics that have multiple redox states can store electrons [142]. Elements such as Fe (+2, +3) and Cu (+1, +2) can reversibly accept and donate electrons and therefore contribute to the ESC. Although some of these inorganics elements are present in wood, based on their abundances (shown in Figure 20) the total amount of electrons they can store, and thus their maximum contribution to the observed ESC, would be negligible [77]. (Note: All seven metals are multi-valent, but only Cu, Fe, Cr, Mn, and Ni are reversibly redox-active and can therefore store electrons.).

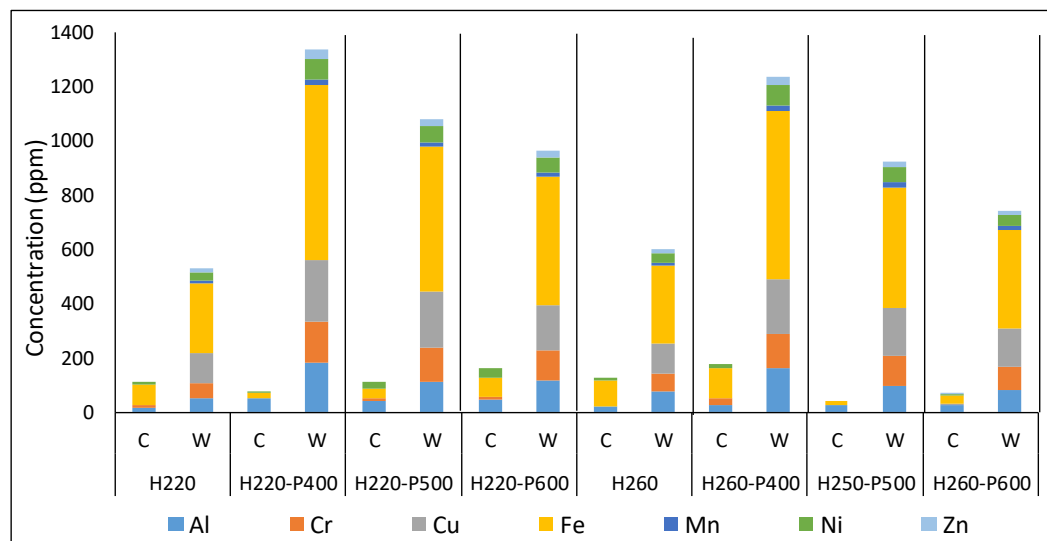


Figure 20: ICP analysis of hydrochars and pyrolyzed hydrochars from cellulose and wood.

3.3.2 Functional groups

Although the surface area of pyrolyzed char was increased by an order of magnitude (as shown in Table 13), the pyrolysis temperature may have an adverse effect on the functional groups on the surface. As functional groups are the main ion-exchange sites, it is important to know their changes with the pyrolysis temperature in order to use them as storage material. The total and individual acidic functional groups are shown in Figure 21. The total acidic functional groups are observed on the C-H200 is $118.0 \pm 14.6 \mu\text{mol/g}$. This number was significantly increased to $926.7 \pm 18.4 \mu\text{mol/g}$ while the pyrolysis was performed of C-H220 at 400°C . This considerable increment might be happened due to two main reasons. Firstly, while the HTC was done at 220°C , hydrolysis of cellulose was just started [39]. As a result, a significant portion of unreacted cellulose remains in the hydrochar. This cellulose takes part in the pyrolysis reaction and creates more functional groups. Secondly, while the functional groups form during the HTC experiment, some of the functional groups might be covered by volatile matters. During the pyrolysis, volatiles started to be removed from the surface and more functional groups were exposed. With the increase of pyrolysis temperature, the total surface functionality decreases on the C-H220. This could be explained from the basis of the polarity index, which is a ratio between oxygen and carbon content. Table 13 shows that the polarity index decreases

with the increase of pyrolysis temperature, which is a hint that the surface is getting more hydrophobic with pyrolysis. The decrease of polarity index (O/C) reveals the reduction of polar groups (-OH and C-O) with pyrolysis temperature [53, 143]. As a result, a decrease in total functional groups was observed. Meanwhile, a different phenomenon was observed during the pyrolysis of C-H260. The total functional groups on the C-H260 was measured of $1268 \pm 23 \mu\text{mol/g}$, which was only decreased with the pyrolysis temperature. A possible reason behind this is that C-H260 is only decomposed and functional groups are polymerized with the increase of pyrolysis temperature. Pyrolyzed hydrochar of W-H220 followed a similar trend of C-H220. However, a little difference was observed for pyrolyzed W-H260 compared to C-H260. The total functional groups increase slightly at P400, possibly because wood is a combination of hemicellulose, cellulose, lignin, and other organic and inorganic constituents.

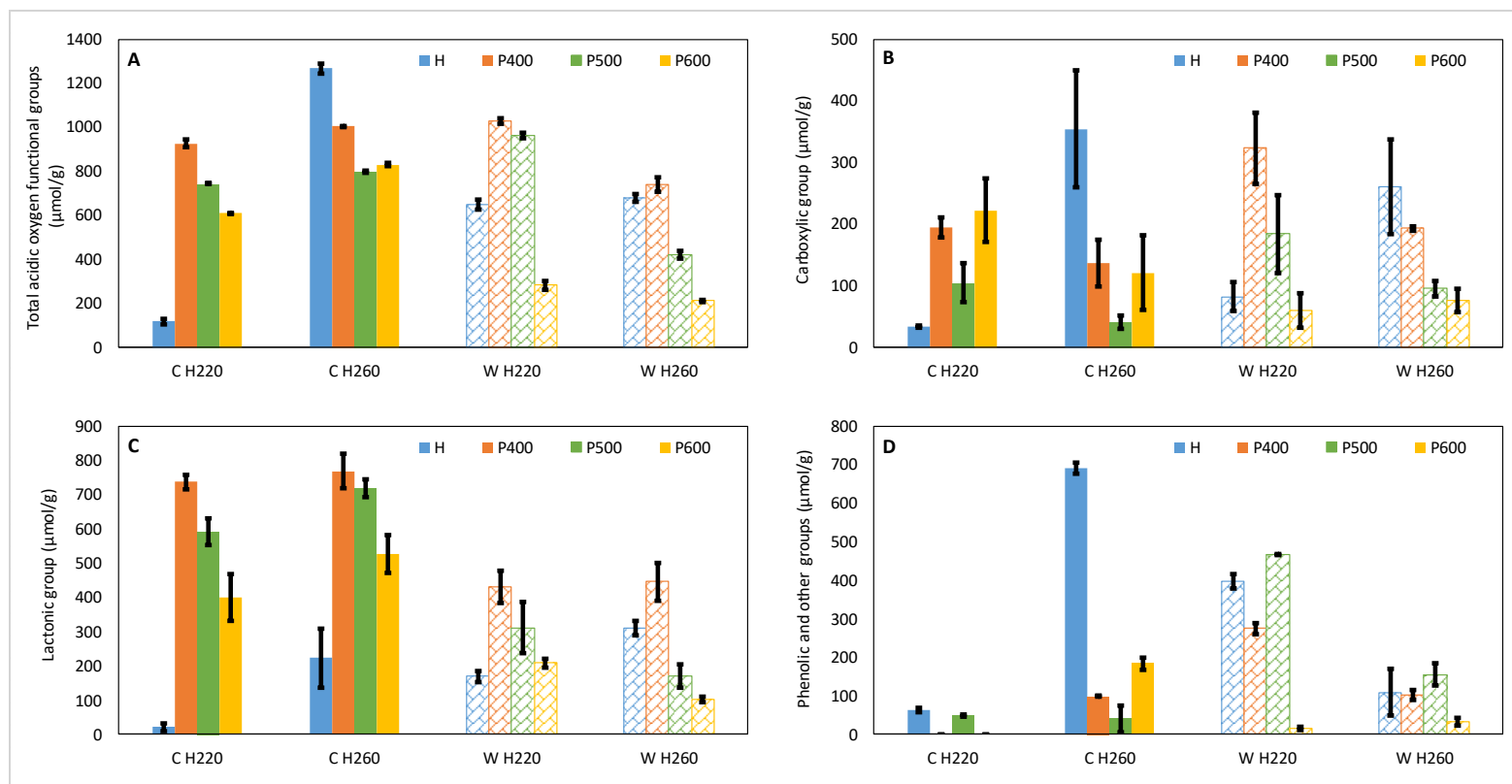


Figure 21: Total and individual oxygen-containing acidic functional groups on chars. A) Total, B) Carboxylic, C) Lactonic, D) Phenolic and other groups

According to literature, lignin degrades between 255–265 °C [119, 129]. So, while the hydrochar was produced from wood at 260 °C, some lignin may remain unreacted. Due to the reaction of that lignin, a slight increase in functionality was observed during P400. The carboxylic group on the cellulose surface was observed 34 ± 2 and 354 ± 95 $\mu\text{mol/g}$ for C-H220 and C-H260, respectively. Similarly, this group on the wood surface was observed 82 ± 24 and 261 ± 76 $\mu\text{mol/g}$ for W-H220 and W-H260, respectively. While the pyrolysis was performed on these samples, wood followed a similar trend as total functional groups. However, a slight deviation was observed for the cellulose when it was pyrolyzed at 600 °C. The carboxylic groups on C-H220-P600 and C-H260-P600 were higher compared to C-H220-P500 and C-H260-P500. As it is already mentioned earlier that with the increase of pyrolysis temperature, some functional groups are polymerized, while some are decomposed. At P600, perhaps the polymerization and decomposition of the carboxylic groups are lower than the formation of the carboxylic groups due to the decomposition of other groups. This could be the reason why the carboxylic groups are higher on the surface of C-H220 and C-H260 when pyrolyzed at P600 compared to P500. FTIR results are shown in Figure 22 also confirmed that the carboxylic bonds at 3300 cm^{-1} , and 1760 cm^{-1} were reduced with the pyrolysis temperature; however, a carboxylic bond at $1706\text{--}1720\text{ cm}^{-1}$ appears at P600.

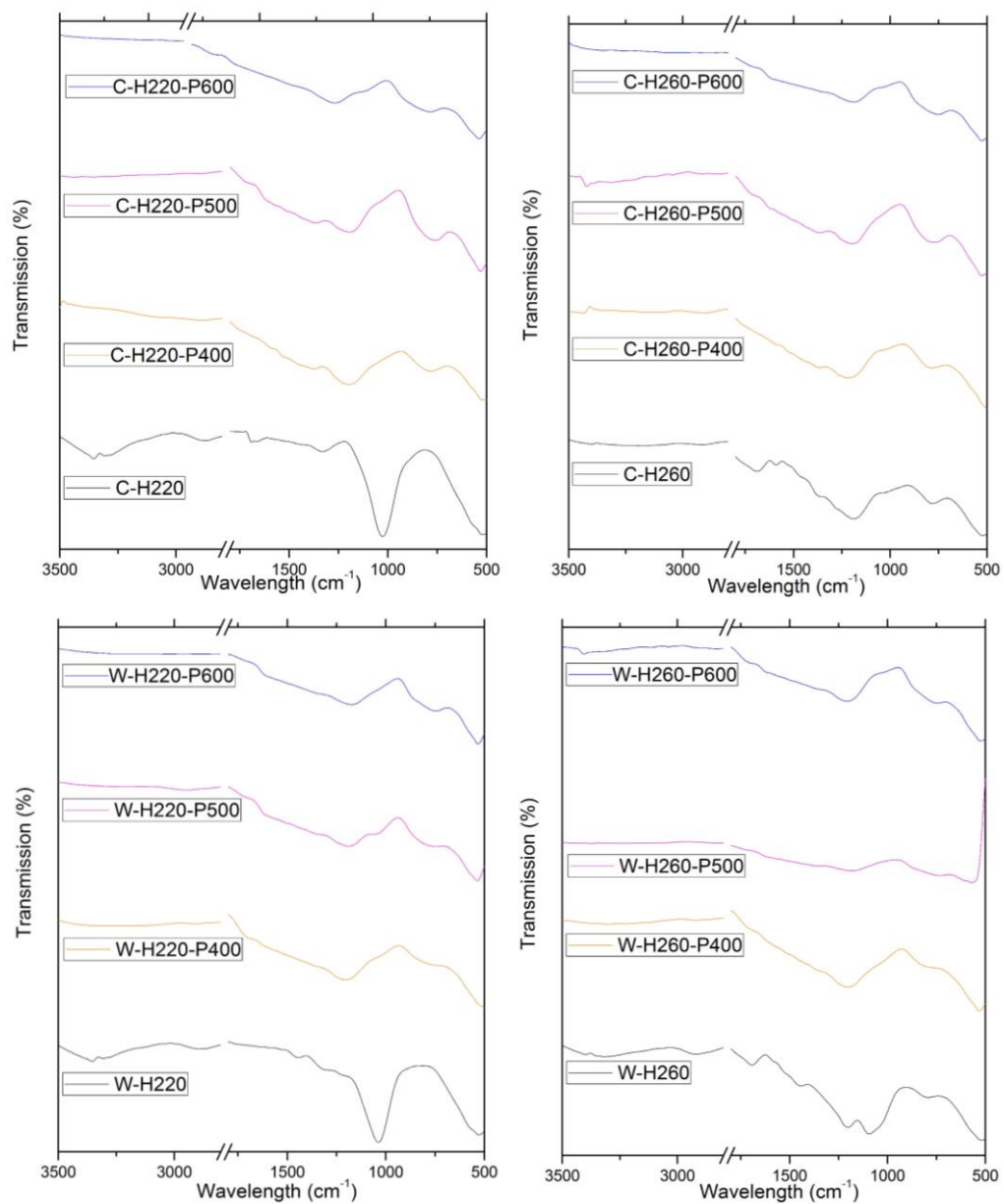


Figure 22: FTIR spectra of cellulose and wood at 200 and 260 °C, and their corresponding pyrolyzed hydrochars at 400, 500, and 600 °C.

The number of lactonic groups increases considerably at P400 compared to their corresponding hydrochars. However, the number decreases from 737.3 ± 21.1 to 401 ± 69 $\mu\text{mol/g}$ and 768 ± 50 to 527 ± 56 $\mu\text{mol/g}$ for C-H220-P600 and C-H260-P600, respectively. Similarly, this number decreases from 430 ± 47 to 208 ± 15 $\mu\text{mol/g}$ and 445 ± 55 to 103 ± 8 $\mu\text{mol/g}$ for W-H220-P600 and W-H260-P600, respectively. An increase of the lactonic group was observed at P400 because C=O remained largely unchanged until this pyrolysis condition [144]. Besides the higher stability, the removal of volatiles may have exposed more esters ($1735\text{--}1750$ cm^{-1}) and aliphatic ketones ($1705\text{--}1725$ cm^{-1}), which are evident in the FTIR spectra of C/W-H220-P400 shown in Figure 22. The number of lactonic groups decreases afterward with the increase of pyrolysis temperature as the C=O bond started to decrease at 500 $^{\circ}\text{C}$ and disappeared at 600 $^{\circ}\text{C}$ [144].

Although the acidic groups other than carboxylic and lactonic groups are often called as “phenolic group” in the literature, it is considered as “phenolic and other groups” in this study [83, 89]. Phenolic and other groups on the hydrochars and pyrolyzed hydrochars did not follow any consistent trend shown in Figure 21D. None of the phenolic and other groups has C=O, which could store electrons. As a result, this group might not be a possible contributor of ESC.

Figure 23 shows the variation of BFGs on pyrolyzed chars. The effect of pyrolysis temperature on BFGs of C-H220 and C-H260 showed a different pattern. The BFGs on C-H220 showed an increasing trend with the pyrolysis temperature, while the BFGs increased around three-fold at P400 and stayed similar at higher pyrolysis temperatures for the C-H260 sample. Despite the fact that the hydrolysis of cellulose just started at 220 °C during HTC, a significant portion of unreacted cellulose remains in the C-H220 sample [80, 145]. In addition, condensation reactions occur during the cooldown of the HTC experiments. This condensation could create a layer that covers the –OH groups on the hydrochar surface [97, 98, 113, 145]. This layer could be removed and exposed to the BFGs during the pyrolysis at low temperatures. Additionally, unreacted cellulose could take part in the reaction with the increase of pyrolysis temperature. Both of these could be the reasons for the increasing trend of BFGs for C-H220 at all pyrolyzed conditions. In contrast, cellulose is fully reacted during HTC at 260 °C. A condensation layer would be the most possible cause of getting low BFGs on the hydrochar. As soon as the layer was removed at P400, there was no more unreacted cellulose remained in C-H260 that can react with the increase of pyrolysis temperature. As a result, after the significant initial increment, the BFGs number remains the same even at higher temperatures, which also proves the thermal stability of C-H260 [43].

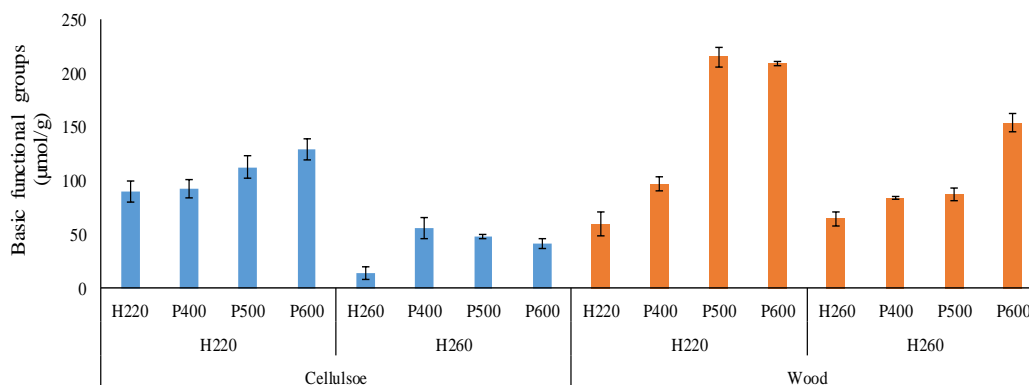


Figure 23: Basic functional groups on pyrolyzed hydrochars produced from cellulose and wood at different temperatures

On the other hand, both W-H220 and W-H260 showed a similar BFGs pattern with the pyrolysis. Both showed that the BFGs increase with the increase of pyrolysis temperature. As wood is a mixture of different components mentioned in the above section, they react at different HTC temperatures between 180–265 °C [103, 119, 145]. As a result, there could be a possibility of some unreacted components of wood in their hydrochar including the condensate layer. According to the literature, the lignocellulosic materials degrade and form biochar (product of pyrolysis) at a pyrolysis temperature range between 200–500 °C where, hemicellulose reacts at 200–300 °C, cellulose reacts at around 400 °C, and lignin reacts at around 500 °C [146]. Therefore, with the increase of pyrolysis temperature, not only the condensate

layer was removed but also the unreacted component was reacted that caused an increasing trend of BFGs on pyrolyzed wood hydrochars.

The FTIR spectra are shown in Figure 22 also confirmed that the intensity of the peaks for a strong alcoholic band at $3200\text{--}3550\text{ cm}^{-1}$, bending alcoholic bond at $1330\text{--}1420\text{ cm}^{-1}$, primary, secondary, and tertiary alcoholic bonds at $1050\text{--}1085\text{ cm}^{-1}$, $1087\text{--}1124\text{ cm}^{-1}$, and $1124\text{--}1205\text{ cm}^{-1}$, respectively vary with the pyrolysis temperature, which could be an indication of the variation of BFGs. In the case of C-H220, a strong peak observed at 3340 cm^{-1} , which indicates an alcoholic bond. With the pyrolysis temperature, although the peak at 3340 cm^{-1} disappeared, some new peaks appeared in the primary ($1050\text{--}1085\text{ cm}^{-1}$), secondary ($1087\text{--}1124\text{ cm}^{-1}$), and tertiary ($1124\text{--}1205\text{ cm}^{-1}$) alcoholic region, which is an indication of the increase of BFGs shown in Figure 22. On the other hand, only a small peak was visible in the bending alcoholic region on C-H260 which is an indication of low BFGs. Along with the pyrolysis temperature, several alcoholic bonds appear at 3425 cm^{-1} , 1140 cm^{-1} , and stayed steady. This behavior of the peaks can easily be correlated with the quantified BFGs discussed in the earlier part. In the case of both wood hydrochars, the peak at 3340 cm^{-1} disappeared with the pyrolysis temperature, but a strong tertiary bond appears at 1200 cm^{-1} , resulting in an increasing trend of BFGs.

3.3.3 pH and pH_{PZC}

As the acidic functional groups decrease with the pyrolysis temperature, the pH of the pyrolyzed chars can be expected to be increased which means they would be less acidic. Figure 24 shows the pH of hydrochars and their pyrolyzed chars. The pH of C-H220 and C-H260 were found 4.9 ± 0.0 and 3.8 ± 0.1 , respectively. Similarly, the values were 4.5 ± 0.1 and 4.0 ± 0.1 for W-H220 and W-H260, respectively. The pH of C-H220 and C-H260 increase with pyrolysis temperature and ended up with 5.4 ± 0.0 and 5.1 ± 0.1 at C-H220-P600 and C-H260-P600, respectively. Similarly, it increases for W-H220 and W-H260 and being ended with 7.2 ± 0.1 and 6.3 ± 0.1 at W-H220-P600 and W-H260-P600, respectively. It is shown in Figure 21 that the carboxylic group decreases and then increases with the pyrolysis temperature, but the lactonic group decreases for cellulose. As a result, it could be hypothesized that the lactonic group might be more dominant to increase the pH of cellulose. However, both groups decrease for wood, which means both groups may have a similar effect on pH. An increase of pH means either a decrease of H^+ ion or proliferation of OH^- . Since dehydration occurred during the pyrolysis, a reduction of OH^- ions could happen on the hydrochar surface. This phenomenon is also supported by the pH of the pyrolyzed char shown in Figure 24. It also shows the measured values of pH_{PZC} for hydrochar at different pyrolysis temperatures. The pH_{PZC} for all pyrolyzed

hydrochars increased with a temperature similar to pH. The pH and pH_{PZC} of C-H220 were observed 4.9 ± 0.0 and 3.4 ± 0.1 , respectively. This indicates that the surface of cellulose hydrochar produced at $220\text{ }^{\circ}\text{C}$ is negatively charged. This char still stayed negatively charged after pyrolysis at $400\text{ }^{\circ}\text{C}$; however, the negativity is reduced. With the increase of pyrolysis temperature, the char transferred from negatively charged to positively charged as the pH_{PZC} is higher than pH. This transformation might be due to the dehydration or degradation of negative ions. The hydrochar surface became more positively charged at P600. A similar phenomenon happened while the pyrolysis was performed on C-H260 at different temperatures.

Although wood hydrochars did not change (negative to positive charge) as cellulose hydrochars, they reduced their negativity with the pyrolysis temperature. The pH and pH_{PZC} of W-H220 were observed 4.5 ± 0.1 and 3.8 ± 0.0 , respectively. With the pyrolysis temperature, the pH_{PZC} was increased; at the same time, the pH also increased. However, it was observed that the pH was always higher than the pH_{PZC} which could possibly mean that the surface of the pyrolyzed W-H220 remained negatively charged. Although it remained negatively charged, the magnitude of the negativity decreased with the pyrolysis temperature. In the case of W-H260, a similar manifestation was observed. A common scenario was observed for both feedstocks, pyrolyzed char reduced their negative charge strength with pyrolysis temperature. As

they were reducing the negative strength, they were supposed to adsorb less proton on the char.

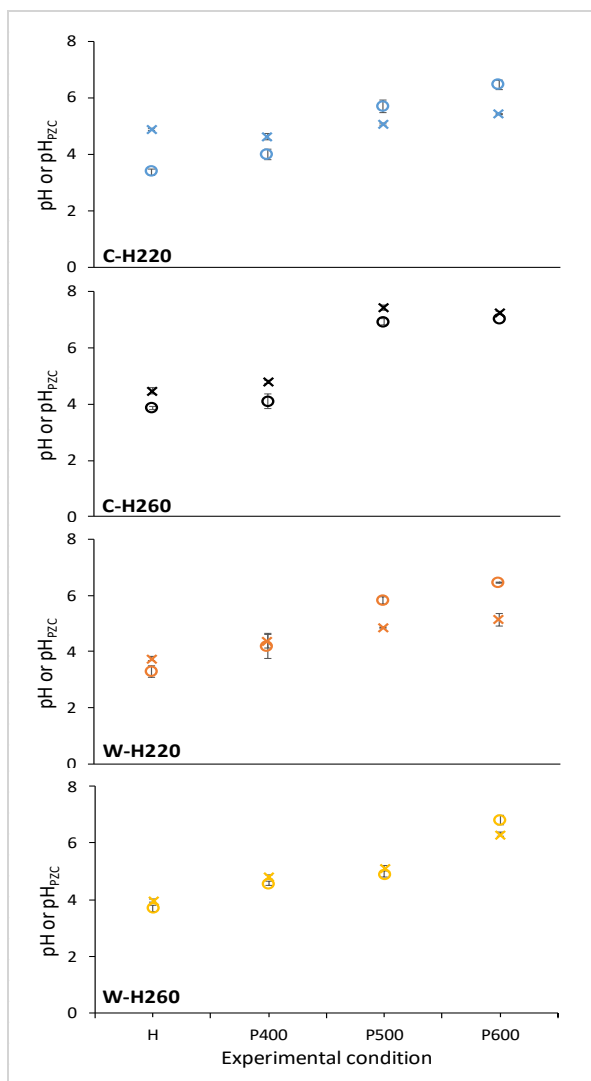


Figure 24: pH and pH_{PZC} of hydrochars and pyrolyzed hydrochars from cellulose and wood; cross markup is for pH and circular markup is for pH_{PZC}.

3.4 Applications

3.4.1 An alternative energy

The world energy demand continues to grow with the increase of populations. The energy demand is projected to reach up to 42 quadrillions British Thermal Unit (BTU) in 2040 to fulfill the needs of 10 billion people [147, 148]. In order to ensure this energy supply is provided in a sustainable manner, fossil fuel industries need to begin integrating with renewable energy sources. Coal power plants, one of the major electricity producers in the U.S., are still expected to provide 17.6 % more electricity in 2040 compared to today [148]. This sustainability problem provides extraordinary potential for coal-like fuels generated from renewable resources. Wet waste biomass, such as PMS, is one of the largest and most abundant sources of renewable energy [149]. In fact, around 16.5 million dry tons of PMS have been produced annually in the U.S. These wastes have been landfilled, land applied, incinerated, or used in other ways (e.g., filler, fibers, composite, etc.) [150]. Due to the strict landfill policies and shortage of lands, incineration is becoming the preferred treatment method despite having incineration costs of around \$13–15 per dry ton [151]. Co-firing PMS with coal in existing coal-fired power plants may reduce the carbon footprint for the power plant, and it may reduce the cost of waste disposal for the paper mill by generating a sellable product rather than waste [152, 153]. However, viable co-firing requires a

feedstock of consistent quality with higher energy density and combustion characteristics compatible with coal. As a result, the HTC of various PMS have been conducted and investigated the fuel properties of the produced hydrochars.

3.4.1.1 Fuel characteristics of hydrochars

It was observed that the carbon contents in the PMS hydrochars were increased with HTC, while oxygen contents were decreased, resulting in increases of HHV_{daf} . While this increase makes the hydrochars more similar to bituminous coal, another factor to consider is that there is clearly a wide range of ash contents observed in PMS samples, which will impact fuel quality. Additionally, the combustion properties of those hydrochars are required to further evaluate the fuel characteristics in order to determine the feasibility of co-combustion with coal. Pyrolysis thermograms of various hydrochars, shown in Figure 25, illustrate the TG curves and DTG curves for hydrochars produced at 260 °C from PS, DPS, PSS₁, PSS₂, PFR, and PTS with respect to TG pyrolysis temperatures. The TG curves for PS-H260, PSS₂-H260, PFR-H260, and PTS-H260 showed a rapid mass loss between 190 to 550 °C, with a maximum mass loss rate of -4.14 , -7.86 , -6.05 , and -6.48 % min^{-1} , respectively. This rapid mass loss could be attributed to the high volatile materials present in these hydrochars [154]. The PSS₂-H260 lost 61 % of its initial mass during the complete pyrolysis stage, which was the maximum among others, while the PS-H260, PFR-

H260, and PTS-H260 have lost 51, 55, and 43 %, respectively. Although PSS₁ and PSS₂ both are mixtures of primary and secondary sludges, the TG curve of PSS₁-H260 exhibited a slow mass loss for the same temperature range with a maximum mass loss rate of $-3.21 \text{ \% min}^{-1}$ compared to PSS₂-H260 and lost 46 % of its initial mass. This is another confirmation that the sources of these samples were different and/or the ratios of primary to secondary sludges are not the same. The TG curve of DPS-H260 displayed a maximum mass loss rate of $-7.13 \text{ \% min}^{-1}$ at a much higher temperature range of 640–780 °C. The presence of higher inorganic compounds or lignin could be the possible reason for this shift towards higher temperatures compared to other sludges [138]. The TG curve for PS, which is dewatered PTS [132], also illustrated its maximum mass loss rate in this temperature range. The DTG curves for all the hydrochars, except for PSS₁-H260 and PSS₂-H260, showed two distinct peaks at two different temperature ranges of 310–400 °C and 640–780 °C, respectively. The DTG curves of PSS₁-H260 and PSS₂-H260 displayed only one major peak in between 310–400 °C. All DTG curves have minor peaks after the major peak in the temperature range of 310–400 °C. The origin of these peaks can be explained from the constituents of PMS. Yanfen *et al.* stated that paper pulp and fiber are the main organic elements of PMS and because of the degradation of hemicellulose, cellulose, and lignin present in the sludges are primarily responsible for these peaks [138]. Previous studies have also found that hemicellulose

decomposes between 200–300 °C during pyrolysis, while cellulose decomposes between 300–400 °C. The pyrolysis of lignin starts above 300 °C and continues for a wide temperature range [133].

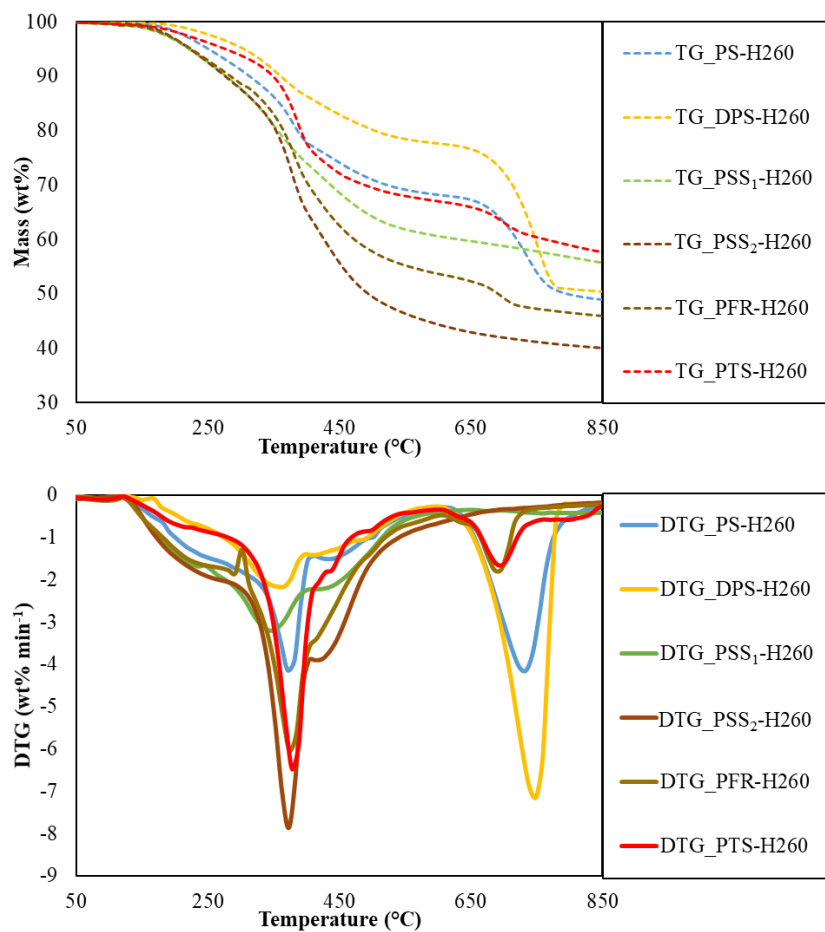


Figure 25: Pyrolysis thermographs (top) and DTG curves (bottom) plotted versus temperature for all 260 °C HTC treated paper mill sludges.

All the peaks illustrated in the DTG curve of Figure 25 (bottom) agree with these findings. The peaks before 400 °C attributed to the complete decomposition of hemicellulose and cellulose and partial decomposition of lignin as it degrades over a wide range of pyrolysis temperatures. The peaks after 400 °C correspond to the complete breaking of lignin [91]. However, the second peak for PS and DPS emerged at 750 °C. The pyrolysis of chemicals (i.e., additives, coagulants, flocculants, CaCO₃, and other minerals) present in the PS and DPS could be the possible reason for the emergence of the second peak at a higher temperature compared to other sludges [138, 155].

Figure 26 shows the co-combustion thermograph of coal, hydrochar of one paper mill sludge (PTS) at 260 °C, and their 50–50 mix. These parameters were selected because the PTS hydrochar saw the greatest energy densification at 260°C. Additionally, 50% mass should allow for both components to show combustions characteristic to determine if any positive or negative synergistic effects exist during co-firing. The PTS hydrothermally treated at 260 °C was co-combusted with coal to examine the combustion characteristics through the TG curve and the first negative derivative of the DTG curve. The TG curve of this PTS hydrochar showed a rapid mass loss of approximately 60 % from 170–350 °C. This rapid mass loss occurred due to the presence of highly volatile materials (~ 45 %) in PTS hydrochar [133]. However, the TG curve for coal displayed a comparatively slow mass loss from

170–608 °C as it contained low volatile materials than PTS hydrochar treated at 260 °C.

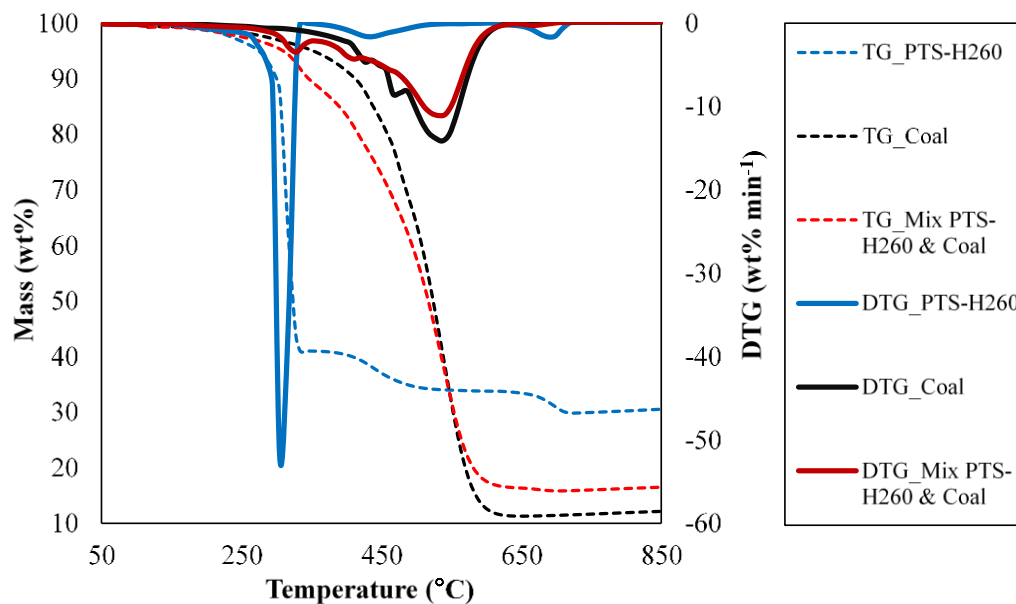


Figure 26: Combustion thermograph and DTG curves plotted versus temperature for 260 °C HTC treated PMS, coal and 50% mixtures of coal and hydrochar (TG nomenclature refers to mass loss on the left axis and DTG can be found on the right axis).

Additional efforts were made to analyze the combustion characteristics of Clarion # 5a coal (VM and FC are 34.3 ± 0.0 and 54.0 ± 0.5 , respectively), all the HTC-260 hydrochars and their 50–50 (wt. % dry basis) mix with coal. During co-combustion, DPS-H260 was not considered as it has low ED compared to other PMS as discussed

in earlier sections. All the parameters of combustion characteristics are presented in Table 14. Ignition and burnout indices were calculated using equations (14) and (15). The ignition temperatures for all the hydrochars produced at 260 °C, except for DPS-H260, were low compared to coal as they contain high volatile material than coal [156]. The presence of high inorganics in DPS could be a reason for high ignition temperature. The other combustion parameters of the same hydrochar also deviated a lot compared to coal. However, when other 260's hydrochars were mixed with coal, these deviations became small. For example, before mixing, the values of ignition temperature, ignition time, burnout temperature, burnout time, DTG_{max} , DTG_{max} time, ignition and burnout indices for PTS-H260 were 294.2 °C, 20.3 min, 342.8 °C, 22.8 min, $-52.1\% \text{ min}^{-1}$, 20.8 min, 1.24×10^{-01} , and 5.40×10^{-03} , respectively. When mixed with coal, these values became 430.5 °C, 26.8 min, 692.0 °C, 39.8 min, $-11.1\% \text{ min}^{-1}$, 31.8 min, 1.31×10^{-02} , and 3.12×10^{-04} , respectively, which were close to the values for coal shown in Table 14. However, in the case of PS-H260, the deviations were still large even though the DTG_{max} value became closer than all the other hydrochars. So, it is evident from Table 14 that combusting hydrochar produced from PMS at 260 °C (except PS) with coal made the co-combusting characteristic similar to coal.

Table 14: Combustion characteristics of determined from combustion TGA data. (Clarion #5a coal (bituminous) was used for co-combustion [134])

Sample	Ignition temperature (°C)	Ignition time (min)	DTG _{max} (% min ⁻¹)	Burnout temperature (°C)	Burnout time (min)	DTG _{max} time (min)	Ignition index, D _i	Burnout index, D _B
PS-H260	380.4	23.8	-19.4	752.5	42.3	25.8	3.17x10 ⁻⁰²	7.19x10 ⁻⁰⁴
DPS-H260	628.1	36.3	-6.6	788.7	44.3	41.8	4.39x10 ⁻⁰³	9.10x10 ⁻⁰⁵
PSS ₁ -H260	262.0	18.8	-8.6	606.4	35.8	20.8	2.21x10 ⁻⁰²	5.88x10 ⁻⁰⁴
PSS ₂ -H260	273.0	19.3	-41.7	557.1	33.3	19.8	1.10x10 ⁻⁰¹	3.26x10 ⁻⁰³
PFR-H260	294.1	20.3	-38.0	708.4	40.8	21.3	8.82x10 ⁻⁰²	2.10x10 ⁻⁰³
PTS-H260	294.2	20.3	-52.1	718.5	41.3	20.8	1.24x10 ⁻⁰¹	2.98x10 ⁻⁰³
Coal	466.7	28.8	-14.2	627.8	36.8	32.3	1.53x10 ⁻⁰²	4.19x10 ⁻⁰⁴
50% Coal+50%PS-H260	305.3	20.8	-14.5	739.4	42.3	21.8	3.22x10 ⁻⁰²	7.49x10 ⁻⁰⁴
50% Coal+50% PSS ₁ -H260	386.3	24.8	-7.0	648.0	37.8	31.8	8.97x10 ⁻⁰³	2.10x10 ⁻⁰⁴
50% Coal+50% PSS ₂ -H260	398.7	24.8	-9.9	660.3	37.8	31.3	1.28x10 ⁻⁰²	3.16x10 ⁻⁰⁴
50% Coal+50% PFR-H260	410.3	25.3	-7.5	701.8	39.8	31.8	9.38x10 ⁻⁰³	2.46x10 ⁻⁰⁴
50% Coal+50% PTS-H260	430.5	26.8	-11.1	692.0	39.8	31.8	1.31x10 ⁻⁰²	3.12x10 ⁻⁰⁴

The combustion indices indicate that hydrochar produced from paper mill sludges have lower ignition temperatures and higher burnout temperatures than raw bituminous coal. However, co-firing with coal and hydrochar showed higher ignition temperatures and lower burnout temperatures. Moreover, most of the hydrochars, specifically hydrochars from primary and secondary sludge, have shown very similar combustion thermograms to coal. In addition, by considering the ash content in the feedstocks and their hydrochars, PSS₂ could be a suitable co-fired option in existing coal-fired power plants.

3.4.2 An adsorbent material

One of the key factors of developing a circular economy is the efficient valorization of agricultural and agro-industrial wastes, such as sunflower stems, walnut shells, olive stones, palm empty fruit bunches, orange peel, grape skin, etc. In particular, most of the orange peel waste is coming from the citrus industry and is commonly known as citrus waste while the grape skin waste is from the winery and is referred to as winery waste. Grapes skin is a rich source of phenolic compounds (both flavonoids and non-flavonoids) and has a very high sugar content [157]. On the other hand, orange peel is acidic. Both wastes are wet and contain a significant amount of moisture. As a result, the use of these wastes directly as fuel and soil improver is economically unfavorable. Therefore, the advancement of the conversion techniques

of the aforementioned wet wastes into valuable materials, such as adsorbents to reduce the environmental liability from juice and winery industries. Therefore, the hydrochars were produced from orange peel and grape skin at various temperatures and studied their dye adsorption potential. The following sections will discuss the findings from the adsorption study.

3.4.2.1 Effect of solution's pH on adsorption

The pH of the solution highly affects the surface charge of the adsorbent, which ultimately controls the adsorption process. The effect of the initial pH of the solution in a range of 3 to 11 was studied for the removal of dye by hydrochar samples as shown in Figure 27. The results indicate that the solution's pH significantly affects the adsorption, particularly under the highest alkaline condition (pH = 11) for both types of hydrochars. The adsorption capacity was found to be slightly lower in acidic environment compared to the neutral condition. Although the adsorption remained more or less similar at pH 8 and 10, it increased around 3 to 4 times at pH 11 compared to the amount adsorbed at pH 7. The reason could be the ion exchange between the hydrochar surface and the cationic dye molecule. At lower initial pH values (3–6), the solution contains an excess amount of hydrogen ions (H^+) which competed with the cationic dye to attack the active sites of the hydrochar.

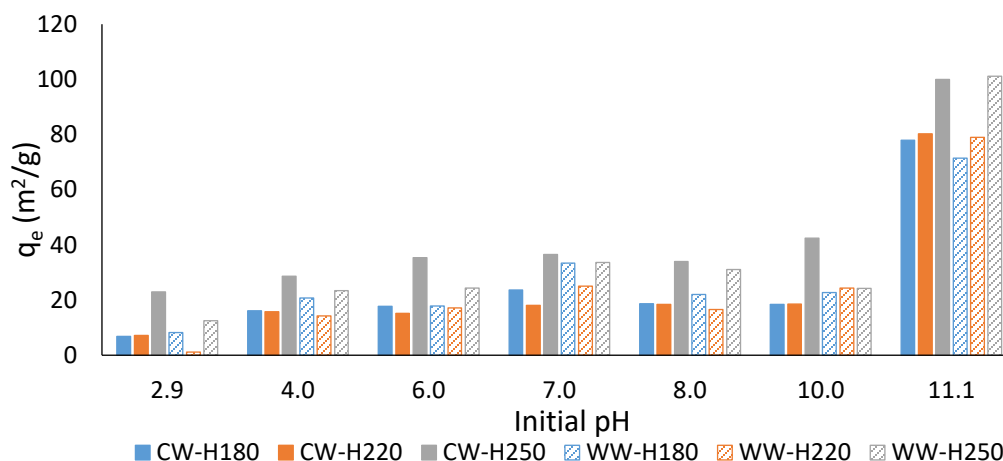


Figure 27: Effect of solution's pH on dye adsorption by hydrochars produced from citrus and winery wastes.

Due to the competition of finding active sites, a decrease of adsorption was observed at lower initial pHs. On the other hand, at higher initial pH (> 7.0) of the solution, the surface attains a negative charge. Thus, an increase in the electrostatic attraction between a positively charged (cationic) dye and a negatively charged adsorbent was achieved, resulting an increase in adsorption [158]. The reason of spectacular growth of the adsorption capacity from pH 10 to 11.1 could be due to the further increase of the dissociation degree of H^+ by the oxygen containing functional groups at elevated pH, resulting to maximize the electronegativity of the hydrochar and the electrostatic attractive force between dye and hydrochar [159-161].

As all of the studied hydrochars have dominant acidic groups on the surface, the adsorption of a basic dye should be suitable. However, having different adsorption capacity indicates that the mechanism of adsorption on CW and WW hydrochars not only involves electrostatic attractions but also involves other interactions, such as pore filling, hydrogen bonding, or π - π interaction [126, 162, 163].

3.4.2.2 Adsorption isotherm

The adsorption isotherm is an indication of the presence of adsorbate in the liquid (contaminated stream) and the solid (adsorbent) phases at a certain temperature. Investigating the adsorption isotherms will allow to understand the type of adsorption whether it is monolayer adsorption (Langmuir) or multilayer adsorption (Freundlich). The adsorption isotherms for the hydrochars at different adsorption temperatures are shown in Figure 28. The corresponding parameters, such as the maximum adsorption capacity, Langmuir and Freundlich coefficients are also shown in Table 15. From Figure 28, it is clear that the adsorption capacity of both CW and WW decreased with the increase of their treatment temperature. For example, CW-H180 showed maximum adsorption capacity (Q_{\max}) 66 mg/g at 4 °C, while CW-H250 showed 29 mg/g at the same adsorption temperature. A similar trend was followed by other samples in this study and is in accordance with what was obtained when using

sewage sludge hydrochars obtained at similar temperatures (namely: 190, 220, and 250 °C) for methylene blue adsorption [162].

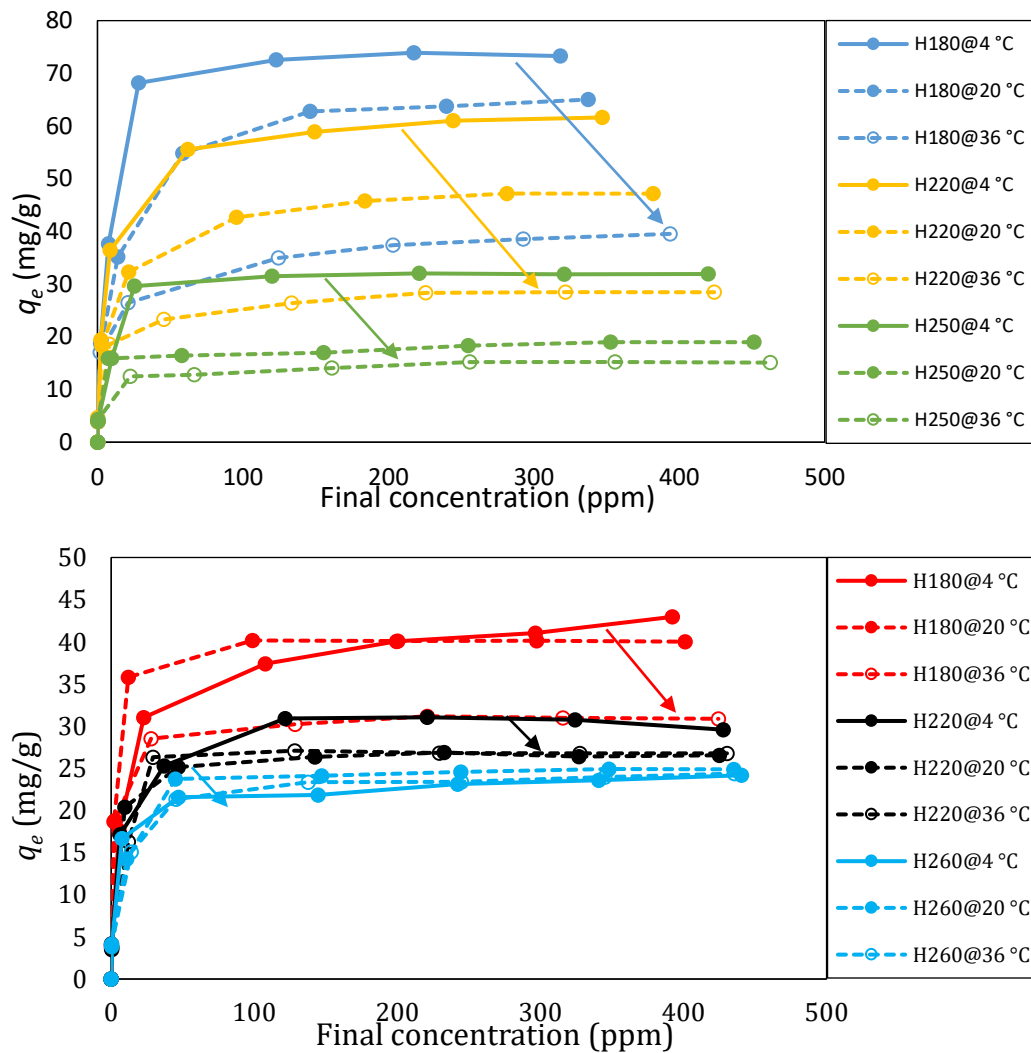


Figure 28: Equilibrium adsorption of dye at different temperatures on hydrochars produced from citrus wastes (top) and winery wastes (bottom).

The Q_{\max} of the hydrochars exhibited the following order: CW-H180 > CW-H220 > CW-H250 and WW-H180 > WW-H220 > WW-H250 as shown in Table 15. In contrast, the BET surface areas were followed opposite trends CW-H250 > CW-H220 > CW-H180 and WW-H250 > WW-H220 > WW-H180 as shown in Table 9. These results demonstrated that other adsorption mechanisms are presented along with pore filling. In this case, the presence of oxygen functional groups could play a role. For example, both CW-H180 and WW-H180 have a lower amount of basic functional groups and a higher amount of carboxylic groups, which could favor the methylene blue adsorption, as it is a cationic or basic dye. In contrast, the basic groups increased with the HTC temperature while the carboxylic groups decreased, which makes the environment adverse to adsorb the dye as a result lower adsorption was observed at a higher temperature. In addition, the presence of lower functional groups per square meter of hydrochar surface could be another reason for the lower adsorption. Similar to the HTC temperature, adsorption capacity was strongly affected by the adsorption temperature shown in Figure 28 and Table 15. The operation temperatures also showed similar trends as the HTC temperature followed. WW-H250 showed minimum effect (about 17 %) of operation temperature on adsorption, while CW-H250 showed the maximum change (about 50 %) in adsorption capacity. Although CW-H250 has the highest surface area among all

studied samples, at the same time, it has the lowest density of functional groups, which could be the determining factor of having the lowest adsorption capacity.

All the isotherms shown in Figure 28 were classified as L-type, which corresponds to the Langmuir isotherm according to the classification. This type of isotherm is characterized by a decreasing slope with the increase of concentration as the vacant sites of the adsorbent decrease as it becomes covered by the adsorbate [164]. This adsorption behavior could also be explained by the high affinity of the adsorbent at low concentrations, which decreases further as concentration increases. The higher correlation coefficients (R^2) of the Langmuir model shown in Table 15 support this hypothesis. The equilibrium data were also fitted to the Freundlich equation and determined the parameters K_F and n_F . The R^2 values of the Freundlich model were found to be significantly lower than the Langmuir model. Ferrentino *et al.* observed a similar finding when using sewage sludge hydrochars obtained at similar temperatures [162]. All the values of dimensionless separation factor (R_L) shown in Table 16 fall between 0–1, which confirm the favorable uptake of the dye. Therefore, it can be concluded that the adsorption of dye onto CW and WW hydrochars mostly followed the Langmuir isotherm rather than the Freundlich isotherm.

Table 15: Methylene blue adsorption by hydrochars produced from citrus and winery wastes: corresponding isotherm parameters from the Langmuir and Freundlich models.

Temperature (°C)	Sample ID	Langmuir parameters			Freundlich parameters		
		Q_{max} (mg/g)	K_L	R^2	K_F	n_F	R^2
4	CW-H180	66.23	0.23	0.99	11.16	2.56	0.87
	CW-H220	60.24	0.21	0.99	10.15	2.79	0.86
	CW-H250	28.57	0.49	0.98	7.13	3.47	0.85
	WW-H180	36.63	0.29	0.99	7.42	3.04	0.89
	WW-H220	28.57	0.40	0.99	6.93	3.52	0.87
	WW-H250	22.83	0.46	0.99	6.55	4.13	0.84
20	CW-H180	51.02	0.34	0.99	9.72	2.68	0.92
	CW-H220	40.00	0.46	0.99	8.96	3.13	0.91
	CW-H250	17.89	1.24	0.99	6.86	5.34	0.82
	WW-H180	36.63	1.01	0.99	11.01	3.86	0.83
	WW-H220	25.97	0.64	0.99	6.99	3.85	0.85
	WW-H250	22.52	0.76	0.98	6.71	4.07	0.92
36	CW-H180	31.65	1.54	0.98	10.25	4.00	0.93
	CW-H220	25.64	1.10	0.99	8.30	4.33	0.92
	CW-H250	14.16	1.59	0.99	5.92	5.87	0.94
	WW-H180	28.65	1.96	0.99	9.64	4.36	0.85
	WW-H220	24.63	1.16	0.98	7.82	4.20	0.89
	WW-H250	21.69	1.11	0.98	6.82	4.25	0.94

Table 16: Separation factor of the Langmuir model.

Feedstock	Initial conc. (ppm)	H180			H220			H250		
		4 °C	20 °C	36 °C	4 °C	20 °C	36 °C	4 °C	20 °C	36 °C
CW	10	0.998	0.997	0.985	0.998	0.995	0.989	0.995	0.988	0.984
	50	0.988	0.983	0.928	0.990	0.977	0.948	0.976	0.941	0.926
	100	0.977	0.967	0.866	0.980	0.956	0.901	0.953	0.889	0.863
	200	0.955	0.936	0.764	0.960	0.915	0.820	0.911	0.800	0.758
	300	0.934	0.907	0.684	0.941	0.878	0.752	0.872	0.728	0.677
	400	0.914	0.880	0.619	0.923	0.844	0.695	0.836	0.667	0.611
	500	0.895	0.854	0.565	0.906	0.812	0.645	0.803	0.616	0.557
WW	10	0.997	0.990	0.981	0.996	0.994	0.989	0.995	0.992	0.989
	50	0.986	0.952	0.911	0.981	0.969	0.945	0.978	0.964	0.947
	100	0.972	0.908	0.836	0.962	0.940	0.896	0.956	0.930	0.900
	200	0.946	0.831	0.718	0.927	0.887	0.811	0.916	0.869	0.818
	300	0.920	0.767	0.630	0.894	0.839	0.741	0.879	0.815	0.750
	400	0.897	0.711	0.560	0.863	0.797	0.682	0.845	0.768	0.692
	500	0.874	0.663	0.505	0.835	0.758	0.632	0.813	0.726	0.643

Moreover, the lower adsorption capacities at higher temperatures demonstrated that the dye removal process by the studied hydrochar could involve physical adsorption. Although adsorption isotherms can contribute to revealing the adsorption mechanism, it is also useful in regards to obtaining thermodynamic parameters.

3.4.2.3 Adsorption thermodynamics

The dye adsorption process could be either physical or chemical or both. The adsorption mechanism of a study is highly directed by its thermodynamic properties, such as ΔG , ΔS , and ΔH . The thermodynamic parameters of adsorption process by CW and WW hydrochars are shown in Table 17. The results revealed that the adsorption phenomenon of both hydrochars occurred spontaneously, as the ΔG values at all temperatures are negative [165]. This finding agreed with the conclusions drawn from the separation factor (R_L) analysis described in the previous section, where all the values of R_L varied between 0 and 1. The results also showed that the ΔG values decreased further about 20 to 25 % and 18 to 25 % for CW and WW, respectively with the increase of adsorption temperature. Additionally, the ΔG values decrease with the increase of HTC temperature. These demonstrated that the adsorption on studied hydrochars was unfavorable at higher temperatures (both HTC and adsorption temperature). A similar observation was found by Tan *et. al.* and Tran *et. al.* where they studied the methylene blue and methylene green adsorption on

activated carbon derived from oil palm fibre and hydrochars derived from golden shower pod, coconut shell, orange peel, respectively [166, 167].

Table 17: Thermodynamic parameters for a dye adsorption process by hydrochars produced from citrus and winery wastes.

Sample ID	Temp. (°C)	Van't Hoff equation	K _C	ΔG (kJ/mol)	ΔH (kJ/mol)	ΔS (J/mol)
CW-H180	4	$y = -4977.2x + 33.0$ $R^2 = 0.873$	4162272	34.66	41.38	274.51
	20		6072126	-39.05		
	36		27363558	-43.44		
CW-H220	4	$y = -4452.3x + 31.2$ $R^2 = 0.997$	3681327	-34.77	37.02	259.14
	20		8233615	-38.91		
	36		19501840	-43.06		
CW-H250	4	$y = -3187.8x + 27.6$ $R^2 = 0.916$	8689631	-37.02	26.50	229.33
	20		22149969	-40.69		
	36		28290480	-44.36		
WW-H180	4	$y = -5154.8x + 34.1$ $R^2 = 0.978$	5112033	-35.75	42.90	283.93
	20		18015640	-40.29		
	36		34805250	-44.84		
WW-H220	4	$y = -2877.2x + 26.1$ $R^2 = 0.991$	7020436	-36.24	23.92	217.21
	20		11333988	-39.72		
	36		20650946	-43.19		
WW-H250	4	$y = -2369.4x + 24.5$ $R^2 = 0.998$	8141606	-36.67	19.70	203.50
	20		13427161	-39.93		
	36		19719331	-43.18		

The ΔH values varied between 41.38 to 26.50 kJ/mol and 42.90 to 19.70 kJ/mol for CW and WW hydrochar, respectively. All of these positive values indicate the adsorption process was endothermic in nature and not governed by the enthalpy [168]. As the process is not governed by the enthalpy, it should be governed by the entropy. The positive values of ΔS indicate that the adsorption of a cationic dye results in an increase of overall entropy in the system, which confirms the adsorption was entropy

governed. The positive values of ΔS further indicated that the degree of freedom of dye increases in the solution, and the organization of the adsorbate at solid/liquid interface becomes more random during the adsorption process [126].

It can be concluded from this study that both CW and WW worked best as adsorbent while they were treated at the lower temperature of 180 °C: at this condition, both CW and WW hydrochars showed the highest active sites per unit area, which translated in their best performances as adsorbent materials.

3.4.3 An electron storage material

A material having high surface area and corresponding surface chemistry is the main consideration for its beneficial applications as soil amendment, carbon sequestration, adsorbent, etc. [52]. Moreover, the surface functionality of carbon material plays an important role in its redox properties (e.g., EEC or ESC) [70, 74-76]. ESC is the amount of electrons that can be stored within a unit mass of char through chemical redox reactions with a reductant or an electron transfer mediator [70, 76-78]. It is important to quantify ESC for the optimal design of carbon-based treatment processes involving the redox transformation of contaminants [169]. Therefore the ESC of various pyrolyzed hydrochars produced from a model biopolymer (cellulose) and biomass (wood) were measured and correlated with the functional groups.

3.4.3.1 ESC of pyrolyzed hydrochar

As shown in Figure 29, both cellulose- and wood-derived pyrolyzed hydrochars contained significant ESCs. For the first redox cycle, the ESCs of cellulose-derived pyrolyzed hydrochars ranged from 1.88 (PT = 600 °C) to 2.43 (400 °C) mmol/g and of wood-derived pyrolyzed hydrochars from 2.06 (600 °C) to 3.25 (400 °C) mmol/g. As was shown in the previous work for SRB, the ESCs of all pyrolyzed hydrochars decreased in subsequent cycles to 1.51–1.86 mmol/g for cellulose-derived pyrolyzed hydrochars and to 1.84–2.91 mmol/g for wood-derived pyrolyzed hydrochars [77]. This decrease in ESC, most marked between the first and second cycles, was attributed to the initial, irreversible reduction of virgin char samples by Ti(III) citrate [77]. The lower values obtained from subsequent cycles were relatively constant and can be regarded as the reversible ESCs of the pyrolyzed hydrochars. Interestingly, wood-derived pyrolyzed hydrochars yielded higher reversible ESCs (81–97 % the value from the first cycle) than cellulose-derived pyrolyzed hydrochars (61–84%), with the P400 cellulose pyrolyzed hydrochars exhibiting the largest decrease. These results suggest that ESC may be a common property of pyrolyzed hydrochars derived from cellulosic biomass and that a portion of the ESCs of the wood pyrolyzed hydrochars originated from its cellulose content. Wood is composed primarily of cellulose, lignin, and hemicellulose, although the composition is variable, depending

on the origin of the wood.[121] While the data suggest cellulose contributed to the ESCs of wood pyrolyzed hydrochars, the fact that cellulose pyrolyzed hydrochars possessed lower ESCs than wood pyrolyzed hydrochars for the same pyrolysis temperature (Figure 29) indicates that other wood components (e.g., lignin) contributed more than cellulose to the total ESCs of wood pyrolyzed hydrochars on the mass basis. It has been suggested that lignin-derived chars possessed twice the (hydro) quinoic functional groups than cellulose- and D-xylose-derived chars, which is consistent with the observation from this study [170].

The ESCs of pyrolyzed hydrochars decreased with increasing pyrolysis temperature from 400-600 °C for both cellulose- and wood-derived pyrolyzed hydrochars. It is known that wood biochar prepared at below 300 °C is primarily composed of residues of biopolymers such as cellulose and lignin [171]. At 350 °C biochar starts to lose the lignocellulosic features and to form aromatic structures with functional groups. As pyrolysis temperature increases to above 400 °C, aromatic C-O groups start to disappear [171]. Klüpfel *et al.* also examined the effect of pyrolysis temperature on biochar ESC from 200 to 700 °C and found that biochars exhibited the greatest ESC around 400–500 °C [76]. Higher pyrolysis temperatures (>500 °C) resulted in reduced abundance of quinones and other redox-active functional groups and hence a lower ESC [76]. In contrast, the effect of HTC temperature on ESC was less apparent. As HTC temperature increased from 220 to 260 °C, the ESCs of wood

pyrolyzed hydrochars decreased slightly while that of the cellulose pyrolyzed hydrochars remained practically the same. Thus, the ESC of pyrolyzed hydrochars was presumably controlled by the pyrolysis temperature rather than the HTC temperature.

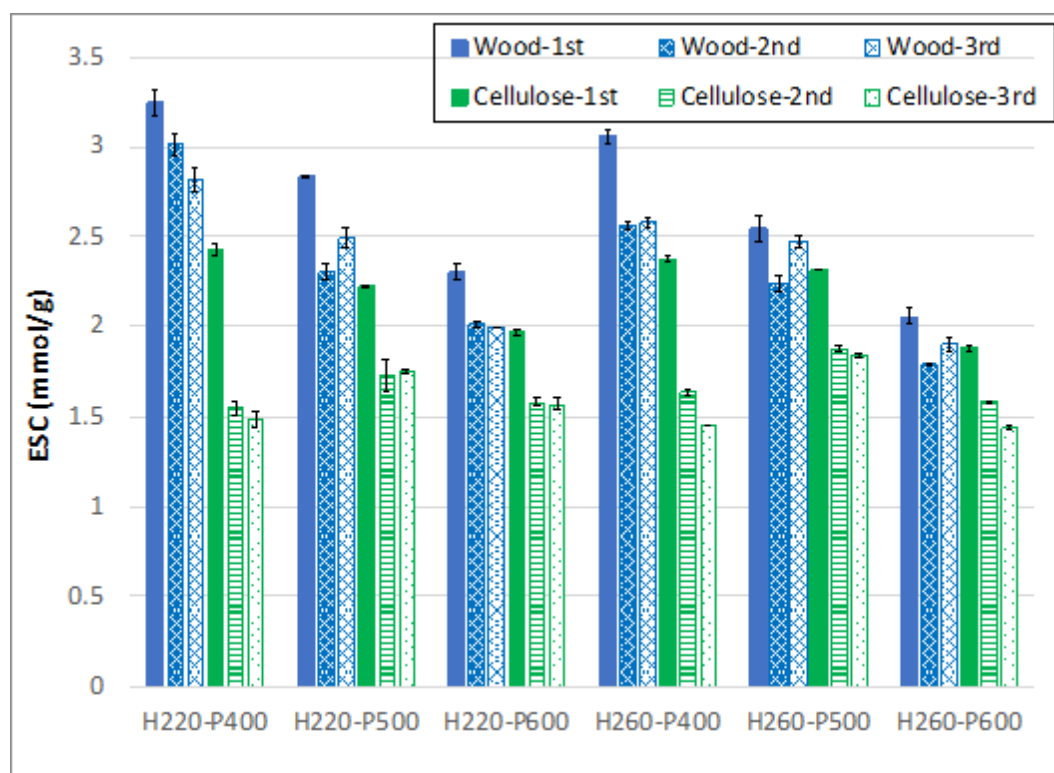


Figure 29: Effect of pyrolysis temperature on the ESC of pyrolyzed hydrochars from cellulose and wood.

A correlation between functional groups and ESC was tried to establish from this study. Figure 30 (top) showed that the lactonic groups followed a similar trend as ESC follows on the pyrolyzed chars. The high R^2 value indicates the data is well fit. The slopes of the two fits are different, which means that the relationship between ESC and functional group (lactonic) could be linear but might not follow a similar slope. It was reported in the literature that the quinone group on biochar is mainly responsible for their ESC [70, 76]. The quinone group contains C=O bonds and these bonds are reduced (to form –OH) during the electron storage. Similarly, the lactonic group on the pyrolyzed hydrochar also has C=O bonds that can be also be reduced with the acceptance of electrons. As a result, the lactonic groups could be responsible for ESC on the pyrolyzed hydrochar. However, the carboxylic group did not follow the linear relationship with ESC shown in Figure 30 (bottom). The reason could be that the carboxylic group is redox-inert and did not reduce by Ti(III) citrate.

A positive correlation between ESC and the lactonic group was observed in this study as discussed in earlier sections. The lactonic group on the surface of pyrolyzed chars has the C=O bond in their structure. The C=O bonds of the lactonic group could have easily be reduced by accepting electrons and become –OH. As the number of lactonic groups decreased with pyrolysis temperature, a decreasing trend of ESC was also observed for both feedstocks. So, further optimization of the pyrolysis condition is required for improving the ESC of pyrolyzed chars.

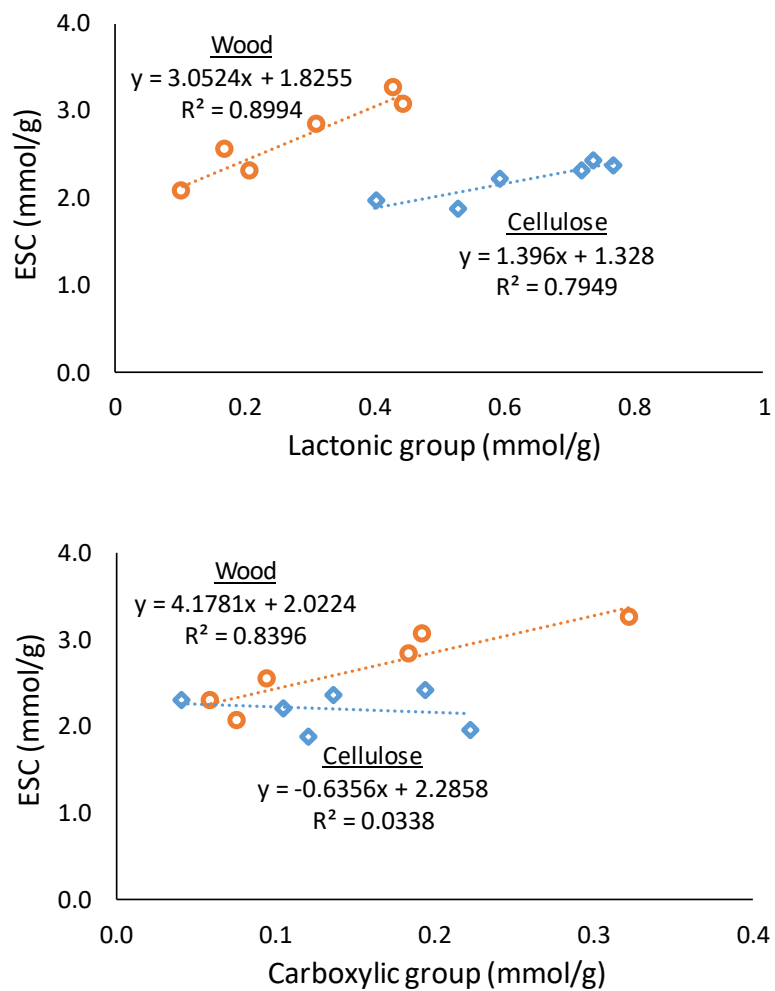


Figure 30: A correlation between ESC and lactonic functional group (top), and between ESC and carboxylic group (bottom).

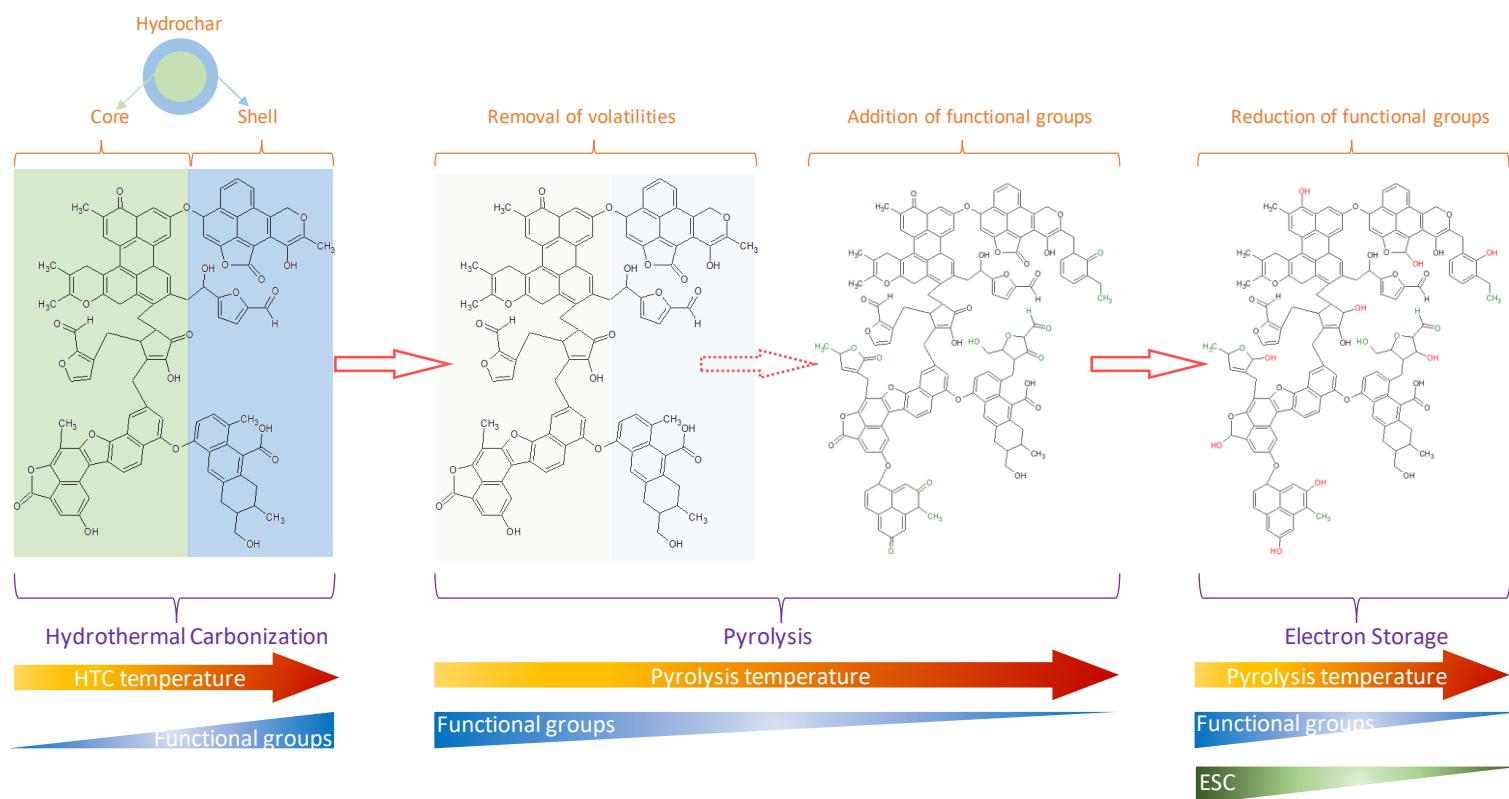


Figure 31: Proposed electron storage mechanism by pyrolyzed hydrochars

Figure 31 shows the overall pathway of electron storage by the hydrochar. During the HTC, the hydrochar was introduced into abundant acidic oxygen-containing functional groups. Some of them are in the core and some of them are in the shell [39]. Few of them could be covered by the volatilities. Pyrolysis of the hydrochar could remove the volatilities and exposed the surface functionality at even lower pyrolysis temperature (400 °C). As a result, a large number of acidic functional groups were observed on the pyrolyzed hydrochar. However, this number was reduced with the pyrolysis temperature, as they might be deformed and/or decomposed at a high pyrolysis temperature.

Limitations: The ESC's of hydrochar samples were unable to be measured using the chemical method because the hydrochars would partially dissolve in Ti(III) citrate solution, rendering the UV-vis absorbance measurement infeasible. Therefore, only the ESC of pyrolyzed hydrochars was quantified, while the change in ESC due to pyrolysis could not be determined.

4 Conclusions

Regardless of the HTT temperature, hydrochar was produced, although solid mass yield decreases with the increase of HTT temperature. This study shows that HTT can increase the surface functionality up to a point, after which excessive dehydration actually removes surface functional groups. The formation, presence, and degradation of these functional groups are reflected in the overall surface composition of the hydrochar. At 260 °C, there are nearly equal amounts of lactonic, carboxylic, and phenolic groups. As HTT temperature rises to 340 °C, the carboxylic groups are almost fully diminished, and the lactonic and phenolic groups are reduced by a third and a half, respectively, compared to C-H260. After supercritical conditions, there is only phenolic groups present at the hydrochar surface. Similarly, the increase in HTT temperature is directly related to the increase in the aromaticity of the hydrochar. It was observed from the SEM images that the particle size of the hydrochar increases until 380 °C and finally collapsed at high temperatures. So, if the hydrochar is meant to be used as an adsorbent, a lower-temperature HTT might be more beneficial than higher HTT temperatures. Furthermore, the hydrochar contains more elemental carbon at high-temperature carbonization, which means the hydrochar will work better as combustion material. Also, this high intense nano

carbon substance might be used as an electrode material. Although the feedstock and hydrochar produced at low temperatures showed polar behavior, it moved toward non-polar characteristics with the treatment temperature.

In regard to see the application of hydrochar as fuel, HTC of various paper mill sludges have been studied. With the exception of DPS, HHV_{daf} and ED ratio were maximized at HTC temperature of 260 °C for all the PMS. Although PMS sludges showed two-staged thermal degradation during pyrolysis, the thermograms revealed that hydrochars produced from different PMS possess different degradation severity. While primary and secondary mix sludges show lower solid mass yields at lower HTC temperatures, the deinked primary sludge shows a higher solid mass yield at similar HTC conditions. Moreover, primary and secondary sludge samples showed anomalies in thermograms between themselves. Although the combustion indices of hydrochars have lower ignition temperatures and higher burnout temperatures compared to bituminous coal, it showed an opposite trend when they were co-fired with coal. So, further investigation is required to find a suitable PMS feedstock for the existing coal-fired power plant to use as co-feed.

The adsorption of a cation dye on CW and WW hydrochars followed a Langmuir monolayer adsorption isotherm. The adsorption of dye on hydrochar is not only governed by the surface area but also the functional groups as well. In addition, if

the adsorption follows the Langmuir isotherm, the functional group density is also important because it will determine how many active sites are available to adsorb the dye molecules. As Langmuir adsorption is a monolayer adsorption, knowing the active sites per unit area of the hydrochar is necessary because it will control the adsorption capacity of the material.

It is noticed that the specific area increases with pyrolysis temperature. In addition, the total acidic groups showed a decreasing trend with the pyrolysis temperature while the individual acidic group (e.g., carboxylic, lactonic, phenolic and others) showed their own trend. Pyrolysis of the hydrochar showed further mass loss, which means hydrochar undergoes further thermal conversion during pyrolysis. However, it was observed that the hydrochar produced at high temperature (260 °C) is thermally more stable than as produced at 220 °C. The ultimate analysis of the pyrolyzed hydrochar showed that the polarity index decreases with the pyrolysis temperature, which indicates that hydrophobicity of the char increases, resulting in a decrease of ESC with the pyrolysis temperature. A positive correlation was observed between ESC and lactonic group. Optimization of pyrolysis of hydrochar might be required to maintain high surface area and abundance of oxygen-containing functional groups for better ESC.

5 Recommendations and future research

Throughout this study, only reaction temperature is considered as a variable, whereas other variables such as reaction time, particle size, and heating-cooling rate are ignored. To design the HTC process, all these variables need to be considered and optimized. As the HTC process requires extra heat, it is essential to do the techno-economic analysis prior to scale up this process.

Thermal activation (pyrolysis) of the hydrochar was conducted to increase the surface area and the surface functionality. During the activation, heating rate could be a potential variable; however, a single heating rate was considered here. As a result, heating rate is recommended to consider as a variable. In addition, chemical activation (i.e., CO₂ activation) could introduce a new surface area. The optimization of the pyrolysis of hydrochar might be required to maintain a high surface area and an abundance of functional groups. This will ultimately increase the application window of the material.

The ESC was measured using a chemical method where titanium citrate was used as an electron donor. However, it is possible to use other electron donors such as Fe (III), Cu (III), etc. to measure the ESC. The produced materials were only tested for

the electron storage capacity. This material could be used for contaminant removal as it has a high surface area and functional groups.

As this is the first step to investigate into the use of hydrochar as electron storage material, only cellulose (model compound) and wood (biomass) were studied to understand the pathway. However, to commercialize this process, it is necessary to conduct a similar study on other wastes, such as sewage sludge, municipal waste, etc. Products from these wastes could be used not only for electron storage, but also for other applications such as contaminant removal, catalyst, etc.

It is found that high-temperature treatment of biomass can still give some char with some surface functionality and high surface area. If one wants to do the hydrothermal liquefaction where the liquid is the main product, one can also use the char as a value-added product as well. For example, this char could be used as electrode materials, fuels, filter media, etc.

6 References

- [1] U. N. E. Programme, "UNEP (United Nations Environment Programme) Converting waste agricultural biomass into a resource," Division of Technology, Industry and Economics International Environmental Technology Centre, Osaka/Shiga, Japan2015.
- [2] N. Jain, H. Pathak, and A. Bhatia, "Sustainable management of crop residues in India," *Current Advances in Agricultural Sciences (An International Journal)*, vol. 6, pp. 1-9, 2014.
- [3] F. a. a. o. t. U. Nations, "World agriculture: towards 2015/2030. Summary report," Rome2002.
- [4] M. T. Reza, "Upgrading biomass by hydrothermal and chemical conditioning," 2013.
- [5] A. Ergüdenler and A. Işığigür, "Agricultural residues as a potential resource for environmentally sustainable electric power generation in Turkey," *Renewable Energy*, vol. 5, pp. 786-790, 1994.
- [6] L. E. d. R. PAULA, P. F. Trugilho, A. Napoli, and M. L. Bianchi, "Characterization of residues from plant biomass for use in energy generation. CERNE [online]. 2011, vol. 17, n. 2," ed: SciELO Brasil, 2011.
- [7] T. Miles Sr and T. Miles Jr, "Environmental implications of increased biomass energy use. Final report," National Renewable Energy Lab., Golden, CO (United States); Miles (Thomas R ...1992.

- [8] G. D. Saratale, R. G. Saratale, J. R. Banu, and J.-S. Chang, "Biohydrogen production from renewable biomass resources," in *Biohydrogen*, ed: Elsevier, 2019, pp. 247-277.
- [9] S. Kumar, "Hydrothermal treatment for biofuels: lignocellulosic biomass to bioethanol, biocrude, and biochar," 2010.
- [10] J. U. Hernández-Beltrán, I. O. Hernández-De Lira, M. M. Cruz-Santos, A. Saucedo-Luevanos, F. Hernández-Terán, and N. Balagurusamy, "Insight into Pretreatment Methods of Lignocellulosic Biomass to Increase Biogas Yield: Current State, Challenges, and Opportunities," *Applied Sciences*, vol. 9, p. 3721, 2019.
- [11] O. Bobleter, "Hydrothermal degradation of polymers derived from plants," *Progress in polymer science*, vol. 19, pp. 797-841, 1994.
- [12] M. Jarvis, "Cellulose stacks up," *Nature*, vol. 426, pp. 611-612, 2003.
- [13] A. Tolbert, H. Akinosho, R. Khunsupat, A. K. Naskar, and A. J. Ragauskas, "Characterization and analysis of the molecular weight of lignin for biorefining studies," *Biofuels, Bioproducts and Biorefining*, vol. 8, pp. 836-856, 2014.
- [14] K. Meyer, A. M. Shirley, J. C. Cusumano, D. A. Bell-Lelong, and C. Chapple, "Lignin monomer composition is determined by the expression of a cytochrome P450-dependent monooxygenase in Arabidopsis," *Proceedings of the National Academy of Sciences*, vol. 95, pp. 6619-6623, 1998.
- [15] G. Gellerstedt, M. Ek, and G. Henriksson, "Wood Chemistry and Wood Biotechnology," ed: Walter de Gruyter, 2009.

- [16] K. Thammassouk, D. Tandjo, and M. H. Penner, "Influence of extractives on the analysis of herbaceous biomass," *Journal of agricultural and food chemistry*, vol. 45, pp. 437-443, 1997.
- [17] M. Ibrahim, "Clean fractionation of biomass-steam explosion and extraction," Virginia Tech, 1998.
- [18] A. V. Bandura and S. N. Lvov, "The ionization constant of water over wide ranges of temperature and density," *Journal of physical and chemical reference data*, vol. 35, pp. 15-30, 2006.
- [19] Y. Marcus, "On transport properties of hot liquid and supercritical water and their relationship to the hydrogen bonding," *Fluid phase equilibria*, vol. 164, pp. 131-142, 1999.
- [20] P. Kritzer and E. Dinjus, "An assessment of supercritical water oxidation (SCWO): existing problems, possible solutions and new reactor concepts," *Chemical Engineering Journal*, vol. 83, pp. 207-214, 2001.
- [21] A. A. Peterson, F. Vogel, R. P. Lachance, M. Fröling, M. J. Antal Jr, and J. W. Tester, "Thermochemical biofuel production in hydrothermal media: a review of sub-and supercritical water technologies," *Energy & Environmental Science*, vol. 1, pp. 32-65, 2008.
- [22] K. Qian, A. Kumar, H. Zhang, D. Bellmer, and R. Huhnke, "Recent advances in utilization of biochar," *Renewable and Sustainable Energy Reviews*, vol. 42, pp. 1055-1064, 2015.

- [23] C. Greenhalf, D. Nowakowski, A. Harms, J. Titiloye, and A. Bridgwater, "A comparative study of straw, perennial grasses and hardwoods in terms of fast pyrolysis products," *Fuel*, vol. 108, pp. 216-230, 2013.
- [24] S. Al Arni, "Comparison of slow and fast pyrolysis for converting biomass into fuel," *Renewable Energy*, vol. 124, pp. 197-201, 2018.
- [25] W.-J. Liu, H. Jiang, and H.-Q. Yu, "Development of biochar-based functional materials: toward a sustainable platform carbon material," *Chemical reviews*, vol. 115, pp. 12251-12285, 2015.
- [26] N. Saha, A. Saba, P. Saha, K. McGaughy, D. Franqui-Villanueva, W. J. Orts, W. M. Hart-Cooper, and M. T. Reza, "Hydrothermal Carbonization of Various Paper Mill Sludges: An Observation of Solid Fuel Properties," *Energies*, vol. 12, p. 858, 2019.
- [27] M. T. Reza, J. Andert, B. Wirth, D. Busch, J. Pielert, J. G. Lynam, and J. Mumme, "Hydrothermal carbonization of biomass for energy and crop production," *Applied Bioenergy*, vol. 1, pp. 11-29, 2014.
- [28] Z. Fang and C. C. Xu, *Near-critical and supercritical water and their applications for biorefineries* vol. 2: Springer, 2014.
- [29] L. Leng, H. Huang, H. Li, J. Li, and W. Zhou, "Biochar stability assessment methods: A review," *Science of the Total Environment*, vol. 647, pp. 210-222, 2019/01/10/ 2019.

- [30] K. Tekin, S. Karagöz, and S. Bektaş, "A review of hydrothermal biomass processing," *Renewable and Sustainable Energy Reviews*, vol. 40, pp. 673-687, 2014/12/01/ 2014.
- [31] D. Kim, K. Lee, and K. Y. Park, "Hydrothermal carbonization of anaerobically digested sludge for solid fuel production and energy recovery," *Fuel*, vol. 130, pp. 120-125, 2014/08/15/ 2014.
- [32] C. He, A. Giannis, and J.-Y. Wang, "Conversion of sewage sludge to clean solid fuel using hydrothermal carbonization: hydrochar fuel characteristics and combustion behavior," *Applied Energy*, vol. 111, pp. 257-266, 2013.
- [33] L.-P. Xiao, Z.-J. Shi, F. Xu, and R.-C. Sun, "Hydrothermal carbonization of lignocellulosic biomass," *Bioresource Technology*, vol. 118, pp. 619-623, 2012/08/01/ 2012.
- [34] L. Calucci, D. P. Rasse, and C. Forte, "Solid-state nuclear magnetic resonance characterization of chars obtained from hydrothermal carbonization of corncob and miscanthus," *Energy & fuels*, vol. 27, pp. 303-309, 2013.
- [35] S. Nizamuddin, N. Mubarak, M. Tiripathi, N. Jayakumar, J. Sahu, and P. Ganesan, "Chemical, dielectric and structural characterization of optimized hydrochar produced from hydrothermal carbonization of palm shell," *Fuel*, vol. 163, pp. 88-97, 2016.

- [36] M. Sevilla, J. A. Maciá-Agulló, and A. B. Fuertes, "Hydrothermal carbonization of biomass as a route for the sequestration of CO₂: Chemical and structural properties of the carbonized products," *Biomass and Bioenergy*, vol. 35, pp. 3152-3159, 2011.
- [37] C. Areeprasert, P. Zhao, D. Ma, Y. Shen, and K. Yoshikawa, "Alternative solid fuel production from paper sludge employing hydrothermal treatment," *Energy & fuels*, vol. 28, pp. 1198-1206, 2014.
- [38] P. Gao, Y. Zhou, F. Meng, Y. Zhang, Z. Liu, W. Zhang, and G. Xue, "Preparation and characterization of hydrochar from waste eucalyptus bark by hydrothermal carbonization," *Energy*, vol. 97, pp. 238-245, 2016.
- [39] M. Sevilla and A. B. Fuertes, "The production of carbon materials by hydrothermal carbonization of cellulose," *Carbon*, vol. 47, pp. 2281-2289, 2009/08/01/ 2009.
- [40] Z. Liu and R. Balasubramanian, "Upgrading of waste biomass by hydrothermal carbonization (HTC) and low temperature pyrolysis (LTP): A comparative evaluation," *Applied Energy*, vol. 114, pp. 857-864, 2014/02/01/ 2014.
- [41] Q. Fan, J. Sun, L. Chu, L. Cui, G. Quan, J. Yan, Q. Hussain, and M. Iqbal, "Effects of chemical oxidation on surface oxygen-containing functional groups and adsorption behavior of biochar," *Chemosphere*, vol. 207, pp. 33-40, 2018/09/01/ 2018.
- [42] F. N. D. Mukome, X. Zhang, L. C. R. Silva, J. Six, and S. J. Parikh, "Use of Chemical and Physical Characteristics To Investigate Trends in Biochar Feedstocks," *Journal of agricultural and food chemistry*, vol. 61, pp. 2196-2204, 2013/03/06 2013.

- [43] N. Saha, D. Xin, P. C. Chiu, and M. T. Reza, "Effect of pyrolysis temperature on acidic oxygen-containing functional groups and electron storage capacities of pyrolyzed hydrochars," *ACS Sustainable Chemistry & Engineering*, vol. 7, pp. 8387-8396, 2019.
- [44] L. Klüpfel, M. Keiluweit, M. Kleber, and M. Sander, "Redox properties of plant biomass-derived black carbon (biochar)," *Environmental science & technology*, vol. 48, pp. 5601-5611, 2014.
- [45] Z. Chen, X. Xiao, B. Chen, and L. Zhu, "Quantification of chemical states, dissociation constants and contents of oxygen-containing groups on the surface of biochars produced at different temperatures," *Environmental science & technology*, vol. 49, pp. 309-317, 2015.
- [46] C. Gai, Y. Guo, T. Liu, N. Peng, and Z. Liu, "Hydrogen-rich gas production by steam gasification of hydrochar derived from sewage sludge," *International Journal of Hydrogen Energy*, vol. 41, pp. 3363-3372, 2016/02/09/ 2016.
- [47] H. N. Tran, C.-K. Lee, T. V. Nguyen, and H.-P. Chao, "Saccharide-derived microporous spherical biochar prepared from hydrothermal carbonization and different pyrolysis temperatures: synthesis, characterization, and application in water treatment," *Environmental technology*, vol. 39, pp. 2747-2760, 2018.
- [48] S. Katyal, K. Thambimuthu, and M. Valix, "Carbonisation of bagasse in a fixed bed reactor: influence of process variables on char yield and characteristics," *Renewable Energy*, vol. 28, pp. 713-725, 2003.

- [49] B. Chen and Z. Chen, "Sorption of naphthalene and 1-naphthol by biochars of orange peels with different pyrolytic temperatures," *Chemosphere*, vol. 76, pp. 127-133, 2009.
- [50] M. K. Rafiq, R. T. Bachmann, M. T. Rafiq, Z. Shang, S. Joseph, and R. Long, "Influence of pyrolysis temperature on physico-chemical properties of corn stover (*Zea mays* L.) biochar and feasibility for carbon capture and energy balance," *PloS one*, vol. 11, p. e0156894, 2016.
- [51] A. Shaaban, S.-M. Se, M. Dimin, J. M. Juoi, M. H. M. Husin, and N. M. M. Mitan, "Influence of heating temperature and holding time on biochars derived from rubber wood sawdust via slow pyrolysis," *Journal of Analytical and Applied Pyrolysis*, vol. 107, pp. 31-39, 2014.
- [52] M. Ahmad, A. U. Rajapaksha, J. E. Lim, M. Zhang, N. Bolan, D. Mohan, M. Vithanage, S. S. Lee, and Y. S. Ok, "Biochar as a sorbent for contaminant management in soil and water: A review," *Chemosphere*, vol. 99, pp. 19-33, 2014/03/01/ 2014.
- [53] B. Chen, D. Zhou, and L. Zhu, "Transitional Adsorption and Partition of Nonpolar and Polar Aromatic Contaminants by Biochars of Pine Needles with Different Pyrolytic Temperatures," *Environmental Science & Technology*, vol. 42, pp. 5137-5143, 2008/07/01 2008.

- [54] M. T. Reza, J. G. Lynam, M. H. Uddin, and C. J. Coronella, "Hydrothermal carbonization: Fate of inorganics," *Biomass and Bioenergy*, vol. 49, pp. 86-94, 2013/02/01/ 2013.
- [55] A. Funke and F. Ziegler, "Hydrothermal carbonization of biomass: A literature survey focusing on its technical application and prospects," in *17th European Biomass Conference and Exhibition. Hamburg, Germany, 2009*, pp. 1037-1050.
- [56] J. A. Libra, K. S. Ro, C. Kammann, A. Funke, N. D. Berge, Y. Neubauer, M.-M. Titirici, C. Fühner, O. Bens, J. Kern, and K.-H. Emmerich, "Hydrothermal carbonization of biomass residuals: a comparative review of the chemistry, processes and applications of wet and dry pyrolysis," *Biofuels*, vol. 2, pp. 71-106, 2011/01/01 2011.
- [57] X. He, Z. Liu, W. Niu, L. Yang, T. Zhou, D. Qin, Z. Niu, and Q. Yuan, "Effects of pyrolysis temperature on the physicochemical properties of gas and biochar obtained from pyrolysis of crop residues," *Energy*, vol. 143, pp. 746-756, 2018.
- [58] M. Mierzwa-Hersztek, K. Gondek, M. Jewiarz, and K. Dziedzic, "Assessment of energy parameters of biomass and biochars, leachability of heavy metals and phytotoxicity of their ashes," *Journal of Material Cycles and Waste Management*, vol. 21, pp. 786-800, 2019/07/01 2019.
- [59] J. Lehmann, J. Gaunt, and M. Rondon, "Bio-char sequestration in terrestrial ecosystems—a review," *Mitigation and adaptation strategies for global change*, vol. 11, pp. 403-427, 2006.

- [60] Y. Wang, R. Yin, and R. Liu, "Characterization of biochar from fast pyrolysis and its effect on chemical properties of the tea garden soil," *Journal of Analytical and Applied Pyrolysis*, vol. 110, pp. 375-381, 2014/11/01/ 2014.
- [61] M. C. Rillig, M. Wagner, M. Salem, P. M. Antunes, C. George, H.-G. Ramke, M.-M. Titirici, and M. Antonietti, "Material derived from hydrothermal carbonization: Effects on plant growth and arbuscular mycorrhiza," *Applied Soil Ecology*, vol. 45, pp. 238-242, 2010/07/01/ 2010.
- [62] N. Saha, M. Volpe, L. Fiori, R. Volpe, A. Messineo, and M. T. Reza, "Cationic Dye Adsorption on Hydrochars of Winery and Citrus Juice Industries Residues: Performance, Mechanism, and Thermodynamics," *Energies*, vol. 13, p. 4686, 2020.
- [63] X. Tan, Y. Liu, G. Zeng, X. Wang, X. Hu, Y. Gu, and Z. Yang, "Application of biochar for the removal of pollutants from aqueous solutions," *Chemosphere*, vol. 125, pp. 70-85, 2015/04/01/ 2015.
- [64] T. M. Vu, D. P. Doan, H. T. Van, T. V. Nguyen, S. Vigneswaran, and H. H. Ngo, "Removing ammonium from water using modified corncob-biochar," *Science of the Total Environment*, vol. 579, pp. 612-619, 2017.
- [65] Y. Li, Z. Wang, X. Xie, J. Zhu, R. Li, and T. Qin, "Removal of Norfloxacin from aqueous solution by clay-biochar composite prepared from potato stem and natural attapulgite," *Colloids and Surfaces A: Physicochemical and Engineering Aspects*, vol. 514, pp. 126-136, 2017/02/05/ 2017.

- [66] T. S. Blankenship II, N. Balahmar, and R. Mokaya, "Oxygen-rich microporous carbons with exceptional hydrogen storage capacity," *Nature communications*, vol. 8, pp. 1-12, 2017.
- [67] M. T. Reza, E. Rottler, L. Herklotz, and B. Wirth, "Hydrothermal carbonization (HTC) of wheat straw: Influence of feedwater pH prepared by acetic acid and potassium hydroxide," *Bioresource technology*, vol. 182, pp. 336-344, 2015.
- [68] M. Sevilla, A. B. Fuertes, and R. Mokaya, "High density hydrogen storage in superactivated carbons from hydrothermally carbonized renewable organic materials," *Energy & Environmental Science*, vol. 4, pp. 1400-1410, 2011.
- [69] L. L. Zhang and X. S. Zhao, "Carbon-based materials as supercapacitor electrodes," *Chemical Society Reviews*, vol. 38, pp. 2520-2531, 2009.
- [70] J. M. Saquing, Y.-H. Yu, and P. C. Chiu, "Wood-Derived Black Carbon (Biochar) as a Microbial Electron Donor and Acceptor," *Environmental Science & Technology Letters*, vol. 3, pp. 62-66, 2016/02/09 2016.
- [71] H. Lu, W. Zhang, Y. Yang, X. Huang, S. Wang, and R. Qiu, "Relative distribution of Pb²⁺ sorption mechanisms by sludge-derived biochar," *Water Research*, vol. 46, pp. 854-862, 2012/03/01/ 2012.
- [72] A. Samsuri, F. Sadegh-Zadeh, and B. Seh-Bardan, "Characterization of biochars produced from oil palm and rice husks and their adsorption capacities for heavy metals," *International Journal of Environmental Science and Technology*, vol. 11, pp. 967-976, 2014.

- [73] Y. Qiu, Z. Zheng, Z. Zhou, and G. D. Sheng, "Effectiveness and mechanisms of dye adsorption on a straw-based biochar," *Bioresource Technology*, vol. 100, pp. 5348-5351, 2009/11/01/ 2009.
- [74] K. Mochidzuki, F. Soutric, K. Tadokoro, M. J. Antal, M. Tóth, B. Zelei, and G. Várhegyi, "Electrical and Physical Properties of Carbonized Charcoals," *Industrial & Engineering Chemistry Research*, vol. 42, pp. 5140-5151, 2003/10/01 2003.
- [75] P. Quin, S. Joseph, O. Husson, S. Donne, D. Mitchell, P. Munroe, D. Phelan, A. Cowie, and L. Van Zwieten, "Lowering N₂O emissions from soils using eucalypt biochar: the importance of redox reactions," *Scientific Reports*, vol. 5, p. 16773, 2015.
- [76] L. Klüpfel, M. Keiluweit, M. Kleber, and M. Sander, "Redox Properties of Plant Biomass-Derived Black Carbon (Biochar)," *Environmental Science & Technology*, vol. 48, pp. 5601-5611, 2014/05/20 2014.
- [77] D. Xin, M. Xian, and P. C. Chiu, "New methods for assessing electron storage capacity and redox reversibility of biochar," *Chemosphere*, vol. 215, pp. 827-834, 2019/01/01/ 2019.
- [78] D. Xin, M. Xian, and P. C. Chiu, "Chemical methods for determining the electron storage capacity of black carbon," *MethodsX*, vol. 5, pp. 1515-1520, 2018/01/01/ 2018.
- [79] F. G. Emmerich, C. Rettori, and C. A. Luengo, "ESR in heat treated carbons from the endocarp of babassu coconut," *Carbon*, vol. 29, pp. 305-311, 1991/01/01/ 1991.

- [80] N. Saha, A. Saba, and M. T. Reza, "Effect of hydrothermal carbonization temperature on pH, dissociation constants, and acidic functional groups on hydrochar from cellulose and wood," *Journal of Analytical and Applied Pyrolysis*, vol. 137, pp. 138-145, 2019/01/01/ 2019.
- [81] J. Schönherr, J. R. Buchheim, P. Scholz, and P. Adelhelm, "Boehm titration revisited (part II): A comparison of boehm titration with other analytical techniques on the quantification of oxygen-containing surface groups for a variety of carbon materials," *C—Journal of Carbon Research*, vol. 4, p. 22, 2018.
- [82] J. Ederer, P. Janoš, P. Ecorchard, V. Štengl, Z. Bělčická, M. Šťastný, O. Pop-Georgievski, and V. Dohnal, "Quantitative determination of acidic groups in functionalized graphene by direct titration," *Reactive and Functional Polymers*, vol. 103, pp. 44-53, 2016.
- [83] S. L. Goertzen, K. D. Thériault, A. M. Oickle, A. C. Tarasuk, and H. A. Andreas, "Standardization of the Boehm titration. Part I. CO₂ expulsion and endpoint determination," *Carbon*, vol. 48, pp. 1252-1261, 2010/04/01/ 2010.
- [84] H. Boehm, "Some aspects of the surface chemistry of carbon blacks and other carbons," *Carbon*, vol. 32, pp. 759-769, 1994.
- [85] M. D. Huff, S. Kumar, and J. W. Lee, "Comparative analysis of pinewood, peanut shell, and bamboo biomass derived biochars produced via hydrothermal conversion and pyrolysis," *Journal of environmental management*, vol. 146, pp. 303-308, 2014/12/15/ 2014.

- [86] N. Fiol and I. Villaescusa, "Determination of sorbent point zero charge: usefulness in sorption studies," *Environmental Chemistry Letters*, vol. 7, pp. 79-84, 2009.
- [87] TAPPI, "Acid-insoluble lignin in wood and pulp (Reaffirmation of T 222 om-02)," 2006.
- [88] R. M. Sequeira and R. B. Lew, "The Carbohydrate Composition of Almond Hulls," *Journal of agricultural and food chemistry*, vol. 18, pp. 950-951, 1970/05/01 1970.
- [89] H.-P. Boehm, "Chapter Thirteen - Surface Chemical Characterization of Carbons from Adsorption Studies," in *Adsorption by Carbons*, E. J. Bottani and J. M.D. Tascón, Eds., ed Amsterdam: Elsevier, 2008, pp. 301-327.
- [90] H. Rong, T. Wang, M. Zhou, H. Wang, H. Hou, and Y. Xue, "Combustion Characteristics and Slagging during Co-Combustion of Rice Husk and Sewage Sludge Blends," *Energies*, vol. 10, p. 438, 2017.
- [91] D. Vamvuka, N. El Chatib, and S. Sfakiotakis, "Measurements of ignition point and combustion characteristics of biomass fuels and their blends with lignite," *Combustion*, vol. 2015, p. 95, 2011.
- [92] H. N. Tran, S.-J. You, and H.-P. Chao, "Thermodynamic parameters of cadmium adsorption onto orange peel calculated from various methods: A comparison study," *Journal of environmental chemical engineering*, vol. 4, pp. 2671-2682, 2016/09/01/ 2016.

- [93] X. Zhou and X. Zhou, "The unit problem in the thermodynamic calculation of adsorption using the Langmuir equation," *Chemical Engineering Communications*, vol. 201, pp. 1459-1467, 2014.
- [94] D. Kim, K. Yoshikawa, and K. Y. Park, "Characteristics of Biochar Obtained by Hydrothermal Carbonization of Cellulose for Renewable Energy," *Energies*, vol. 8, pp. 14040-14048, 2015.
- [95] N. Saha, K. McGaughey, and M. T. Reza, "Elucidating hydrochar morphology and oxygen functionality change with hydrothermal treatment temperature ranging from subcritical to supercritical conditions," *Journal of Analytical and Applied Pyrolysis*, vol. 152, p. 104965, 2020.
- [96] Y. Yu, X. Lou, and H. Wu, "Some recent advances in hydrolysis of biomass in hot-compressed water and its comparisons with other hydrolysis methods," *Energy & fuels*, vol. 22, pp. 46-60, 2008.
- [97] A. Funke and F. Ziegler, "Hydrothermal carbonization of biomass: a summary and discussion of chemical mechanisms for process engineering," *Biofuels, Bioproducts and Biorefining*, vol. 4, pp. 160-177, 2010.
- [98] M. T. Reza, M. H. Uddin, J. G. Lynam, S. K. Hoekman, and C. J. Coronella, "Hydrothermal carbonization of loblolly pine: reaction chemistry and water balance," *Biomass Conversion and Biorefinery*, vol. 4, pp. 311-321, 2014.

- [99] R. Demir-Cakan, N. Baccile, M. Antonietti, and M.-M. Titirici, "Carboxylate-rich carbonaceous materials via one-step hydrothermal carbonization of glucose in the presence of acrylic acid," *Chemistry of materials*, vol. 21, pp. 484-490, 2009.
- [100] T. Wang, Y. Zhai, Y. Zhu, C. Li, and G. Zeng, "A review of the hydrothermal carbonization of biomass waste for hydrochar formation: Process conditions, fundamentals, and physicochemical properties," *Renewable and Sustainable Energy Reviews*, vol. 90, pp. 223-247, 2018.
- [101] S. T. Sundar, M. M. Sain, and K. Oksman, "Characterization of microcrystalline cellulose and cellulose long fiber modified by iron salt," *Carbohydrate Polymers*, vol. 80, pp. 35-43, 2010/03/25/ 2010.
- [102] A. Y. Chaerunisaa, S. Sriwidodo, and M. Abdassah, "Microcrystalline Cellulose as Pharmaceutical Excipient," in *Pharmaceutical Formulation Design-Recent Practices*, ed: IntechOpen, 2019.
- [103] A. A. Peterson, F. Vogel, R. P. Lachance, M. Fröling, J. M. J. Antal, and J. W. Tester, "Thermochemical biofuel production in hydrothermal media: A review of sub- and supercritical water technologies," *Energy & Environmental Science*, vol. 1, pp. 32-65, 2008.
- [104] F. Liu, R. Yu, and M. Guo, "Hydrothermal carbonization of forestry residues: influence of reaction temperature on holocellulose-derived hydrochar properties," *Journal of Materials Science*, vol. 52, pp. 1736-1746, 2017.

- [105] W. Chen, H. Yu, Y. Liu, P. Chen, M. Zhang, and Y. Hai, "Individualization of cellulose nanofibers from wood using high-intensity ultrasonication combined with chemical pretreatments," *Carbohydrate Polymers*, vol. 83, pp. 1804-1811, 2011.
- [106] A. Marinovic, F. D. Pileidis, and M.-M. Titirici, "Hydrothermal carbonisation (HTC): history, state-of-the-art and chemistry," *Porous Carbon Materials from Sustainable Precursors*, p. 129, 2015.
- [107] M. Inagaki, K. C. Park, and M. Endo, "Carbonization under pressure," *New Carbon Materials*, vol. 25, pp. 409-420, 2010/12/01/ 2010.
- [108] X. Lu, B. Jordan, and N. D. Berge, "Thermal conversion of municipal solid waste via hydrothermal carbonization: Comparison of carbonization products to products from current waste management techniques," *Waste Management*, vol. 32, pp. 1353-1365, 2012/07/01/ 2012.
- [109] N. Saha and M. T. Reza, "Effect of pyrolysis on basic functional groups of hydrochars," *Biomass Conversion and Biorefinery*, 2019/08/23 2019.
- [110] P. T. Williams and J. Onwudili, "Composition of products from the supercritical water gasification of glucose: a model biomass compound," *Industrial & Engineering Chemistry Research*, vol. 44, pp. 8739-8749, 2005.
- [111] G. Ying, H.-p. CHEN, W. Jun, S. Tao, Y. Hai-Ping, and W. Xian-Hua, "Characterization of products from hydrothermal liquefaction and carbonation of biomass model compounds and real biomass," *Journal of Fuel Chemistry and Technology*, vol. 39, pp. 893-900, 2011.

- [112] M. Volpe and L. Fiori, "From olive waste to solid biofuel through hydrothermal carbonisation: The role of temperature and solid load on secondary char formation and hydrochar energy properties," *Journal of Analytical and Applied Pyrolysis*, vol. 124, pp. 63-72, 2017.
- [113] M. Lucian, M. Volpe, L. Gao, G. Piro, J. L. Goldfarb, and L. Fiori, "Impact of hydrothermal carbonization conditions on the formation of hydrochars and secondary chars from the organic fraction of municipal solid waste," *Fuel*, vol. 233, pp. 257-268, 2018/12/01/ 2018.
- [114] N. Way, "Safety data sheet," 2016.
- [115] A. Jain, R. Balasubramanian, and M. P. Srinivasan, "Hydrothermal conversion of biomass waste to activated carbon with high porosity: A review," *Chemical Engineering Journal*, vol. 283, pp. 789-805, 2016/01/01/ 2016.
- [116] P. Mosur, Y. M. Chernoberezhskii, and A. Lorentsson, "Electrosurface properties of microcrystalline cellulose dispersions in aqueous solutions of aluminum chloride, nitrate, and sulfate," *Colloid Journal*, vol. 70, pp. 462-465, 2008.
- [117] I. A. Udoetok, R. M. Dimmick, L. D. Wilson, and J. V. Headley, "Adsorption properties of cross-linked cellulose-epichlorohydrin polymers in aqueous solution," *Carbohydrate polymers*, vol. 136, pp. 329-340, 2016.
- [118] M. Sevilla and A. B. Fuertes, "Chemical and structural properties of carbonaceous products obtained by hydrothermal carbonization of saccharides," *Chemistry–A European Journal*, vol. 15, pp. 4195-4203, 2009.

- [119] S. K. Hoekman, A. Broch, and C. Robbins, "Hydrothermal Carbonization (HTC) of Lignocellulosic Biomass," *Energy & Fuels*, vol. 25, pp. 1802-1810, 2011/04/21 2011.
- [120] Z. Fang, T. Sato, R. L. Smith Jr, H. Inomata, K. Arai, and J. A. Kozinski, "Reaction chemistry and phase behavior of lignin in high-temperature and supercritical water," *Bioresource Technology*, vol. 99, pp. 3424-3430, 2008.
- [121] M. M. Mian and G. Liu, "Recent progress in biochar-supported photocatalysts: synthesis, role of biochar, and applications," *RSC Advances*, vol. 8, pp. 14237-14248, 2018.
- [122] H. Jin, E. Sun, Y. Xu, R. Guo, M. Zheng, H. Huang, and S. Zhang, "Hydrochar derived from anaerobic solid digestates of swine manure and rice straw: a potential recyclable material," *BioResources*, vol. 13, pp. 1019-1034, 2018.
- [123] M. T. Reza, M. H. Uddin, J. G. Lynam, and C. J. Coronella, "Engineered pellets from dry torrefied and HTC biochar blends," *Biomass and Bioenergy*, vol. 63, pp. 229-238, 2014.
- [124] M. Schwanninger, J. Rodrigues, H. Pereira, and B. Hinterstoisser, "Effects of short-time vibratory ball milling on the shape of FT-IR spectra of wood and cellulose," *Vibrational Spectroscopy*, vol. 36, pp. 23-40, 2004.
- [125] H. S. Kambo and A. Dutta, "A comparative review of biochar and hydrochar in terms of production, physico-chemical properties and applications," *Renewable and Sustainable Energy Reviews*, vol. 45, pp. 359-378, 2015.

- [126] H. N. Tran, S.-J. You, and H.-P. Chao, "Fast and efficient adsorption of methylene green 5 on activated carbon prepared from new chemical activation method," *Journal of environmental management*, vol. 188, pp. 322-336, 2017.
- [127] C. Sheng and J. Azevedo, "Estimating the higher heating value of biomass fuels from basic analysis data," *Biomass and Bioenergy*, vol. 28, pp. 499-507, 2005.
- [128] C. Zhao, E. Jiang, and A. Chen, "Volatile production from pyrolysis of cellulose, hemicellulose and lignin," *Journal of the Energy Institute*, vol. 90, pp. 902-913, 2017.
- [129] S. Kang, X. Li, J. Fan, and J. Chang, "Characterization of hydrochars produced by hydrothermal carbonization of lignin, cellulose, D-xylose, and wood meal," *Industrial & Engineering Chemistry Research*, vol. 51, pp. 9023-9031, 2012.
- [130] M. Mäkelä, V. Benavente, and A. Fullana, "Hydrothermal carbonization of lignocellulosic biomass: Effect of process conditions on hydrochar properties," *Applied Energy*, vol. 155, pp. 576-584, 2015.
- [131] Y. Lin, X. Ma, X. Peng, S. Hu, Z. Yu, and S. Fang, "Effect of hydrothermal carbonization temperature on combustion behavior of hydrochar fuel from paper sludge," *Applied Thermal Engineering*, vol. 91, pp. 574-582, 2015.
- [132] G. M. Scott and A. Smith, "Sludge characteristics and disposal alternatives for the pulp and paper industry," in *Tappi International Environmental Conference*, 1995, pp. 269-269.

- [133] A. Saba, P. Saha, and M. T. Reza, "Co-Hydrothermal Carbonization of coal-biomass blend: Influence of temperature on solid fuel properties," *Fuel Processing Technology*, vol. 167, pp. 711-720, 2017.
- [134] G. Garcia, J. Arauzo, A. Gonzalo, J. Sánchez, and J. Abrego, "Influence of feedstock composition in fluidised bed co-gasification of mixtures of lignite, bituminous coal and sewage sludge," *Chemical Engineering Journal*, vol. 222, pp. 345-352, 2013.
- [135] H. Grénman, K. Eränen, J. Krogell, S. Willför, T. Salmi, and D. Y. Murzin, "Kinetics of aqueous extraction of hemicelluloses from spruce in an intensified reactor system," *Industrial & Engineering Chemistry Research*, vol. 50, pp. 3818-3828, 2011.
- [136] P. McKendry, "Energy production from biomass (part 1): overview of biomass," *Bioresource Technology*, vol. 83, pp. 37-46, 2002.
- [137] G. D. Stricker, R. M. Flores, M. H. Trippi, M. S. Ellis, C. M. Olson, J. E. Sullivan, and K. I. Takahashi, *Coal quality and major, minor, and trace elements in the Powder River, Green River, and Williston Basins, Wyoming and North Dakota*: US Department of the Interior, US Geological Survey, 2007.
- [138] L. Yanfen and M. Xiaoqian, "Thermogravimetric analysis of the co-combustion of coal and paper mill sludge," *Applied Energy*, vol. 87, pp. 3526-3532, 2010.
- [139] Y. Gao, X. Wang, J. Wang, X. Li, J. Cheng, H. Yang, and H. Chen, "Effect of residence time on chemical and structural properties of hydrochar obtained by hydrothermal carbonization of water hyacinth," *Energy*, vol. 58, pp. 376-383, 2013.

- [140] J. G. Lynam, M. T. Reza, W. Yan, V. R. Vásquez, and C. J. Coronella, "Hydrothermal carbonization of various lignocellulosic biomass," *Biomass Conversion and Biorefinery*, vol. 5, pp. 173-181, 2015.
- [141] K. McGaughy and M. T. Reza, "Recovery of macro and micro-nutrients by hydrothermal carbonization of septage," *Journal of agricultural and food chemistry*, vol. 66, pp. 1854-1862, 2018.
- [142] K. Zhang, Z. Hu, Z. Tao, and J. Chen, "Inorganic & organic materials for rechargeable Li batteries with multi-electron reaction," *Science China Materials*, vol. 57, pp. 42-58, 2014/12/01 2014.
- [143] Z. Chen, B. Chen, and C. T. Chiou, "Fast and Slow Rates of Naphthalene Sorption to Biochars Produced at Different Temperatures," *Environmental Science & Technology*, vol. 46, pp. 11104-11111, 2012/10/16 2012.
- [144] Y. Chun, G. Sheng, C. T. Chiou, and B. Xing, "Compositions and Sorptive Properties of Crop Residue-Derived Chars," *Environmental Science & Technology*, vol. 38, pp. 4649-4655, 2004/09/01 2004.
- [145] M. Sevilla and A. B. Fuertes, "Chemical and Structural Properties of Carbonaceous Products Obtained by Hydrothermal Carbonization of Saccharides," *Chemistry – A European Journal*, vol. 15, pp. 4195-4203, 2009/04/14 2009.

- [146] S. Rangabhashiyam and P. Balasubramanian, "The potential of lignocellulosic biomass precursors for biochar production: performance, mechanism and wastewater application-a review," *Industrial Crops and Products*, vol. 128, pp. 405-423, 2019.
- [147] D. Shaykheeva, M. Panasyuk, I. Malganova, and I. Khairullin, "World population estimates and projections: Data and methods," *J. Econ. Econ. Educ. Res*, vol. 17, pp. 237-247, 2016.
- [148] U. S. E. I. Administration, "Annual Energy Outlook 2016 with projections to 2040," 27 July 2020 2016.
- [149] M. Langholtz, B. Stokes, and L. Eaton, "2016 Billion-ton report: Advancing domestic resources for a thriving bioeconomy, Volume 1: Economic availability of feedstock," *Oak Ridge National Laboratory, Oak Ridge, Tennessee, managed by UT-Battelle, LLC for the US Department of Energy*, vol. 2016, pp. 1-411, 2016.
- [150] M. Bird and J. Talberth, "Washington State Department of Ecology Industrial Footprint Project," 2008.
- [151] T. R. Aspitarte, "Methods for pulp and paper mill sludge utilization and disposal," 1973.
- [152] T.-Y. Mun, T. Z. Tumsa, U. Lee, and W. Yang, "Performance evaluation of co-firing various kinds of biomass with low rank coals in a 500 MWe coal-fired power plant," *Energy*, vol. 115, pp. 954-962, 2016.

- [153] M.-Y. Tsai, K.-T. Wu, C.-C. Huang, and H.-T. Lee, "Co-firing of paper mill sludge and coal in an industrial circulating fluidized bed boiler," *Waste Management*, vol. 22, pp. 439-442, 2002.
- [154] S. A. El-Sayed and M. Mostafa, "Pyrolysis characteristics and kinetic parameters determination of biomass fuel powders by differential thermal gravimetric analysis (TGA/DTG)," *Energy conversion and management*, vol. 85, pp. 165-172, 2014.
- [155] M. Volpe, J. L. Goldfarb, and L. Fiori, "Hydrothermal carbonization of *Opuntia ficus-indica* cladodes: Role of process parameters on hydrochar properties," *Bioresource Technology*, vol. 247, pp. 310-318, 2018.
- [156] M. Varol, A. Atımtay, B. Bay, and H. Olgun, "Investigation of co-combustion characteristics of low quality lignite coals and biomass with thermogravimetric analysis," *Thermochimica Acta*, vol. 510, pp. 195-201, 2010.
- [157] V. Lavelli, L. Torri, G. Zeppa, L. Fiori, and G. Spigno, "Recovery of winemaking by-products for innovative food application," 2016.
- [158] M. M. Abd El-Latif and A. M. Ibrahim, "Adsorption, kinetic and equilibrium studies on removal of basic dye from aqueous solutions using hydrolyzed Oak sawdust," *Desalination and Water Treatment*, vol. 6, pp. 252-268, 2009/06/01 2009.
- [159] Y. Kuang, X. Zhang, and S. Zhou, "Adsorption of methylene blue in water onto activated carbon by surfactant modification," *Water*, vol. 12, p. 587, 2020.

- [160] V. Garg, R. Gupta, A. B. Yadav, and R. Kumar, "Dye removal from aqueous solution by adsorption on treated sawdust," *Bioresource Technology*, vol. 89, pp. 121-124, 2003.
- [161] C. Namasivayam, D. Prabha, and M. Kumutha, "Removal of direct red and acid brilliant blue by adsorption on to banana pith," *Bioresource Technology*, vol. 64, pp. 77-79, 1998.
- [162] R. Ferrentino, R. Ceccato, V. Marchetti, G. Andreottola, and L. Fiori, "Sewage Sludge Hydrochar: An Option for Removal of Methylene Blue from Wastewater," *Applied Sciences*, vol. 10, p. 3445, 2020.
- [163] M. Kermanioryani, M. I. A. Mutalib, K. A. Kurnia, K. C. Lethesh, S. Krishnan, and J.-M. Leveque, "Enhancement of π - π aromatic interactions between hydrophobic Ionic Liquids and Methylene Blue for an optimum removal efficiency and assessment of toxicity by microbiological method," *Journal of Cleaner Production*, vol. 137, pp. 1149-1157, 2016/11/20/ 2016.
- [164] D. L. Sparks, "Environmental soil chemistry," *Elsevier*, 2003.
- [165] A. Nasrullah, B. Saad, A. H. Bhat, A. S. Khan, M. Danish, M. H. Isa, and A. Naeem, "Mangosteen peel waste as a sustainable precursor for high surface area mesoporous activated carbon: Characterization and application for methylene blue removal," *Journal of Cleaner Production*, vol. 211, pp. 1190-1200, 2019/02/20/ 2019.

- [166] H. N. Tran, S.-J. You, and H.-P. Chao, "Insight into adsorption mechanism of cationic dye onto agricultural residues-derived hydrochars: negligible role of π - π interaction," *Korean Journal of Chemical Engineering*, vol. 34, pp. 1708-1720, 2017.
- [167] I. Tan, B. Hameed, and A. Ahmad, "Equilibrium and kinetic studies on basic dye adsorption by oil palm fibre activated carbon," *Chemical Engineering Journal*, vol. 127, pp. 111-119, 2007.
- [168] P. J. Dauenhauer and O. A. Abdelrahman, "A universal descriptor for the entropy of adsorbed molecules in confined spaces," *ACS central science*, vol. 4, pp. 1235-1243, 2018.
- [169] J. Tian, V. Miller, P. C. Chiu, J. A. Maresca, M. Guo, and P. T. Imhoff, "Nutrient release and ammonium sorption by poultry litter and wood biochars in stormwater treatment," *Science of The Total Environment*, vol. 553, pp. 596-606, 2016/05/15/ 2016.
- [170] D. Mai, R. Wen, W. Cao, B. Yuan, Y. Liu, Q. Liu, and G. Qian, "Effect of Heavy Metal (Zn) on Redox Property of Hydrochar Produced from Lignin, Cellulose, and d-Xylose," *ACS Sustainable Chemistry & Engineering*, vol. 5, pp. 3499-3508, 2017/04/03 2017.
- [171] X. Cao, J. J. Pignatello, Y. Li, C. Lattao, M. A. Chappell, N. Chen, L. F. Miller, and J. Mao, "Characterization of Wood Chars Produced at Different Temperatures Using Advanced Solid-State ^{13}C NMR Spectroscopic Techniques," *Energy & Fuels*, vol. 26, pp. 5983-5991, 2012/09/20 2012.

Appendix A

HTC reaction mechanism

Biomass mainly consists of hemicellulose, cellulose, and lignin; they are converted to hydrochar at different rates via different mechanisms. The detailed mechanisms of hydrochar formation from cellulose are shown in Figure A1. In the first step, long-chain cellulose hydrolyze when hydronium ions catalyze the hydrolysis from different oligomers and then further hydrolyze to glucose, which partly isomerizes to fructose [1, 2]. The oligomers also hydrolyze into their monomers, which undergo dehydration and fragmentation reactions leading to the formation of different soluble products, such as 1,6-anhydroglucose, erythrose, furfural-like compounds (i.e. 5-hydroxymethylfurfural, furfural, 5-methyl furfural) [1, 3, 4]. These intermediates subsequently take part in polymerization and condensation reactions and formed soluble polymers [5]. These reactions may be tempted by dehydration or aldol condensation that resulted from the aromatization of polymers and formation of different functional groups such as C=O, C=C, -OH, etc. [6]. Furthermore, the aromatized molecules formed the aromatic cluster, and when the concentration of this cluster reaches at supersaturation point, a burst nucleation takes place. The nuclei then grows outwards by diffusion towards the surface of the solution. The species present in the solution are linked to the surface of the microspheres via the reactive oxygen functionalities (hydroxyl, carbonyl, carboxylic, etc.). As a result, once the growth process stops, the outer surface of the hydrochar particles will contain a high concentration of oxygen functional groups.

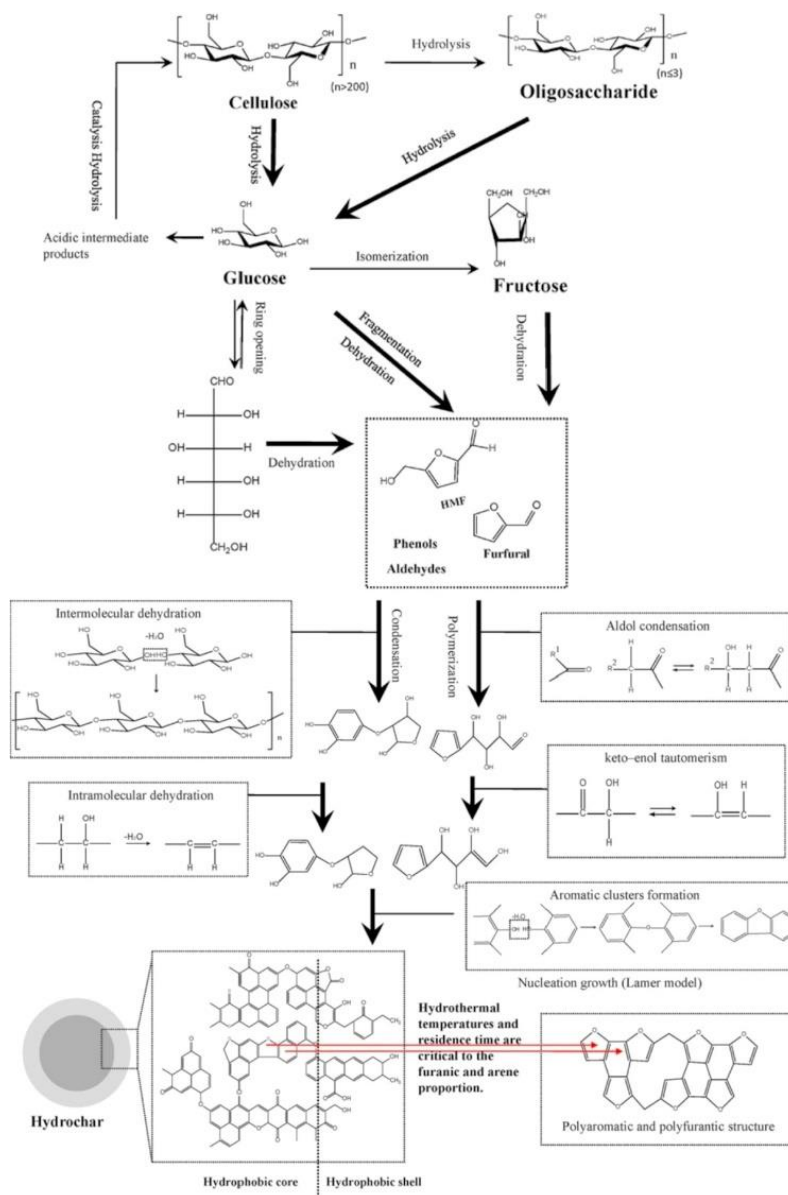


Figure A1: HTC of cellulose: hydrochar formation mechanism [7].

Similar to cellulose, hemicellulose (xylan) is hydrolyzed into xylose in the first step followed by the formation of another important intermediate such as furfural [8-11].

Later on, this furfural is working as the precursor during the char formation via polymerization [12]. The detailed mechanism of hydrochar formation from hemicellulose is illustrated in Figure A2.

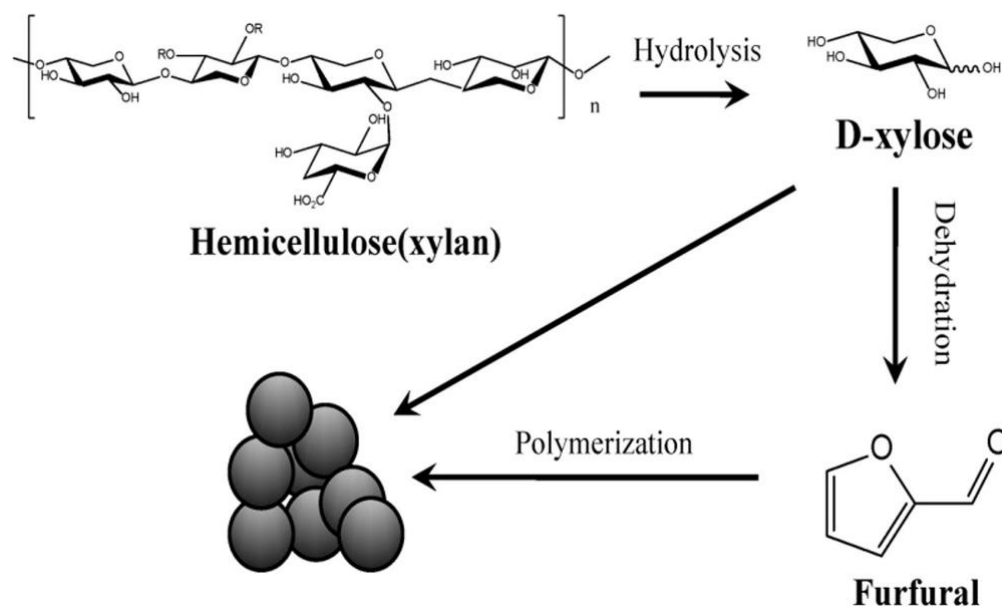


Figure A2: HTC of hemicellulose: Hydrochar formation mechanism [7].

Although a fraction of lignin can be dissolved in water at 200 °C, the majority of lignin fragments are hard to be dissolved and dispersed onto aqueous media as the HTC temperature (typically upto 260 °C) is not high enough [11]. In addition, the high molecular weight and the complex structure make the reaction mechanism more complicated. A detailed mechanism of hydrochar formation from lignin is demonstrated in Figure A3. This formation is occurred at around 265 °C [11]. Firstly,

the lignin dissolved and decomposed by hydrolysis and dealkylation in a homogeneous reaction and form phenolic products such as syringols, guaiacols, catechols, and phenols. These intermediates then undergo a cross-linking reaction and repolymerized into phenolic char [7]. Finally, the part of lignin, that could not be dissolved in water is converted into polyaromatic hydrochar via solid-solid reactions similar to the pyrolysis mechanism [13].

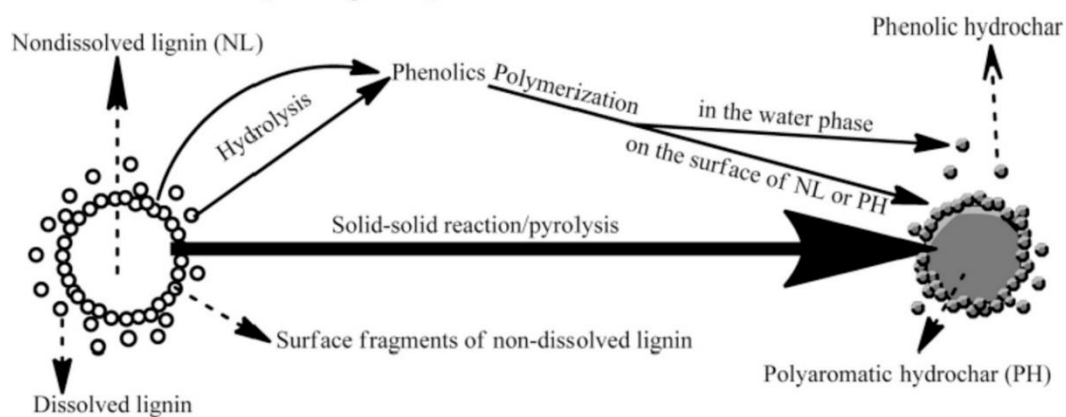


Figure A3: Proposed formation pathways of lignin hydrochar [11].

References

- [1] M. Sevilla and A. B. Fuertes, "The production of carbon materials by hydrothermal carbonization of cellulose," *Carbon*, vol. 47, pp. 2281-2289, 2009.
- [2] M. Sasaki, Z. Fang, Y. Fukushima, T. Adschiri, and K. Arai, "Dissolution and hydrolysis of cellulose in subcritical and supercritical water," *Industrial & Engineering Chemistry Research*, vol. 39, pp. 2883-2890, 2000.
- [3] T. M. Aida, Y. Sato, M. Watanabe, K. Tajima, T. Nonaka, H. Hattori, and K. Arai, "Dehydration of D-glucose in high temperature water at pressures up to 80 MPa," *The Journal of supercritical fluids*, vol. 40, pp. 381-388, 2007.
- [4] B. M. Kabyemela, T. Adschiri, R. M. Malaluan, and K. Arai, "Glucose and fructose decomposition in subcritical and supercritical water: detailed reaction pathway, mechanisms, and kinetics," *Industrial & Engineering Chemistry Research*, vol. 38, pp. 2888-2895, 1999.
- [5] F. Salak Asghari and H. Yoshida, "Acid-catalyzed production of 5-hydroxymethyl furfural from D-fructose in subcritical water," *Industrial & Engineering Chemistry Research*, vol. 45, pp. 2163-2173, 2006.
- [6] R. Bacon and M. Tang, "Carbonization of cellulose fibers—II. Physical property study," *Carbon*, vol. 2, pp. 221-225, 1964.

- [7] T. Wang, Y. Zhai, Y. Zhu, C. Li, and G. Zeng, "A review of the hydrothermal carbonization of biomass waste for hydrochar formation: Process conditions, fundamentals, and physicochemical properties," *Renewable and Sustainable Energy Reviews*, vol. 90, pp. 223-247, 2018.
- [8] C. He, A. Giannis, and J.-Y. Wang, "Conversion of sewage sludge to clean solid fuel using hydrothermal carbonization: hydrochar fuel characteristics and combustion behavior," *Applied Energy*, vol. 111, pp. 257-266, 2013.
- [9] J. Qi and L. Xiuyang, "Kinetics of non-catalyzed decomposition of D-xylose in high temperature liquid water," *Chinese Journal of Chemical Engineering*, vol. 15, pp. 666-669, 2007.
- [10] N. Paksung and Y. Matsumura, "Decomposition of xylose in sub-and supercritical water," *Industrial & Engineering Chemistry Research*, vol. 54, pp. 7604-7613, 2015.
- [11] S. Kang, X. Li, J. Fan, and J. Chang, "Characterization of hydrochars produced by hydrothermal carbonization of lignin, cellulose, D-xylose, and wood meal," *Industrial & Engineering Chemistry Research*, vol. 51, pp. 9023-9031, 2012.
- [12] C. Promdej and Y. Matsumura, "Temperature effect on hydrothermal decomposition of glucose in sub-and supercritical water," *Industrial & Engineering Chemistry Research*, vol. 50, pp. 8492-8497, 2011.

- [13] Z. Fang, T. Sato, R. L. Smith Jr, H. Inomata, K. Arai, and J. A. Kozinski, "Reaction chemistry and phase behavior of lignin in high-temperature and supercritical water," *Bioresource Technology*, vol. 99, pp. 3424-3430, 2008.

Appendix B

Pyrolysis reaction mechanism

Similar to the HTC, different components of the biomass converted to biochar at different rates via different mechanisms under pyrolysis condition. The hemicellulose pyrolysis mechanism is characterized by a decreasing degree of polymerization. It firstly depolymerized into oligosaccharides, followed by the cleavage of glycosidic linkage of xylan chain and rearrangement of the depolymerized molecules to produce 1, 4-anhydro-D-xylopyranose [1].

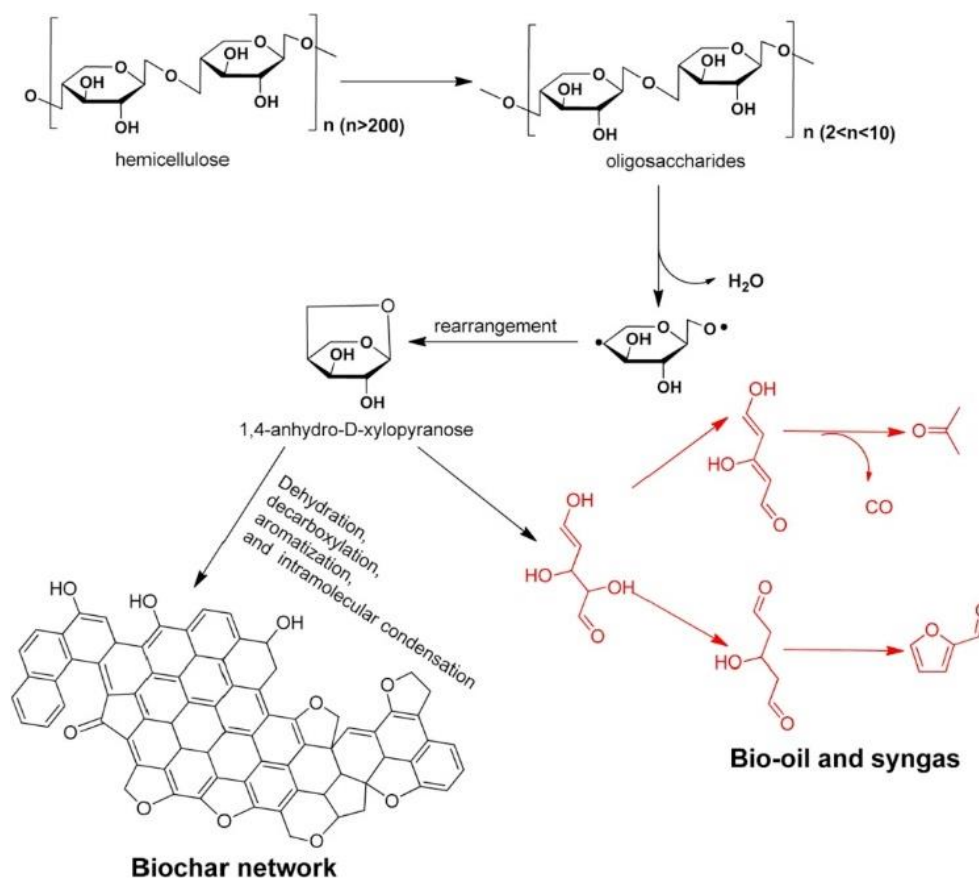


Figure B1: Pyrolysis of hemicellulose: biochar formation mechanism [2].

It can further undergo several reactions such as dehydration, decarboxylation, aromatization and intramolecular condensation to produce biochar [3-7]. The detailed decomposition mechanism of hemicellulose under the pyrolysis condition is shown in Figure B1.

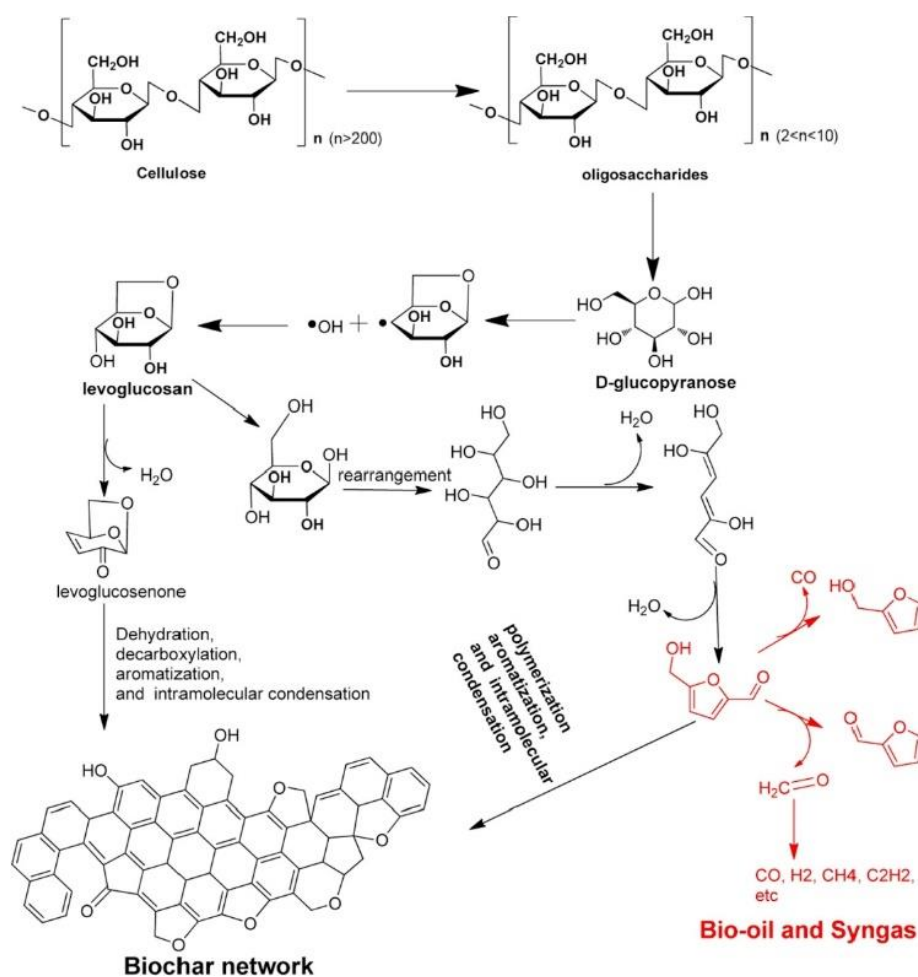


Figure B2: Pyrolysis of cellulose: biochar formation mechanism [2].

Similar to the hemicellulose, cellulose has a similar pyrolysis mechanism. A detailed mechanism of cellulose decomposition under the pyrolysis condition is illustrated in Figure B2. Basically, it reduces from the long-chain carbon to shortchains by decomposition and charring. In the first step of the pyrolysis process, cellulose depolymerized into oligosaccharides followed by the formation of D-glucopyranose, which undergoes an intramolecular rearrangement to form levoglucosan [8]. The formation of biochar from the levoglucosan can occur in two ways. Firstly, levoglucosan leads to the formation of levoglucosenone via a dehydration process. This levoglucosenone undergoes several reactions such as dehydration, decarboxylation, aromatization, and intramolecular condensation to finally form biochar. Secondly, levoglucosan can undertake a series of rearrangement and dehydration process to form hydroxymethylfurfural (HMF), which either can be decomposed into bio-oil and syngas or undergoes a series of polymerization, aromatization, and intramolecular condensation reactions to produce biochar [2].

As lignin is more complex in structure, it also has a complex decomposition mechanism. A free radical reaction is one of the dominant pathways [9-12]. According to these mechanisms, free radicals are generated by the breaking of the β -O-4 lignin linkage, which can capture the protons of other species with weak C-H or O-H bonds and form decomposed compounds. The radicals are passed on to others, which leads to chain propagation. The chain reactions are terminated by the collision

of two radicals and formation of stable compounds. The observation of free radicals in pyrolysis process is not easy; thus the exact mechanism of lignin decomposition remains challenging [2]. The detailed mechanism of lignin decomposition under the pyrolysis condition is demonstrated in Figure B3.

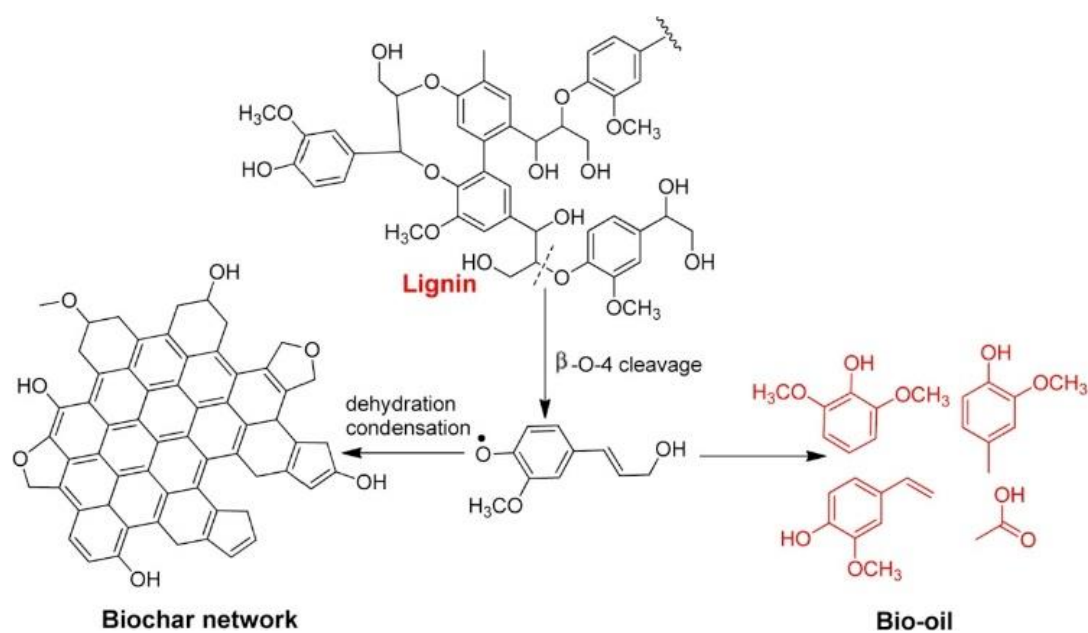


Figure B3: Pyrolysis of lignin: biochar formation mechanism [2].

References

- [1] D. Shen, S. Gu, and A. V. Bridgwater, "Study on the pyrolytic behaviour of xylan-based hemicellulose using TG–FTIR and Py–GC–FTIR," *Journal of Analytical and Applied Pyrolysis*, vol. 87, pp. 199-206, 2010.
- [2] W.-J. Liu, H. Jiang, and H.-Q. Yu, "Development of biochar-based functional materials: toward a sustainable platform carbon material," *Chemical reviews*, vol. 115, pp. 12251-12285, 2015.
- [3] B. Peters, "Prediction of pyrolysis of pistachio shells based on its components hemicellulose, cellulose and lignin," *Fuel processing technology*, vol. 92, pp. 1993-1998, 2011.
- [4] Y. Peng and S. Wu, "The structural and thermal characteristics of wheat straw hemicellulose," *Journal of Analytical and Applied Pyrolysis*, vol. 88, pp. 134-139, 2010.
- [5] J. Huang, C. Liu, H. Tong, W. Li, and D. Wu, "Theoretical studies on pyrolysis mechanism of xylopyranose," *Computational and Theoretical Chemistry*, vol. 1001, pp. 44-50, 2012.
- [6] P. R. Patwardhan, R. C. Brown, and B. H. Shanks, "Product distribution from the fast pyrolysis of hemicellulose," *ChemSusChem*, vol. 4, pp. 636-643, 2011.

- [7] M. Z. Sefain, S. F. El - Kalyoubi, and N. Shukry, "Thermal behavior of holo - and hemicellulose obtained from rice straw and bagasse," *Journal of Polymer Science: Polymer Chemistry Edition*, vol. 23, pp. 1569-1577, 1985.
- [8] S. Li, J. Lyons-Hart, J. Banyasz, and K. Shafer, "Real-time evolved gas analysis by FTIR method: an experimental study of cellulose pyrolysis," *Fuel*, vol. 80, pp. 1809-1817, 2001.
- [9] M. Kosa, H. Ben, H. Theliander, and A. J. Ragauskas, "Pyrolysis oils from CO₂ precipitated Kraft lignin," *Green Chemistry*, vol. 13, pp. 3196-3202, 2011.
- [10] S. Chu, A. V. Subrahmanyam, and G. W. Huber, "The pyrolysis chemistry of a β -O-4 type oligomeric lignin model compound," *Green Chemistry*, vol. 15, pp. 125-136, 2013.
- [11] J. Cho, S. Chu, P. J. Dauenhauer, and G. W. Huber, "Kinetics and reaction chemistry for slow pyrolysis of enzymatic hydrolysis lignin and organosolv extracted lignin derived from maplewood," *Green Chemistry*, vol. 14, pp. 428-439, 2012.
- [12] W. Mu, H. Ben, A. Ragauskas, and Y. Deng, "Lignin pyrolysis components and upgrading—technology review," *Bioenergy research*, vol. 6, pp. 1183-1204, 2013.

Appendix C

Journal publications and conference presentations

Peer-reviewed articles

1. **N. Saha**, A. Saba, and T. Reza, “Effect of hydrothermal carbonization temperature on pH, dissociation constants, and acidic functional groups on hydrochar from cellulose and wood,” *Journal of Analytical and Applied Pyrolysis*, 2019, vol. 137, p. 138-145. <https://doi.org/10.1016/j.jaap.2018.11.018>.
2. **N. Saha**, D. Xin, P. Chiu, and T. Reza, “Effect of pyrolysis temperature on acidic oxygen-containing functional groups and electron storage capacities of pyrolyzed hydrochars,” *ACS Sustainable Chem. Eng.*, 2019, 7, 8387-8396. <https://doi.org/10.1021/acssuschemeng.9b00024>.
3. **N. Saha**, A. Saba, P. Saha, K. McGaughy, D. Franqui-Villanueva, W. J. Orts, W. M. Hart-Cooper, and T. Reza, “Hydrothermal carbonization of various paper mill sludges: an observation of solid fuel properties,” *Energies*, 12, 2019, 858-868. <https://doi.org/10.3390/en12050858>.
4. **N. Saha** and T. Reza, “Effect of pyrolysis on basic functional groups of hydrochars,” *Biomass Conversion and Biorefinery*, 2019,1, 1-8. <https://doi.org/10.1007/s13399-019-00504-3>.
5. A. Saba, **N. Saha**, K. C. Williams, C. J. Coronella, and T. Reza, “Binder-free torrefied biomass pellets: significance of torrefaction temperature and pelletization parameters by multivariate analysis,” *Biomass Conversion and*

- Biorefinery*, 2020. <https://doi.org/10.1007/s13399-020-00737-7>.
6. **N. Saha**, K. McGaughy, M. Held, and T. Reza, “Hydrothermal degradation of β -estradiol and oxytetracycline at selective reaction severities” *SN Applied Sciences*, 2020. <https://doi.org/10.1007/s42452-020-03436-0>.
 7. **N. Saha**, M. Volpe, L. Fiori, R. Volpe, A. Messineo, and T. Reza, “Cationic dye adsorption on hydrochars of winery and citrus juice industries residues: performance, mechanism, and thermodynamics” *Energies*, vol. 13, p. 4686, 2020. <https://doi.org/10.3390/en13184686>.
 8. **N. Saha**, K. McGaughy, and T. Reza, “Elucidating hydrochar morphology and oxygen functionality change with hydrothermal treatment temperature ranging from subcritical to supercritical conditions” *Journal of Analytical and Applied Pyrolysis*, vol. 152, p. 104965, 2020. <https://doi.org/10.1016/j.jaap.2020.104965>
 9. **N. Saha**, A. Saba, K. McGaughy, and T. Reza, “Effect of supercritical water temperature and Pd/C catalyst on upgrading fuel characteristics of gumweed-derived solvent extracted biocrude” *Biomass Conversion and Biorefinery*, 2020. <https://doi.org/10.1007/s13399-020-01050-z>.
 10. **N. Saha**, H. Uddin, and T. Reza, “Preliminary Safety Evaluation of Solvothermal Liquefaction Process of Plastic Wastes using Toluene as Solvent” *Clean Technologies and Environmental Policy*, 2021.
 11. M.Rifat Hasan, **N. Saha**, Thomas Quaid, and T. Reza, “Formation of Carbon

Quantum Dots via Hydrothermal Carbonization: Investigate the Effect of Precursors” *Energies*, 2021. <https://doi.org/10.3390/en14040986>.

12. A. I. Sultana, **N. Saha**, and T. Reza, “Synopsis of Factors Affecting Hydrogen Storage in Biomass-Derived Activated Carbons” *Sustainability*, 2021. <https://doi.org/10.3390/su13041947>.
13. **N. Saha**, K. McGaughy, S. Davis, and T. Reza, “Assessing Hydrothermal Carbonization as Sustainable Home Sewage Management for Rural Counties: A Case Study from Appalachian Ohio” *Science of the Total Environment*, 2021 (under-review).
14. D. Xin, **N. Saha**, T. Reza, J. Hudson, and P. Chiu, “Pyrolysis Creates Electron Storage Capacity of Black Carbon (Biochar) from Lignocellulosic Biomass” *ACS Sustainable Chem. Eng.*, 2021 (under-review).

Invited talks

1. **N. Saha**, and T. Reza, “Solvothermal Conversion: Crude Oil Production from Waste Plastics,” AIChE Annual Meeting 2020, San Francisco, CA.
2. **N. Saha**, A. I. Sultana, and T. Reza, “Hydrogen Storage in Superactivated Hydrochars,” 2000339, ASABE Annual International Meeting 2020, Virtual Event.

Conference oral presentations

1. **N. Saha**, M. Volpe, L. Fiori, R. Volpe, A. Messineo, and T. Reza, “A

- Thermodynamics Study of Methylene Blue Adsorption on Hydrochars Produced from Orange Peel and Grape Skin,” AIChE Annual Meeting 2020, San Francisco, CA.
2. **N. Saha**, K. McGaugy, and T. Reza, “Effect of Hydrothermal Treatment Temperature on Surface Morphology and Oxygen Functionality of Hydrochar Produced from Cellulose,” AIChE Annual Meeting 2020, San Francisco, CA.
 3. **N. Saha** and T. Reza, “Quantitative Risk Assessment of Solvothermal Conversion of Waste Plastics,” AIChE Annual Meeting 2020, San Francisco, CA.
 4. A. I. Sultana, **N. Saha**, and T. Reza, “Gas Storage in Superactivated Hydrochars Synthesized from Anaerobic Digested Food Waste,” AIChE Annual Meeting 2020, San Francisco, CA.
 5. **N. Saha**, M. Volpe, L. Fiori, R. Volpe, A. Messineo, and T. Reza, “Effect of Hydrothermal Carbonization Temperature on Acidic and Basic Groups of Hydrochars Produced from Orange Peel and Grape Skin,” 768c, AIChE Annual Meeting 2019, Orlando, FL.
 6. **N. Saha** and T. Reza, “Hydrothermal Degradation of Emerging Pollutants from Water,” 670c, AIChE Annual Meeting 2019, Orlando, FL.
 7. **N. Saha** and T. Reza, “Super Activated Hydrochar for Hydrogen Storage,” 613b, AIChE Annual Meeting 2019, Orlando, FL.

8. **N. Saha**, K. McGaughy, O. N. Safsari, T. L. Westover, and T. Reza, "Fate of Inorganics during Hydrothermal Carbonization of High Ash Fraction of Air Classified Biomass," 613f, AIChE Annual Meeting 2019, Orlando, FL.
9. K. McGaugy, A. Saba, **N. Saha**, and T. Reza, "Techno-Economic Analysis of Septic Tank Waste Treatment in a Centralized Hydrothermal Treatment Facility," 587i, AIChE Annual Meeting 2019, Orlando, FL.
10. **N. Saha**, D. Xin, P. Chiu, T. Reza, "Effect of Pyrolysis Temperature on Various Acidic and Basic Functional Groups on Hydrochar," 258th ACS National Meeting 2019, July 2019, San Diego, CA.
11. **N. Saha**, D. Xin, P. Chiu, and T. Reza, "Effect of Pyrolysis on Oxygen Functional Groups of Hydrochars," 1900902, ASABE Annual International Meeting 2019, Boston, MA.
12. **N. Saha**, D. Xin, P. Chiu, and T. Reza, "Effect of Pyrolysis Temperature on Acidic and Basic Functional Groups of Hydrochar," Biochar & Bioenergy 2019, Fort Collins, CO.
13. T. Reza, **N. Saha**, D. Xin, and P. Chiu "Fate of oxygen functional groups upon pyrolysis of hydrochars," 2nd HTC Symposium, May 2019, Berlin, Germany.
14. **N. Saha**, A. Saba, and T. Reza, "Effect of Activation Temperature on Oxygen Functional Groups and Corresponding Electron Exchange Capacities on

Hydrochar,” 411c, AIChE Annual Meeting 2018, Pittsburgh, PA.

15. **N. Saha** and T. Reza, “Hydrothermal Degradation of Hormones and Antibiotics,” 721g, AIChE Annual Meeting 2018, Pittsburgh, PA.
16. **N. Saha**, S. Mazumder, A. Saba, T. Reza, “Quantification of chemical states, dissociation constants, and oxygen functional groups on hydrochar,” 255th ACS National Meeting 2018, March 2018, New Orleans, LA.

Conference posters

1. **N. Saha** and T. Reza, “Hydrothermal degradation of β -estradiol and oxytetracycline at selective reaction severities,” 2019 College of Engineering and Science Doctoral Candidate Research Showcase, Florida Institute of Technology, Melbourne, FL.
2. **N. Saha** and T. Reza, “Hydrothermal Degradation of Emerging Pollutants from Water,” Ohio University Student Expo 2019, Athens, OH.
3. Adam Huges, **N. Saha**, and T. Reza, “Study of Methylene Blue Adsorption on Pyrolyzed Hydrochars,” Ohio University Student Expo 2019, Athens, OH.
4. **N. Saha** and T. Reza, “Quantification of Chemical States, Point-of-Zero Charge, Dissociation Constants, and Oxygen Functional Groups on Hydrochar,” Ohio University Student Expo 2018, Athens, OH.
5. **N. Saha** and T. Reza, “Hydrothermal Treatment of Paper Mill Sludge: Nutrient Characterization,” 199c, AIChE Annual Meeting 2018, Pittsburgh, PA.

Appendix D

Copyright permission from the publisher

Elsevier

9/24/2020

Rightslink® by Copyright Clearance Center



RightsLink®



Home



Help



Email Support



Sign In



Create Account



Effect of hydrothermal carbonization temperature on pH, dissociation constants, and acidic functional groups on hydrochar from cellulose and wood

Author: Nepu Saha, Akbar Saba, M. Toufiq Reza

Publication: Journal of Analytical and Applied Pyrolysis

Publisher: Elsevier

Date: January 2019

© 2018 Elsevier B.V. All rights reserved.

Please note that, as the author of this Elsevier article, you retain the right to include it in a thesis or dissertation, provided it is not published commercially. Permission is not required, but please ensure that you reference the journal as the original source. For more information on this and on your other retained rights, please visit: <https://www.elsevier.com/about/our-business/policies/copyright#Author-rights>

[BACK](#)

[CLOSE WINDOW](#)

© 2020 Copyright - All Rights Reserved | [Copyright Clearance Center, Inc.](#) | [Privacy statement](#) | [Terms and Conditions](#)
 Comments? We would like to hear from you. E-mail us at customer-care@copyright.com

3/18/2021

Rightslink® by Copyright Clearance Center



RightsLink®



Home



Help



Email Support



Sign In



Create Account



Elucidating hydrochar morphology and oxygen functionality change with hydrothermal treatment temperature ranging from subcritical to supercritical conditions

Author: Nepu Saha, Kyle McGaughey, M. Toufiq Reza

Publication: Journal of Analytical and Applied Pyrolysis

Publisher: Elsevier

Date: November 2020

© 2020 Elsevier B.V. All rights reserved.

Journal Author Rights

Please note that, as the author of this Elsevier article, you retain the right to include it in a thesis or dissertation, provided it is not published commercially. Permission is not required, but please ensure that you reference the journal as the original source. For more information on this and on your other retained rights, please visit: <https://www.elsevier.com/about/our-business/policies/copyright#Author-rights>

BACK

CLOSE WINDOW

© 2021 Copyright - All Rights Reserved | Copyright Clearance Center, Inc. | [Privacy statement](#) | [Terms and Conditions](#)
 Comments? We would like to hear from you. E-mail us at customercare@copyright.com

ACS publications

3/18/2021

Rightslink® by Copyright Clearance Center



RightsLink®



Home



Help



Email Support



Sign In



Create Account

Effect of Pyrolysis Temperature on Acidic Oxygen-Containing Functional Groups and Electron Storage Capacities of Pyrolyzed Hydrochars



Author: Nepu Saha, Danhui Xin, Pei C. Chiu, et al

Publication: ACS Sustainable Chemistry & Engineering

Publisher: American Chemical Society

Date: May 1, 2019

Copyright © 2019, American Chemical Society

PERMISSION/LICENSE IS GRANTED FOR YOUR ORDER AT NO CHARGE

This type of permission/license, instead of the standard Terms & Conditions, is sent to you because no fee is being charged for your order. Please note the following:

- Permission is granted for your request in both print and electronic formats, and translations.
- If figures and/or tables were requested, they may be adapted or used in part.
- Please print this page for your records and send a copy of it to your publisher/graduate school.
- Appropriate credit for the requested material should be given as follows: "Reprinted (adapted) with permission from (COMPLETE REFERENCE CITATION). Copyright (YEAR) American Chemical Society." Insert appropriate information in place of the capitalized words.
- One-time permission is granted only for the use specified in your request. No additional uses are granted (such as derivative works or other editions). For any other uses, please submit a new request.

[BACK](#)
[CLOSE WINDOW](#)

© 2021 Copyright - All Rights Reserved | Copyright Clearance Center, Inc. | [Privacy statement](#) | [Terms and Conditions](#)
 Comments? We would like to hear from you. E-mail us at customer@copyright.com

Springer nature

3/18/2021

RightsLink Printable License

**SPRINGER NATURE LICENSE
TERMS AND CONDITIONS**

Mar 18, 2021

This Agreement between Florida Institute of Technology -- Nepu Saha ("You") and Springer Nature ("Springer Nature") consists of your license details and the terms and conditions provided by Springer Nature and Copyright Clearance Center.

License Number 5032010721802

License date Mar 18, 2021

Licensed Content
Publisher Springer NatureLicensed Content
Publication Biomass Conversion and Biorefinery

Licensed Content Title Effect of pyrolysis on basic functional groups of hydrochars

Licensed Content
Author Nepu Saha et al

Licensed Content Date Aug 23, 2019

Type of Use Thesis/Dissertation

Requestor type academic/university or research institute

Format electronic

Portion full article/chapter

Will you be
translating? no

3/18/2021

RightsLink Printable License

Circulation/distribution 1 - 29

Author of this Springer Nature content yes

Title Behavior of selective oxygen functional groups upon hydrothermal carbonization and pyrolysis of biomass and their roles on selective applications

Institution name Florida Institute of Technology

Expected presentation date May 2021

Requestor Location Florida Institute of Technology
150 W University Blvd
Apt 5
MELBOURNE, FL 32901
United States
Attn: Florida Institute of Technology

Total 0.00 USD

Terms and Conditions

**Springer Nature Customer Service Centre GmbH
Terms and Conditions**

This agreement sets out the terms and conditions of the licence (the **Licence**) between you and Springer Nature Customer Service Centre GmbH (the **Licensor**). By clicking 'accept' and completing the transaction for the material (**Licensed Material**), you also confirm your acceptance of these terms and conditions.

1. Grant of License

1. 1. The Licensor grants you a personal, non-exclusive, non-transferable, world-wide licence to reproduce the Licensed Material for the purpose specified in your order only. Licences are granted for the specific use requested in the order and for no other use, subject to the conditions below.

1. 2. The Licensor warrants that it has, to the best of its knowledge, the rights to license reuse of the Licensed Material. However, you should ensure that the material you are requesting is original to the Licensor and does not carry the copyright of

another entity (as credited in the published version).

1. 3. If the credit line on any part of the material you have requested indicates that it was reprinted or adapted with permission from another source, then you should also seek permission from that source to reuse the material.

2. Scope of Licence

2. 1. You may only use the Licensed Content in the manner and to the extent permitted by these Ts&Cs and any applicable laws.

2. 2. A separate licence may be required for any additional use of the Licensed Material, e.g. where a licence has been purchased for print only use, separate permission must be obtained for electronic re-use. Similarly, a licence is only valid in the language selected and does not apply for editions in other languages unless additional translation rights have been granted separately in the licence. Any content owned by third parties are expressly excluded from the licence.

2. 3. Similarly, rights for additional components such as custom editions and derivatives require additional permission and may be subject to an additional fee. Please apply to Journalpermissions@springernature.com/bookpermissions@springernature.com for these rights.

2. 4. Where permission has been granted **free of charge** for material in print, permission may also be granted for any electronic version of that work, provided that the material is incidental to your work as a whole and that the electronic version is essentially equivalent to, or substitutes for, the print version.

2. 5. An alternative scope of licence may apply to signatories of the [STM Permissions Guidelines](#), as amended from time to time.

3. Duration of Licence

3. 1. A licence for is valid from the date of purchase ('Licence Date') at the end of the relevant period in the below table:

Scope of Licence	Duration of Licence
Post on a website	12 months
Presentations	12 months
Books and journals	Lifetime of the edition in the language purchased

4. Acknowledgement

4. 1. The Licensor's permission must be acknowledged next to the Licenced Material in print. In electronic form, this acknowledgement must be visible at the same time as the figures/tables/illustrations or abstract, and must be hyperlinked to the journal/book's homepage. Our required acknowledgement format is in the Appendix below.

5. Restrictions on use

5. 1. Use of the Licensed Material may be permitted for incidental promotional use and minor editing privileges e.g. minor adaptations of single figures, changes of format, colour and/or style where the adaptation is credited as set out in Appendix 1 below. Any other changes including but not limited to, cropping, adapting, omitting material that affect the meaning, intention or moral rights of the author are strictly prohibited.

5. 2. You must not use any Licensed Material as part of any design or trademark.

5. 3. Licensed Material may be used in Open Access Publications (OAP) before publication by Springer Nature, but any Licensed Material must be removed from OAP sites prior to final publication.

6. Ownership of Rights

6. 1. Licensed Material remains the property of either Licensor or the relevant third party and any rights not explicitly granted herein are expressly reserved.

7. Warranty

IN NO EVENT SHALL LICENSOR BE LIABLE TO YOU OR ANY OTHER PARTY OR ANY OTHER PERSON OR FOR ANY SPECIAL, CONSEQUENTIAL, INCIDENTAL OR INDIRECT DAMAGES, HOWEVER CAUSED, ARISING OUT OF OR IN CONNECTION WITH THE DOWNLOADING, VIEWING OR USE OF THE MATERIALS REGARDLESS OF THE FORM OF ACTION, WHETHER FOR BREACH OF CONTRACT, BREACH OF WARRANTY, TORT, NEGLIGENCE, INFRINGEMENT OR OTHERWISE (INCLUDING, WITHOUT LIMITATION, DAMAGES BASED ON LOSS OF PROFITS, DATA, FILES, USE, BUSINESS OPPORTUNITY OR CLAIMS OF THIRD PARTIES), AND WHETHER OR NOT THE PARTY HAS BEEN ADVISED OF THE POSSIBILITY OF SUCH DAMAGES. THIS LIMITATION SHALL APPLY NOTWITHSTANDING ANY FAILURE OF ESSENTIAL PURPOSE OF ANY LIMITED REMEDY PROVIDED HEREIN.

8. Limitations

8. 1. **BOOKS ONLY:** Where 'reuse in a dissertation/thesis' has been selected the following terms apply: Print rights of the final author's accepted manuscript (for clarity, NOT the published version) for up to 100 copies, electronic rights for use only on a personal website or institutional repository as defined by the Sherpa guideline (www.sherpa.ac.uk/romeo/).

8. 2. For content reuse requests that qualify for permission under the [STM Permissions Guidelines](#), which may be updated from time to time, the STM Permissions Guidelines supersede the terms and conditions contained in this licence.

9. Termination and Cancellation

9. 1. Licences will expire after the period shown in Clause 3 (above).
9. 2. Licensee reserves the right to terminate the Licence in the event that payment is not received in full or if there has been a breach of this agreement by you.

Appendix 1 — Acknowledgements:

For Journal Content:

Reprinted by permission from [the Licensor]: [Journal Publisher (e.g. Nature/Springer/Palgrave)] [JOURNAL NAME] [REFERENCE CITATION (Article name, Author(s) Name), [COPYRIGHT] (year of publication)]

For Advance Online Publication papers:

Reprinted by permission from [the Licensor]: [Journal Publisher (e.g. Nature/Springer/Palgrave)] [JOURNAL NAME] [REFERENCE CITATION (Article name, Author(s) Name), [COPYRIGHT] (year of publication), advance online publication, day month year (doi: 10.1038/sj.[JOURNAL ACRONYM].)]

For Adaptations/Translations:

Adapted/Translated by permission from [the Licensor]: [Journal Publisher (e.g. Nature/Springer/Palgrave)] [JOURNAL NAME] [REFERENCE CITATION (Article name, Author(s) Name), [COPYRIGHT] (year of publication)]

Note: For any republication from the British Journal of Cancer, the following credit line style applies:

Reprinted/adapted/translated by permission from [the Licensor]: on behalf of Cancer Research UK: : [Journal Publisher (e.g. Nature/Springer/Palgrave)] [JOURNAL NAME] [REFERENCE CITATION (Article name, Author(s) Name), [COPYRIGHT] (year of publication)]

For Advance Online Publication papers:

Reprinted by permission from The [the Licensor]: on behalf of Cancer Research UK: [Journal Publisher (e.g. Nature/Springer/Palgrave)] [JOURNAL NAME] [REFERENCE CITATION (Article name, Author(s) Name), [COPYRIGHT] (year of publication), advance online publication, day month year (doi: 10.1038/sj.[JOURNAL ACRONYM].)]

For Book content:

Reprinted/adapted by permission from [the Licensor]: [Book Publisher (e.g. Palgrave Macmillan, Springer etc) [Book Title] by [Book author(s)] [COPYRIGHT] (year of publication)]

Other Conditions:

Version 1.3

3/18/2021

RightsLink Printable License

Questions? customercare@copyright.com or +1-855-239-3415 (toll free in the US) or +1-978-646-2777.
